PHOTON COUNTING RECEIVERS FOR OPTICAL COMMUNICATION THROUGH THE TURBULENT ATMOSPHERE

Kaliappan Shanmuganathan
B.Sc., Madras University, 1966
M.Sc., Madurai University, 1968

A dissertation submitted to the faculty
of the Oregon Graduate Center
in partial fulfillment of the
requirements for the degree
Doctor of Philosophy
in
Applied Physics & Electronic Science

March 12, 1980

The dissertation "Photon Counting Receivers for Optical Communication Through the Turbulent Atmosphere" by Kaliappan Shanmuganathan has been examined and approved by the following Examination Committee:

CHARLES M. McINTYRE, Thesis Advisor
Assistant Professor

J. FRED HOLMES
Professor

RICHARD A. ELLIOTT
Associate Professor

FRANK M. HAUSER
Associate Professor

"The secret things belong to the Lord our God; but the things that are revealed belong to us and to our children for ever . . ."

Deut. 29:29
New Oxford Annotated Bible
Revised Standard Version

ACKNOWLEDGEMENTS

The author wishes to express his sincere thanks to all who helped and supported him in this endeavor. In particular: to Glen Robinson, Gordon Frost and Carl Miller for their assistance in fabrication of the experimental system; to Phil Pincus, Jim Churnside, Dale Larson and Rao Gudimetla, my good friends and one-time fellow students, for their invaluable help through discussion, suggestions and also in the field site work; to the members of my thesis committee (in particular, Dick Elliott) for their suggestions and comments in preparing the thesis; to Nancy Christie for typing the thesis.

Above all, I am very grateful to Chuck McIntyre for his support, assistance and guidance which made this work possible and for the patience and understanding he exhibited throughout.

DEDICATION

This work is dedicated to my teachers.

TABLE OF CONTENTS

Chapter

LIST OF TABLES

LIST OF ILLUSTRATIONS

ABSTRACT

PHOTON COUNTING RECEIVERS FOR OPTICAL COMMUNICATION

THROUGH THE TURBULENT ATMOSPHERE

Kaliappan Shanmuganathan, Ph.D.
Oregon Graduate Center, 1980

Supervising Professor: Charles M. McIntyre

Direct detection, photon counting receivers for use in optical communication through the clear air, turbulent atmosphere have been examined. In particular, spatial diversity arrays to overcome the effect of fading due to atmospheric turbulence are considered. Experimental results are compared with theoretical results for an optimum receiver structure based upon Bayes criterion of minimum probability of error. In addition, certain suboptimum receivers with simpler structures are derived directly from the optimum receiver. These receivers, along with an adaptive threshold receiver, are considered in order to examine the tradeoff between performance and complexity. The results indicate that the adaptive threshold reciever is a good compromise for information rates that are high with respect to scintillation frequencies, a relatively unrestrictive condition.

CHAPTER 1

INTRODUCTION

Using a laser beam for communication through the atmosphere may have several advantages. It offers extremely high bandwidth and since a laser beam is highly directional, private communication is possible. In addition, a range of cheap, reliable functional devices (polarizers, modulating crystals, etc.) and very sensitive, low noise detectors are available. There has been considerable work in the past to understand the optical properties of the atmosphere and to develop receiver structures to process the signal in an optimal way. A typical optical communication system is shown in Figure 1.

Both coherent detection (also referred to as heterodyne detection) and direct detection (also called incoherent detection) have been considered for use in these communication systems. In coherent detection, the received optical wave is mixed with that of a local oscillator (Figure 2). The resulting wave is then detected to generate an IF signal and proper filtering of the IF signal recovers the original signal. This technique is usually preferred in radio and microwave communication, but in optical communication this technique poses some problems. The need for a local oscillator with good frequency stability and critical alignment with the received wave introduce cost and complexity. In addition, the fluctuations in the phase and angle of arrival of the received wave due to turbulence

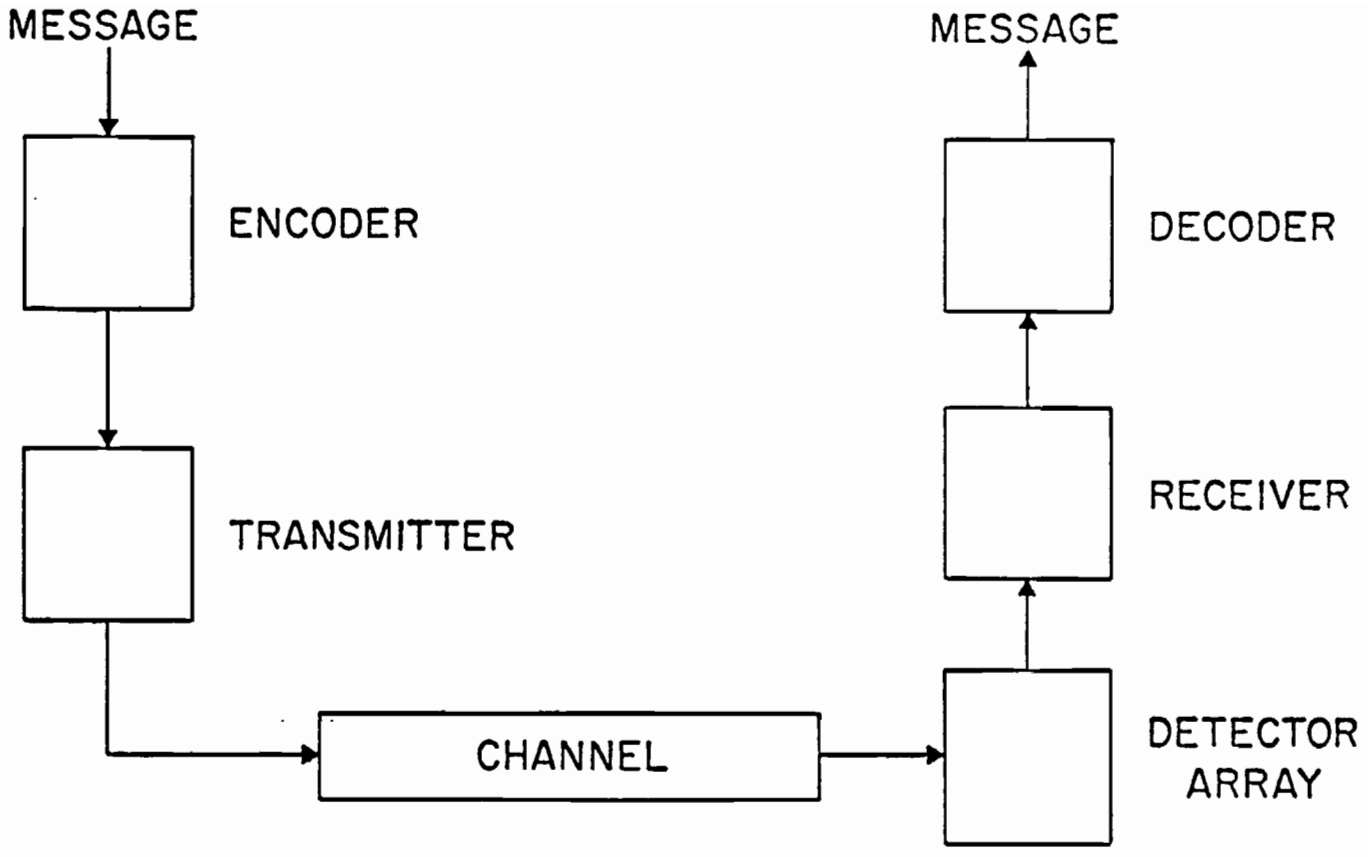

Figure 1. **Block diagram of general optical communication system. Specific receiver structures will be examined for channels through the clear-air turbulent atmosphere.**

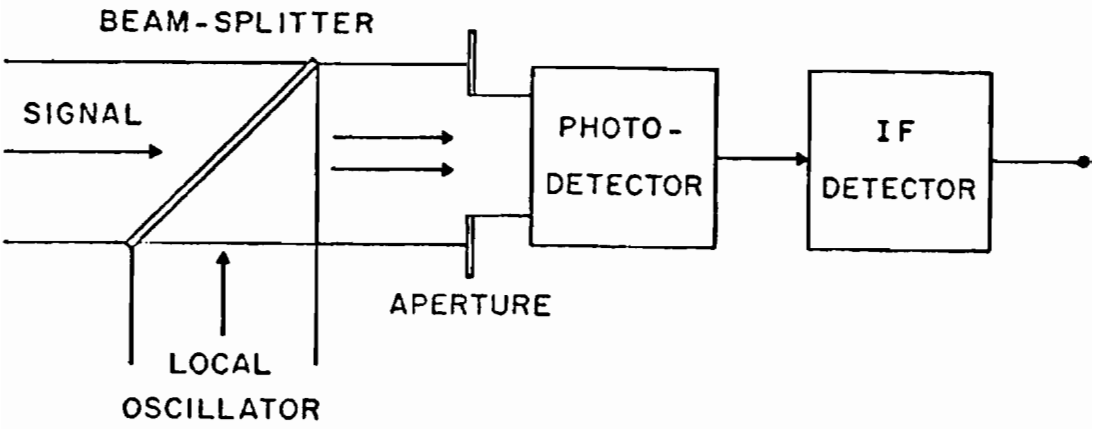

Figure 2. Block diagram of a generalized optical heterodyne receiver.

also cause problems. Therefore direct detection, in spite of its higher sensitivity to background radiation, has been favored in the optical region.

Receiver structures using direct detection for optical communication through the atmosphere have been discussed by several authors.[1,2] A recent and complete treatment by Teich and Rosenberg[3] is the one that is of interest in this work. In their work, lognormal statistics are assumed for the fading due to turbulence, and the limiting case of photon counting is considered. First, a most general receiver structure is developed and found to be very complex. The next simpler case of the optimum receiver using a diversity-array of detectors, in which the fading at each detector can be considered independent, is the basis for the current investigation. An outline of this development is given in the next chapter.

The structure of the optimum receiver, in spite of its relative simplicity compared to the more general case, is also somewhat complex. In this thesis, three additional receiver structures are considered. Two of them are suboptimum receivers derived directly from the optimum receiver, and the third is an adaptive threshold receiver. All three are considerably simplified relative to the optimum receiver.

An experimental photon counting receiver was fabricated to measure the performance of the above receivers. The objective was three-fold:

1) The theoretical calculations by Teich and Rosenberg show a relatively high error rate for the optimum receiver structure. This is due to the severe fading due to turbulence.[4] This effect can be counteracted to some extent by using large aperture receivers. However, when the turbulence is severe, the apertures must be extremely large. This is not desirable for practical purposes. Consequently a diversity-array, in which the individual elements are spaced to provide independent fading at each element, is examined to find useful levels of performance.

2) To compare experimental results with theoretical values.

3) To compare the error rates of the receivers with one another in order to explore the trade-off between their performance and complexity.

The experiment and the results are presented in Chapter 4. The results can be summarized as follows:

1) By using a diversity-array of four detectors, error rates of the order of 10^{-4} are observed. In the experiment, only point detectors were used, because it was desired to explore the worst case. In practice each detector can have a finite size and thereby reduce the scintillation and consequently the error rate to some extent. The resulting error rates can therefore be better than 10^{-4}.

2) It is found that the theoretical curves for the probability density functions agree very well with the experimentally measured ones. For this reason, there is also good agreement between the predicted and measured values of error rates for the optimum receiver. This means, therefore, that the theory can be confidently used in designing and predicting the performance of photon counting communication systems using a laser beam through a clear turbulent atmosphere.

3) When the scintillation frequencies are sufficiently smaller than the bit rates, the adaptive threshold receiver performs better than all other receivers. It is also found to be the least complex of all. (However, it is pointed out that the optimum receiver uses a likelihood function that has only a finite number of discrete values. This fact can be used to reduce its complexity considerably. This is especially so in the case of multi-detector arrays.) The two suboptimum receivers perform very poorly compared to both the optimum receiver and the adaptive threshold receiver.

CHAPTER 2

THE ATMOSPHERE AND OPTICAL COMMUNICATION

Technological developments in the field of semiconductors have made cheap and efficient photo detection possible. This, together with the advance in optical fiber technology, has made communication through optical fibers a reality today. But optical communication through the atmosphere is still in the budding. Some experimental studies have been done in Japan and Russia.[5,6] An engineering feasibility model for a satellite to earth communication link by NASA has been reported.[7] This model is to be space tested using a satellite to be launched in the early 1980's. To explore and exploit the possibilities, however, more work is needed.

Problems Associated with the Atmosphere

Laser communication through the atmosphere obviously requires a good understanding of the atmosphere as an optical channel. The effects of the atmosphere on laser propagation can be broadly divided into two categories. First, there is scattering due to dust, haze, fog, clouds, rain, etc.[8] Recently there have been numerous studies on the particulate scattering of laser beams. Most of them pertain to obtaining information about the particles in the atmosphere, but many also deal with the problems related to communication.

R. R. Meier, et al., study the scattering of UV radiation from a point source using Monte Carlo simulation.[9] G. W. Kattawar et al., treat the effects of radiance and polarization for the case where diffusive scattering is very prominent.[10] B. W. Fowler et al., obtain a numerical solution to the three-dimensional radiative transfer equation in Ref. 8 for a foggy medium.[11] Also there have been some interesting theoretical calculations regarding the possibility of burning a hole through clouds and fog using high power lasers.[12,13] A summary of the phenomenon of light scattering in the atmosphere may be found in Ref. 14. Some of the experimental investigations and their results can be found in Refs. 5, 15-17.

The second deleterious effect that the atmosphere has on laser beam propagation is that due to turbulence. In this case the phase and amplitude of the optical wave change randomly both in space and in time at the receiver plane. Unlike particulate scattering which occurs only in the presence of clouds, fog, etc., the turbulence effects are always present and any receiver system using a laser beam through the atmosphere must take this into account. In recent years there has been considerable progress towards the understanding of this phenomenon. A detailed account of this phenomenon is given in Refs. 18-20. A very brief outline is given in the next section.

Turbulence

Turbulence of the atmosphere is the random variation in space and time of the index of refraction which is mainly caused by random

fluctuations in the temperature of the atmosphere.[18] These fluctuations may be supposed to be encompassed by two scales: an inner scale ℓ_o and an outer scale L_o. Considering only the spatial fluctuations, ℓ_o is the smallest distance over which the spatial covariance factor differs from unity and L_o is the largest distance over which it differs from zero. Obviously, these quantitlies ℓ_o and L_o are not easily measurable. Their primary use is in formulating a theoretical model for the turbulence.

It is convenient to represent the spatial variations of the index of refraction of the atmosphere in terms of a structure function defined as,

$$D_n(r) = \left\langle \left[n(\vec{r}_1) - n(\vec{r}_2) \right]^2 \right\rangle \tag{1}$$

where $n(\vec{r})$ is the index of refraction at a point in the atmosphere represented by the vector $\vec{r}$. $D_n(r)$ has been found to be proportional to $r^{2/3}$ where $r = |\vec{r}_1 - \vec{r}_2|$.[18] The structure function can be written

$$D_n(r) = C_n^2 \; r^{2/3}, \; \ell_o << r << L_o \tag{2}$$

where C_n^2 is a parameter representative of the magnitude of the fluctuations in the index of refraction.

For an isotropic medium, the spatial wave number spectrum of the fluctuations in the index of refraction, for well developed turbulence is approximately given by[19]

$$\phi_n(\kappa) = 0.033 \; C_n^2 \; \kappa^{-11/3} \; \exp(-\kappa^2/\kappa_m^2). \tag{3}$$

In the above κ is the spatial wave number of the fluctuations in refractive index and $\kappa_m = 2\pi/\ell_o$. Equation (3) is a good approximation for $\kappa \lesssim 2\pi/L_o$.

Because of the random refractive index, different portions of the optical wave undergo different random phase changes. At some points in the receiver plane these waves may add up in phase. However, at other points, the random phases may cause a severe fading in amplitude. It has been observed experimentally that the resulting distribution of amplitude (or intensity) obeys lognormal statistics described by

$$f(A) = \frac{1}{A\sqrt{2\pi\sigma_\chi^2}} \exp\left[- \frac{\ell nA - <\ell nA>)^2}{2\sigma_\chi^2} \right] \tag{4}$$

where A is the normalized amplitude, σ_χ^2 is the variance of the logarithm of the amplitude, and f(A) is the probability density function of the amplitude. When the turbulence is very severe ($\sigma_\chi^2 \simeq 0.6$) there is some deviation from the lognormal distribution.[21] However, for many practical purposes, the lognormal distribution appears to be an adequate approximation.

Assuming a spherical wave, an approximate expression for the variance of log amplitude for a homogeneous medium is given by[19]

$$\sigma_\chi^2 = 2\pi^2 k^2 L \int_o^\infty \left\{ 1 - \left(\frac{2\pi k}{\kappa^2 L}\right)^{1/2} \left[\cos\left(\frac{\kappa^2 L}{4k}\right) \cdot C\left(\left(\frac{\kappa^2 L}{2\pi k}\right)^{1/2}\right) + \sin\left(\frac{\kappa^2 L}{4k}\right) S\left(\left(\frac{\kappa^2 L}{2\pi k}\right)^{1/2}\right) \right] \right\} \phi_n(\kappa)\kappa d\kappa \tag{5}$$

where L is the path length, k is the optical wave number of the laser and

$$C(x) = \int_0^x \cos \frac{\pi t^2}{2} \, dt \quad \text{and}$$

$$S(x) = \int_0^x \sin \frac{\pi t^2}{2} \, dt .$$

For a homogeneous isotropic medium the above equation can be reduced by using equation (3). Thus,

$$\sigma_\chi^2 = 0.124 \, C_n^2 \, k^{7/6} \, L^{11/6}, \quad \ell_o^2/\lambda \ll L \tag{6a}$$

where λ is the wavelength. Also, it can be shown that

$$\sigma_I^2 = 0.5 \, C_n^2 \, k^{7/6} \, L^{11/6} \tag{6b}$$

where σ_I^2 is the variance of log intensity. The above expression is valid for $\sigma_\chi^2 \leqslant 0.1$. Experiments[22,23] show that σ_χ^2 increases with L until $\sigma_\chi^2 \simeq 0.7$. Further increases in L cause very little change. This phenomenon is referred to as saturation of the variance of log amplitude. Using equation (2) an expression for the covariance of log amplitude, b (ρ), for the case of a spherical wave can also be derived:[19]

$$b_\chi(\rho) = 1 - 2.2 \left(\frac{k\rho^2}{L}\right)^{5/6} + 1.71 \left(\frac{k\rho^2}{L}\right) + 0.05 \left(\frac{k\rho^2}{L}\right)^{17/6} - 0.08 \left(\frac{k\rho^2}{L}\right)^2 \tag{7}$$

where $\ell_o^2/\lambda \ll L$ and $\ell_o \ll \rho \ll (\lambda L)^{1/2}$.

The temporal fluctuations in the refractive index cause a corresponding fluctuation in the amplitude (or intensity) at any given point in the receiver plane, referred to as scintillation. Among other things, scintillation is affected by the wind velocity across the path of the beam. The relationship between scintillation frequency and the wind velocity is usually described by using Taylor's hypothesis.[18,20]

Some of the recent theoretical work explains the saturation phenomenon,[24,25] indicating that at very high values of integrated path turbulence, as in equation (6), ($\sigma_I^2 >> 100$) the fluctuations in intensity are described by an exponential distribution rather than a lognormal distribution. However, this requires extremely long paths and is difficult to observe experimentally. As such, the predicted exponential distribution for the intensity is less useful than the lognormal distribution.

In recent work[26] Bissonnette, et al., suggest an exponential Bessel distribution for the fading due to turbulence. However, their theoretical justification for such a distribution appears to be questionable. Also from a practical point of view this distribution involves parameters that are more difficult to measure than the parameter (σ_I^2) needed in the case of a lognormal distribution.

In the subsequent treatment we will assuma a lognormal distribution for the irradiance fluctuations due to turbulence.

CHAPTER 3

THEORY OF PHOTON COUNTING RECEIVER

Theory of Optimum Receiver

In this section we outline the development of the optimum receiver by Teich and Rosenberg.[3] The theory is applicable for the case of a non-focused laser beam passing through a clear air, turbulent atmosphere. Only the photon counting (or more correctly, photoelectron counting) case is considered. Lognormal statistics are assumed for the fluctuations in irradiance due to turbulence. It must be mentioned here that their theoretical treatment is more general than is needed for our purposes. In this work we will consider only the very special case of the receiver defined in the next paragraph, since it is not possible to experimentally investigate all the receivers that the theory could cover.

The communication system considered in this thesis uses binary coded amplitude modulation. Sending a laser pulse during a bit interval will correspond to a hypothesis H_1 and not sending a laser pulse during a bit interval will correspond to a hypothesis H_0. The a priori probabilities of H_1 and H_0 are equal. The system uses a simple Bayes criterion of minimum probability of error in the decision making process.

(To avoid a possible confusion later on we may point out here the terminology used: When the transmitter sends a laser pulse

during a bit interval this will be referred to as "The transmitter sends an H_1 bit." When the transmitter does not send any laser pulse during a bit interval, this will be referred to as "The transmitter sends an H_0 bit.")

First, a list of all the assumptions used at various stages of the theoretical development will be given. The list will indicate the extent of usefulness as well as the limitations of the theory.

1) Only the effects of clear air turbulence will be considered. Other effects like particulate scattering, etc. will not be considered.

2) The background radiation is modeled as a white, zero mean, stationary, complex Gaussian process. At low energies, this becomes a Poisson process because of the discrete nature of the photons.

3) The background radiation is additive and the effects of cross mixing between background and signal are negligible.

4) The detector area is assumed to be small enough to ensure complete first order spatial coherence of the field over the detector area of each detector. This condition will be met if the dimensions of the detector-surface are much smaller than $\sqrt{\lambda L}$, the Fresnel zone size, with λ the wave length and L the path length. Actually, this assumption is made only to avoid carrying cumbersome integrals over the detector area. The theory itself will hold good irrespective of the detector area if the reduced variance of the log-intensity due to aperture averaging over large detector surfaces is used in the calculations. This is because it has been observed

that intensity scintillations of the light collected by a large area still obey a log-normal distribution with reduced variance for log-intensity.[27]

5) The individual photoelectrons are resolved and the number of unresolved cases, if present, are negligible.

6) Fluctuations in the laser output energy are negligible. This will be generally true if the laser oscillates far above threshold.

7) The average background radiation and its statistics are the same for all detectors in the array.

8) The mean value of the irradiance due to the laser beam, and its statistics are the same for all detectors in the array.

9) Finally, $T << \frac{1}{f_c}$ where T is the bit interval and f_c is the characteristic frequency of the turbulence fluctuations (typically a few hundred Hz).

Keeping the above assumptions in mind, an expression for the conditional probabilities for the signal (photons) detected at the receiver is derived. First one may omit the effect of turbulence and write the probability density function for the case of a steady flow of photons. Then the turbulence effects can be taken into account and the resulting density function written.

Consider one bit interval between t_1 and $t_1 + T$. Assume the energy received by one detector during this interval is E_T.

$$E_T = \int_{t_1}^{t_1 + T} \beta \, |V(t')|^2 \, dt' \tag{9}$$

where $V(t')$ is the field due to the signal and β is a constant representing the area of the detector (assumption 4). If, during this interval, n photoelectrons are detected,

$$n = \frac{E_T \eta}{h\nu} \tag{10}$$

where η is the quantum efficiency and $h\nu$ the energy in a single photon. Since the counting of random events obeys Poisson statistics, the number of photo-electrons counted should fluctuate about a mean value W, where

$$W = \langle n \rangle = \left\langle \frac{E_T \eta}{h\nu} \right\rangle . \tag{11}$$

Therefore, for one detector the probability density of the photo-electron count can be written as

$$P_a(n) = \frac{W^n \exp(-W)}{n!} . \tag{12}$$

If during the bit interval considered, a hypothesis H_0 was sent, then $W = N_B$ for all detectors in the array, where N_B is the average number of photoelectrons due to the background (assumption 7).

Therefore, the probability density function for n, the number of photoelectrons counted during T for H_0, for one detector is

$$P_a(n) = \frac{N_B^n \exp(-N_B)}{n!} \tag{13}$$

If we consider an array of D detectors, the density function can be written as

$$P_o(\vec{n}) = \prod_{i=1}^{D} \frac{N_B^{n_i} \exp(-N_B)}{n_i!} \tag{14}$$

where n_i is the number of photoelectrons counted at the ith detector and

$$\vec{n} = \begin{pmatrix} n_1 \\ n_2 \\ \cdot \\ \cdot \\ \cdot \\ n_D \end{pmatrix} \tag{15}$$

If we consider only the bit intervals in which hypothesis H_1 were sent, the average number of photoelectron counts would be

$$W = ZN_S + N_B \tag{16}$$

where N_S is the average number of photoelectrons due to the laser and Z, the fading factor due to turbulence effects. By assumption 8, N_S is the same for all detectors, but Z need not be the same. However, by assumptions 1 and 8, Z is statistically identical for

all the detectors. Consequently, given Z, and considering only one detector, the conditional probability density function for n, the number of photoelectron counts when H_1 is sent is

$$P_b(n|Z) = \frac{(ZN_S + N_B)^n \exp\left[-(ZN_S + N_B)\right]}{n!} \quad . \tag{17}$$

For the case of an array of detectors the conditional probability density function takes the form

$$P_c(\vec{n}|\vec{Z}) = \prod_{i=1}^{D} \frac{(Z_i N_S + N_B)^{n_i} \exp\left[-(Z_i N_S + N_B)\right]}{n_i!} \quad , \text{ where } \vec{Z} = \begin{pmatrix} Z_1 \\ Z_2 \\ \vdots \\ Z_D \end{pmatrix} \quad . \tag{18}$$

Under the assumption of lognormal statistics for the fading, the probability density function for $\vec{Z}$ is given as

$$P_Z(\vec{Z}) = \frac{1}{(2\Pi)^{D/2} \ |\Lambda|^{1/2} \ (Z_1 \ Z_2 \ \ldots \ Z_D)} \exp\left[-\frac{(\vec{X})^{\dagger}(\Lambda)^{-1}(\vec{X})}{2}\right] \tag{19}$$

where the vector $\vec{X}$ has components given by $\left\{X_i = \ell n Z_i + \frac{\sigma_I^2}{2}\right\}$ and Λ is the log-irradiance covariance matrix whose elements are

$$\Lambda_{ij} = \begin{cases} C_{\ell nI}(r_i, r_j) & i \neq j \\ C_{\ell nI}(r_i, r_j) = \sigma_I^2 & i = j \end{cases} \qquad i = 1, 2 \ldots D \tag{20}$$

By assumption 9 the *fading* vector $\vec{Z}$ does not change over the period T.

Combining equations (18) and (19) we get the probability density function for the hypothesis H_1 including the turbulence (lognormal) as well as the counting (Poisson) statistics.

$$P_d(\vec{n}) = \int_0^\infty P_c(\vec{n}|\vec{Z})\, P_Z(\vec{Z})\, d\vec{Z}$$

$$= \int_0^\infty \cdots \int_0^\infty \prod_{i=1}^{D} \left\{ \frac{(Z_i N_S + N_B)^{n_i} \exp\left[-(Z_i N_S + N_B)\right]}{n_i!} \right\} P_Z(Z_1, Z_2 \ldots Z_D) dZ_1 \ldots dZ_D \tag{21}$$

Teich and Rosenberg apply the method of steepest descents[3] to reduce the above integrals to get

$$P_1(\vec{n}) = \frac{\left\{ \prod_{i=1}^{D} \frac{(Z_{io} N_S + N_B)^{n_i} \exp\left[-(Z_{io} N_S + N_B)\right]}{n_i!} \right\} \exp\left[-\frac{(\vec{X}_o)^\dagger (\Lambda)^{-1} (\vec{X}_o)}{2} \right]}{|\Lambda|^{\frac{1}{2}} \, |-B^*|^{\frac{1}{2}}} \tag{22}$$

where the relevant quantities are defined below.

$$X_{io} = \ell n Z_{io} + \tfrac{1}{2}\sigma_I^2 \tag{23}$$

$$Q_i^{(1)} = \frac{n_i Z_{io} N_S}{Z_{io} N_S + N_B} - Z_{io} N_S \tag{24}$$

$$Q_{ij}^{(2)} = \left[\frac{n_i Z_{io} N_S N_B}{(Z_{io} N_S + N_B)^2} - Z_{io} N_S \right] \delta_{ij} \tag{24a}$$

and

$$B^* = \begin{bmatrix} Q_{11}^{(2)} & Q_{12}^{(2)} & \cdots & Q_{1D}^{(2)} \\ Q_{21}^{(2)} & Q_{22}^{(2)} & \cdots & Q_{2D}^{(2)} \\ \vdots & \vdots & & \vdots \\ Q_{D1}^{(2)} & Q_{D2}^{(2)} & & Q_{DD}^{(2)} \end{bmatrix} - \Lambda^{-1} \tag{25}$$

The quantity $\vec{Z}_o$ is the stationary value of $\vec{Z}$ obtained from the equation

$$Q^{(1)} - \Lambda^{-1}\vec{X} = 0 \tag{26}$$

Equations (14) and (22) give the photoelectron counting distributions when the hypotheses H_0 and H_1 respectively are sent.

Consider a single detector receiver. Suppose during a bit interval the detector counts n photoelectrons. Using this information, a decision has to be made as to whether H_0 or H_1 was sent from the transmitter. This can be done by evaluating a quantity called the likelihood ratio.[28] If $P_0(n)$ and $P_1(n)$ are the probability densities for receiving n photoelectron counts for the hypotheses H_0 and H_1 respectively, then the likelihood ratio is defined as

$$\underline{\Lambda}(n) = \frac{P_1(n)}{P_0(n)} \tag{27}$$

According to the Bayes criterion of minimum probability of error, the decision rule is then $\underline{\Lambda}(n) \underset{H_0}{\overset{H_1}{\gtrless}} 1$. That is, decide in favor of H_1 if $\underline{\Lambda}(n) > 1$, and H_0 if $\underline{\Lambda}(n) < 1$. Often it is preferred to

use another quantity called the likelihood function, L(n), for making the decision. L(n) is simply $\ell n \underline{\Lambda}(n)$. In terms of L(n), the decision rule is $L(n) \underset{H_0}{\overset{H_1}{\gtrless}} 0$.

Considering a receiver system using an array of D detectors, we can write the corresponding likelihood ratio from equations (14) and (22).

$$\underline{\Lambda}(\vec{n}) = \prod_{i=1}^{D} \left\{ \left(\frac{Z_{io} N_S}{N_B} + 1 \right)^{n_i} \exp \left[-Z_{io} N_S \right] \right\} \frac{\exp \left\{ - \frac{\vec{X}_o^{\dagger} \Lambda^{-1} \vec{X}_o}{2} \right\}}{|\Lambda|^{\frac{1}{2}} |-B^*|^{\frac{1}{2}}} \quad . \tag{28}$$

The corresponding liklihood function is given by

$$L(\vec{n}) = \sum_{i=1}^{D} \left\{ n_i \ell n \left(\frac{Z_{io} N_S}{N_B} + 1 \right) - Z_{io} N_S \right\} - \frac{\vec{X}_o^{\dagger} \Lambda^{-1} \vec{X}_o}{2} - \frac{\ell n |\Lambda|}{2} - \frac{\ell n |-B^*|}{2} \quad . \tag{29}$$

The resulting receiver structure is shown in Figure 3. As can be seen, this receiver structure is very complicated, especially because of the covariance terms.

For a case where the fading of the signals at each of the detectors may be considered to be independent, the likelihood function, and hence the resulting receiver structure, take a simpler form. Such independent fading is possible if the detectors are sufficiently far apart from each other. The likelihood function then is

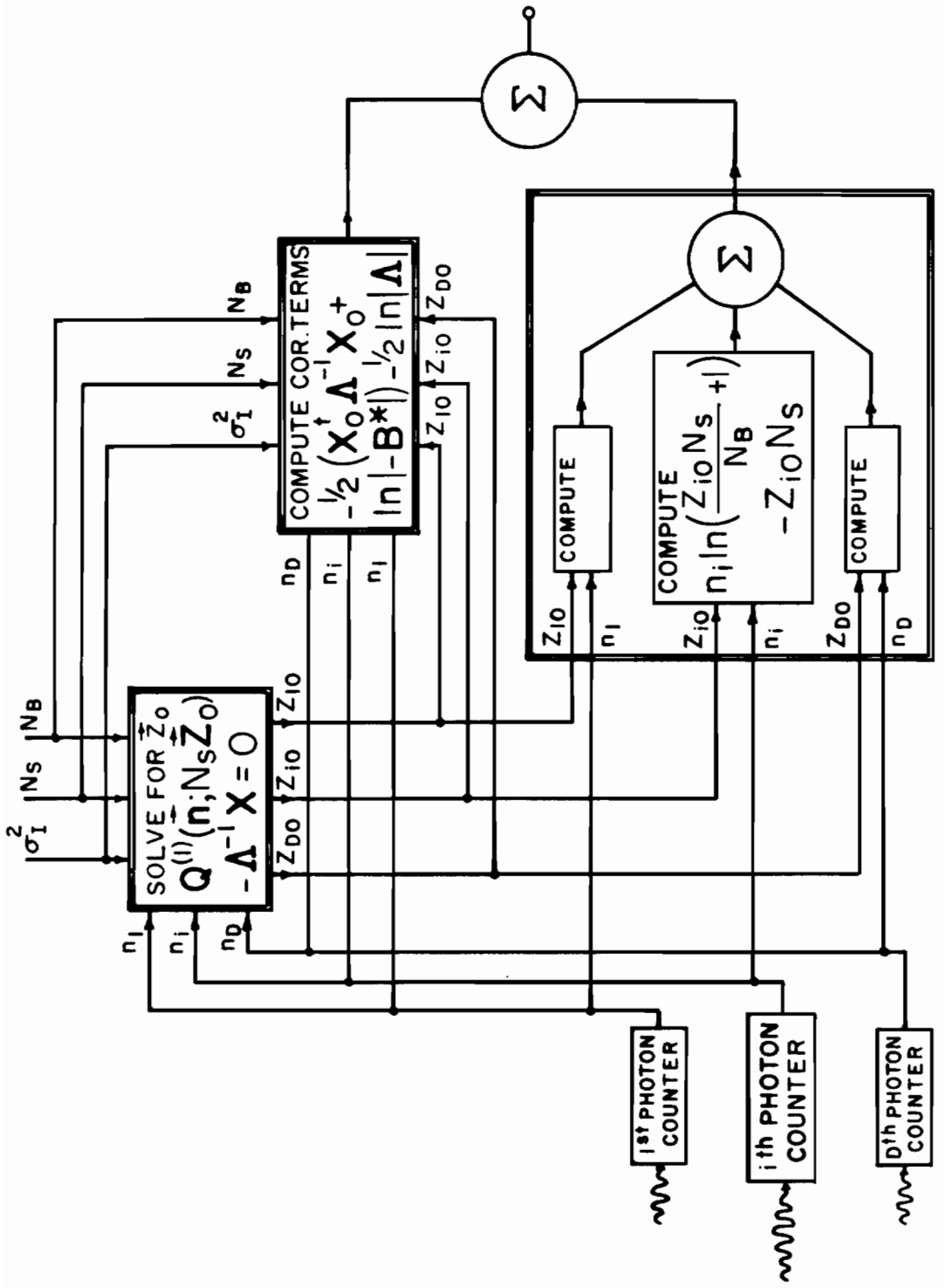

Figure 3. Optimum receiver structure for partially correlated fading at the detectors.

$$L(\vec{n}) = \sum_{i=1}^{D} \left[n_i \ell n \left(\frac{Z_{io} N_S}{N_B} + 1 \right) - Z_{io} N_S - \frac{\left[\ell n Z_{io} + \sigma_I^2/2 \right]^2}{2\sigma_I^2} \right.$$

$$\left. - \tfrac{1}{2} \ell n \left\{ \sigma_I^2 \left(\frac{-n_i Z_{io} N_S N_B}{(Z_{io} N_S + N_B)^2} + Z_{io} N_S \right) + 1 \right\} \right] \qquad (30)$$

where Z_{io} is now obtained from an uncoupled set of equations given by

$$\frac{n_i Z_{io} N_S}{Z_{io} N_S + N_B} - Z_{io} N_S - \frac{\ell n Z_{io} + (\sigma_I^2/2)}{\sigma_I^2} = 0, \qquad i = 1, 2 \ldots D. \qquad (31)$$

The receiver structure corresponding to the likelihood function given in equation (30) is shown in Figure 4. This receiver will henceforth be called the approximate optimum receiver, or simply AOR.

Suboptimum Receiver

From a point of view of practical construction, even the AOR is relatively complicated. More complexity means more cost and in a sense, less reliability. This, therefore, calls for further reduction to simpler structures, and a better trade-off between complexity and performance, if that is possible. We now consider a few possibilities.

Suboptimum Receiver I (SOR I):

We start with the expression for the likelihood function as given in equation (30). An investigation of the relative importance

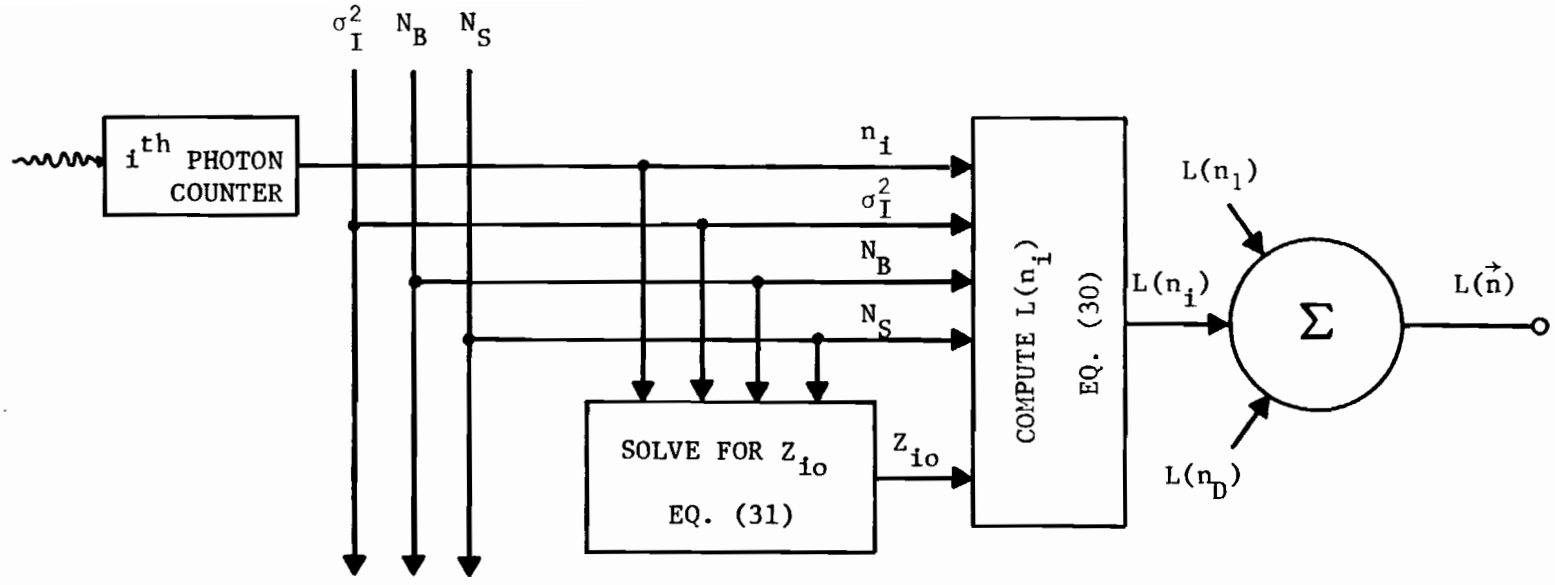

$$L(\vec{n}) = \sum_{i=1}^{D} \left[n_i \ell n \left(\frac{Z_{io} N_S}{N_B} + 1 \right) - Z_{io} N_S - \frac{\left[\ell n Z_{io} + \sigma_I^2/2 \right]^2}{2\,\sigma_I^2} - \tfrac{1}{2} \ell n \left\{ \sigma_I^2 \left(\frac{-n_i Z_{io} N_S N_B}{(Z_{io} N_S + N_B)^2} + Z_{io} N_S \right) + 1 \right\} \right] \quad (30)$$

$$\frac{n_i Z_{io} N_S}{Z_{io} N_S + N_B} - Z_{io} N_S - \frac{\ell n Z_{io} + (\sigma_I^2/2)}{\sigma_I^2} = 0 \quad (31)$$

Figure 4. Approximate optimum receiver (AOR) with independent fading at detectors.

of the four terms on the RHS shows that the last two terms are, in general, considerably smaller than the first two. The actual values of these four terms are listed in Table I for certain typical combinations of σ_I^2 , N_S and N_B and near the corresponding threshold count n_T. The values of the four terms are presented for the threshold counts, because the decision making for H_0 or H_1 is critical only near the threshold. As can be seen, the last two terms are very small compared to the first two in most of the cases. As such, there is some justification to drop the last two terms to make the receiver structure a simpler one. Alternatively, one can look at this approximation this way: The solution of equation (31) for Z_{io} gives an estimated value of the actual fading Z_i. If we assume that this estimated value for Z_i is very nearly the exact value of Z_i, then it can be shown that the last two terms in the square bracket in equation (30) drop out. This results in a simpler equation for the likelihood function:

$$L(n) = \sum_{i=1}^{D} \left[N_i \ell n \left(\frac{Z_{io} N_S}{N_B} + 1 \right) - Z_{io} N_S \right] \qquad (32)$$

where Z_{io} is given by equation (31). The corresponding receiver structure is given in Figure 5.

Suboptimum Receiver II (SOR II):

Another possible approximation results from a consideration of equation (31) for Z_{io}. An investigation shows that the values of Z_{io}

TABLE I

TYPICAL VALUES FOR THE TERMS IN THE LIKELIHOOD FUNCTION OF EQUATION (30)

N_B	N_S	σ_I^2	T_1	$-T_2$	$-T_3$	$-T_4$
1.0	2.0	0.01	1.09	1.96	0.008	0.008
1.0	2.0	0.10	0.996	1.76	0.058	0.069
1.0	2.0	0.5	0.764	0.115	0.094	0.185
1.0	2.0	2.5	0.351	0.470	0.019	0.212
1.0	10.0	0.01	9.36	9.39	0.167	0.043
1.0	10.0	0.1	6.03	6.46	0.747	0.239
1.0	10.0	0.5	4.71	3.81	0.512	0.489
10.0	10.0	0.01	9.48	9.68	0.039	0.03
10.0	10.0	0.1	8.21	7.97	0.155	0.186
10.0	10.0	0.5	5.50	5.27	0.153	0.386
10.0	10.0	2.5	3.36	2.95	0.000	0.489

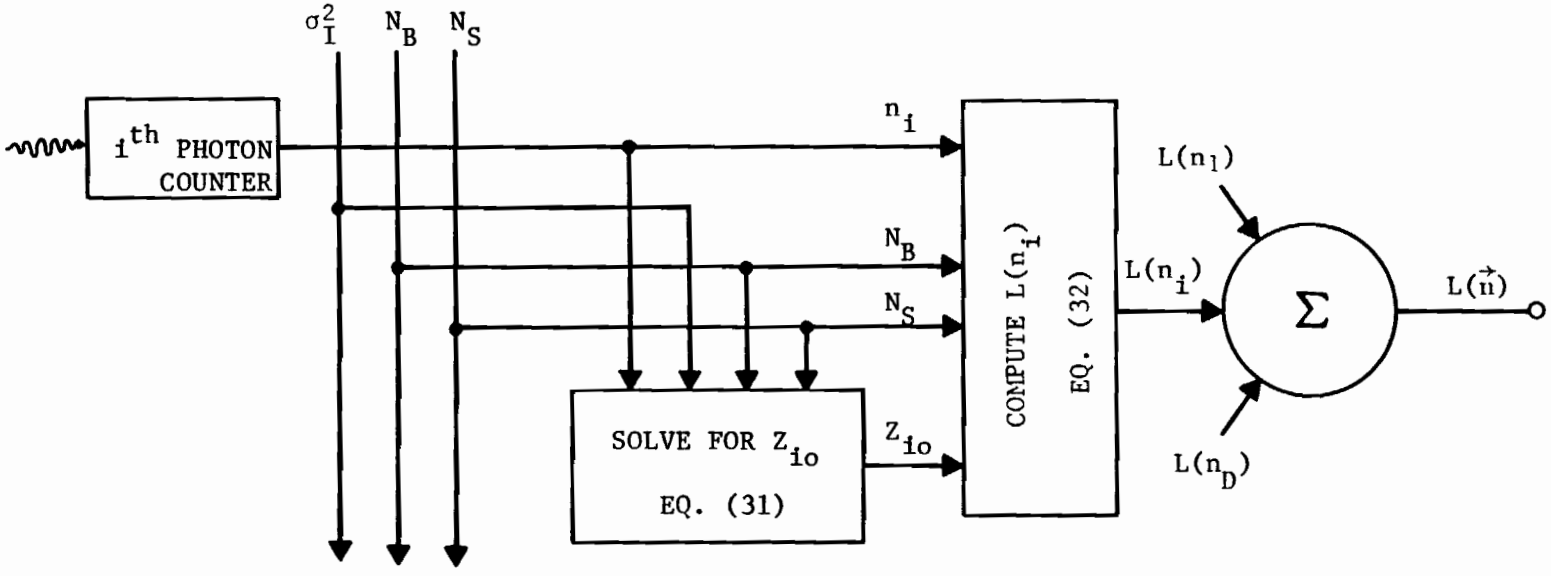

$$L(n) = \sum_{i=1}^{D} \left[N_i \ell n \left(\frac{Z_{io} N_S}{N_B} + 1 \right) - Z_{io} N_S \right] \tag{32}$$

$$\frac{n_i Z_{io} N_S}{Z_{io} N_S + N_B} - Z_{io} N_S - \frac{\ell n Z_{io} + (\sigma_I^2/2)}{\sigma_I^2} = 0, \tag{31}$$

Figure 5. Receiver structure for suboptimum receiver I (SOR I).

only rarely fall outside the range of 0.1 and 10.0. The value of σ_i^2 is never more than about 3.0. Therefore, the third term on the LHS is of the order of unity. For reasonably large values of N_S (and hence n_i) the first two terms on the LHS of the equation will dominate. In such a case, we could drop the third term, approximating the equation for Z_{io} as

$$\frac{n_i Z_{io} N_S}{Z_{io} N_S + N_B} - Z_{io} N_S = 0 \text{ (or) } Z_{io} = \frac{n_i - N_B}{N_S} \quad . \tag{33}$$

We might note that n_i may be less than or equal to N_B, in which case, according to equation (33), Z_{io} can take negative or zero values. This, of course, is not permitted, A more correct way of writing the above equation is

$$Z_{io} = \frac{n_i - N_B}{N_S} \text{ or 0.1, whichever is larger.} \tag{34}$$

The resulting receiver structure is shown in Figure 6.

Adaptive Threshold Receiver (ATR):

The above simplified receiver structures resulting from approximations for the equations for the likelihood function and the stationary value of Z should be expected to perform poorer than the approximate optimum receiver (AOR). An interesting case of a receiver using an averaged threshold has been suggested by McIntyre and Churnside.[29] They point out that if the bit rate is large,

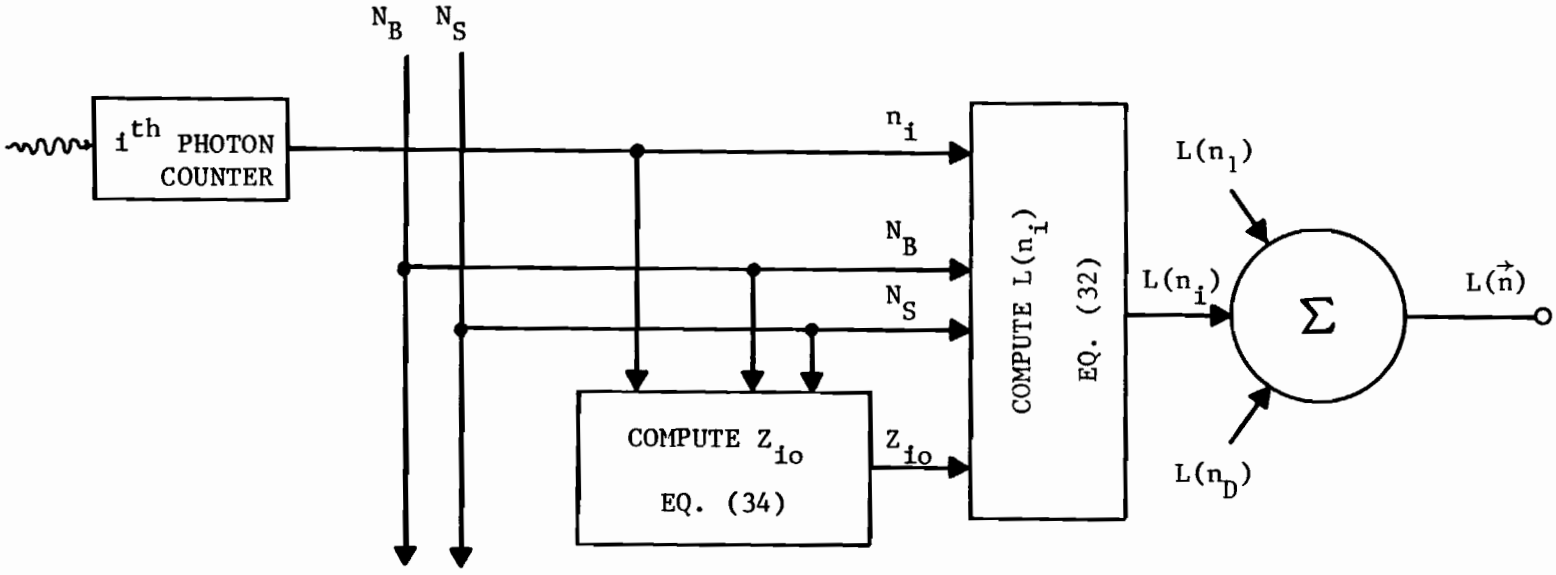

$$L(n) = \sum_{i=1}^{D} \left[N_i \ell n \left(\frac{Z_{io} N_S}{N_B} + 1 \right) - Z_{io} N_S \right] \tag{32}$$

$$Z_{io} = \frac{n_i - N_B}{N_S} \quad \text{or 0.1, whichever is larger.} \tag{34}$$

Figure 6. Receiver structure for suboptimum receiver II (SOR II).

instead of using n_i it is possible to use $\bar{n}_i$, the value for the photoelectron count averaged over a properly chosen number of bits, to calculate Z_{io}. They further show that if the number of bits averaged over can be large enough, a receiver that is both simpler in structure and better in performance can result, especially for high levels of turbulence.

We consider equation (31) again. Modifying this equation to replace n_i with $N\bar{n}_i$, where N is the number of bits averaged over, one gets

$$\frac{N\bar{n}_i Z_{io} N_S}{Z_{io} N_S + 2N_B} - \frac{NZ_{io}N_S}{2} - \frac{\ell n Z_{io} + \sigma_I^2/2}{\sigma_I^2} = 0 \tag{35}$$

As explained earlier, the last term on the LHS is of the order of unity and can be dropped without introducing much error if $N\bar{n}_i$ is large enough. The resulting equation can then be solved for Z_{io}.

$$Z_{io} = \frac{2(\bar{n}_i - N_B)}{N_S} \tag{36}$$

If we treat this value of Z_{io} as the exact value for fading, then we can substitute in equation (32) to get

$$L(\vec{n}) = \sum_{i=1}^{D} \left[n_i \ell n\left(\frac{2\bar{n}_i}{N_B} - 1\right) - 2\bar{n}_i + 2N_B \right] \tag{37}$$

The corresponding receiver structure is shown in Figure 7.

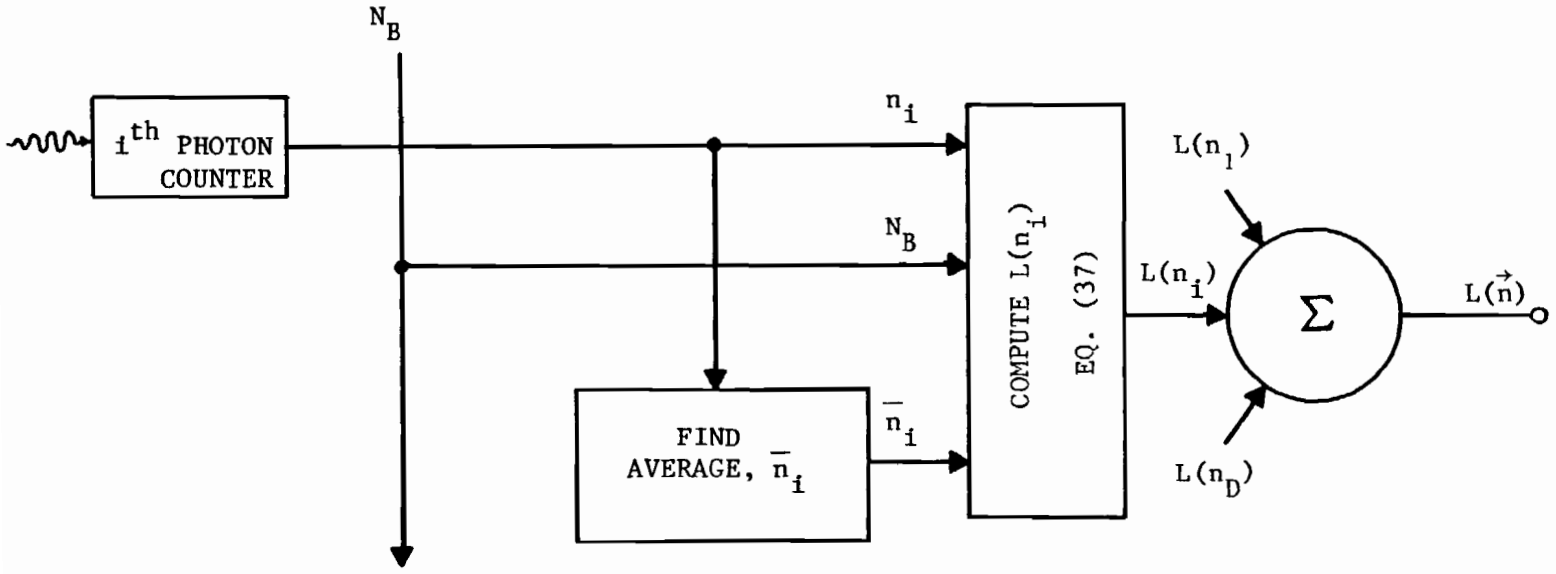

$$L(\vec{n}) = \sum_{i=1}^{D} \left[n_i \ell n\left(\frac{2\bar{n}_i}{N_B} - 1\right) - 2\bar{n}_i + 2N_B \right] \qquad (37)$$

Figure 7. Receiver structure for adaptive threshold receiver (ATR).

Comparing Figure 7 with Figure 4 will show a three-fold simplification. First, the likelihood function is simpler. Second, the solution of an implicit equation for Z_{io} is replaced by a straightforward averaging. Third, the need to feed in the values σ_I^2 and N_S does not exist. The better performance of this receiver over that of the AOR in certain cases (high values for σ_I^2) is a result of the fact that through the averaging process information in more than one bit is used in the decision making.

Receiver With Stored Likelihood Function (RWSLF):

If the laser beam used for communication is strong enough, the light wave received can be considered to be continuous. In such a case, any intrinsic fluctuations in the intensity (apart from the turbulence fluctuations) would be Gaussian in nature. On the other hand, at low intensities the light received would be discontinuous due to the quantum nature of light. The intrinsic fluctuations would then be Poisson. The boundary between the two regimes is not a sharp one. However, when N_S, $N_B \lesssim 40$ which is the regime we are concerned with in this work, the fluctuations are Poisson.

When N_S, $N_B \lesssim 40$ the photoelectron count during any bit interval is likely to exceed 100 only rarely. Even if more than 100 photoelectrons were counted during any bit interval, one could treat it as if no more than 100 photo-electrons were counted without increasing the overall error probability more than 10^{-10}, which is negligible.

Consequently, in the case of a photon counting receiver, one may never have to count more than about 100 photoelectrons.

The likelihood functions in equations (30) and (32) are functions σ_I^2, N_S, N_B and n_i. By the assumptions listed earlier σ_I^2, N_S and N_B are the same for all detectors in the receiver array. Also it is reasonable to assume that σ_I^2, N_S and N_B do not change significantly over a period of about a minute. For such brief periods, $L(\sigma_I^2, N_S, N_B, n_i) \rightarrow L(n_i)$ is a function of only n_i. Since n_i takes values only from 0 to about 100, L(n) needs to take only about 101 different values. Therefore, instead of calculating L(n) for each detector for each bit (as the receiver structures in Figures 4-6 indicate), one could calculate the 101 values of L(n), store them in a memory, and use them over again. Since σ_I^2, N_S and N_B change only very slowly, the values of L(n) need to be calculated afresh only every minute or so. This would result in a considerable saving in computing power. For example, a receiver operating at 10^5 bits/sec, and using an array of four detectors, will need 4×10^5 calculations per second. By the above method, an RWSLF would need only about 101 calculations per minute. The receiver structure for RWSLF is shown in Figure 8. As can be seen, either AOR or SOR I or SOR II can be brought into an RWSLF configuration. This is not possible with ATR, since here the likelihood function is a function of $\bar{n}_i$, whose values are continuous.

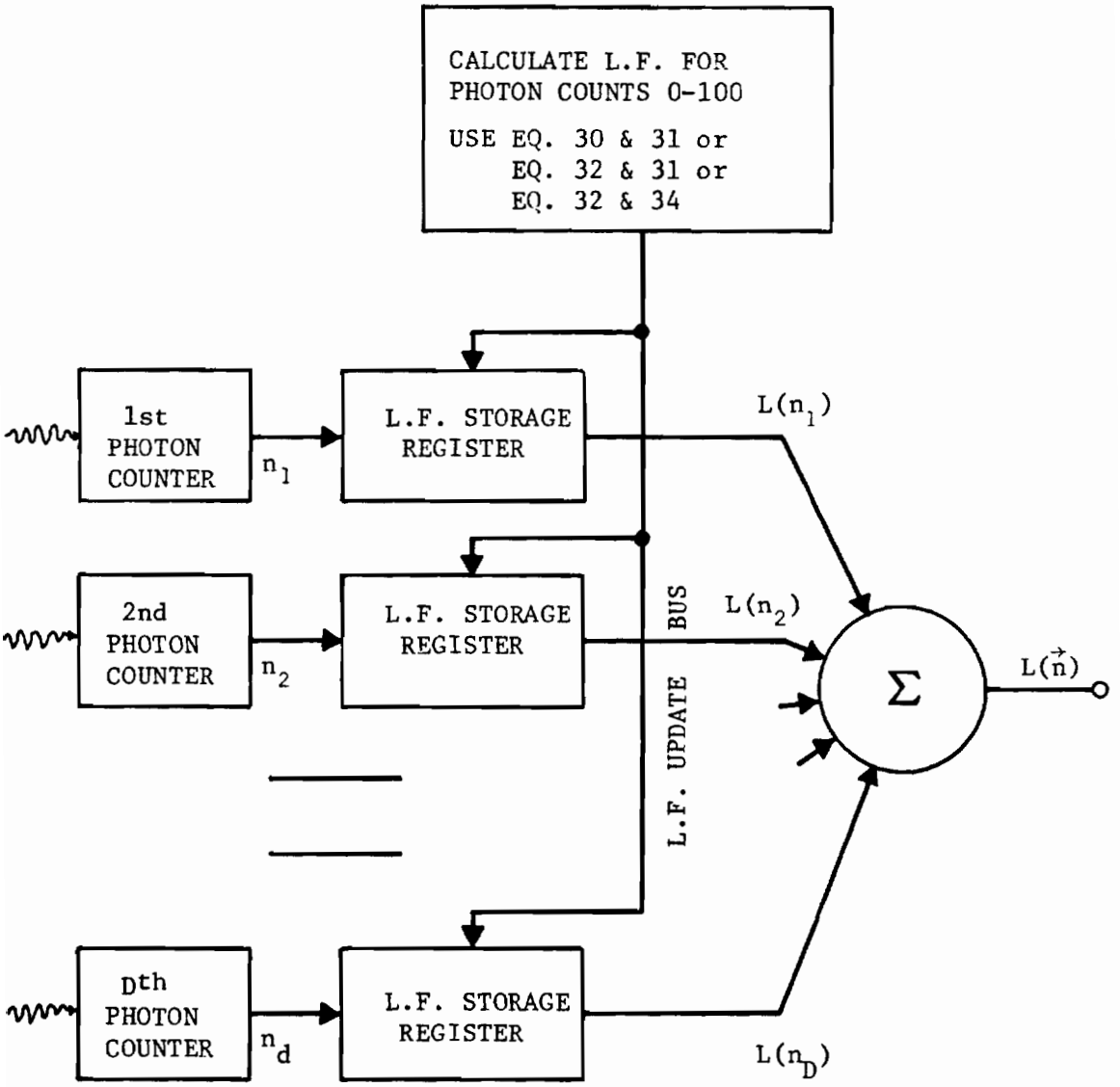

Figure 8. Receiver structure with stored likelihood function.

Estimation of Relative Complexity in Terms of Necessary Computing Power

The complexity of the receiver structures considered in the preceding sections of this chapter depend on the complexity of the functions to be computed and the equations to be solved. The computation and solving operations can be performed either by analog or digital methods. Analog methods are usually much faster and may be needed if the bit rate is very large. However, analog computing and equation solving devices are difficult to build and are less accurate than their digital counterparts. If the bit rate is not much greater than about 10^5/sec, real time digital processing is possible using modern microprocessors, and may be the most appropriate to use in the above-mentioned receivers. In such a case, it is possible to get an estimate of the relative complexity and cost by performing the relevant operations in a digital computer, and noting the processing time as a measure of the computing power needed. This was done using specially written algorithms, and the results are shown in Table II.

While the figures in Table II indicate the relative complexity of the indicated operations, it must be remembered that the actual computing power necessary depends very much on the rate at which these operations need to be performed. Consider, for example, a communication system with a bit rate of 10^5/sec and using an array

TABLE II

COMPLEXITY OF RECEIVER OPERATIONS IN TERMS OF DIGITAL COMPUTATION TIME

Receiver	Operation	Time
AOR SOR I	Solve for Z_{io} (0.1% or less error) $\frac{n_i Z_{io} N_S}{Z_{io} N_S + N_B} - Z_{io} N_S - \frac{\ell n Z_{io} + \sigma_I^2}{\sigma_I^2} = 0$	100 Units
SOR II	Compute Z_{io} $Z_{io} = \frac{n_i - N_B}{N_S}$	0.5 Units
AOR	Compute Expression $\left[n_i \ell n \left(\frac{Z_{io} N_S}{N_B} + 1 \right) - Z_{io} N_S - \frac{(\ell n Z_{io} + \sigma_I^2/2)^2}{2\sigma_I^2} \right.$ $\left. - 1/2 \ \ell n \left\{ \sigma_I^2 \left(\frac{-n_i Z_{io} N_S N_B}{(Z_{io} N_S + N_B)^2} + Z_{io} N_S \right) + 1 \right\} \right]$	19 Units
SOR I SOR II	Compute Expression $\left[n_i \ell n \left(\frac{Z_{io} N_S}{N_B} + 1 \right) - Z_{io} N_S \right]$	5.0 Units
ATR	Compute Expression $\left[n_i \ell n \left(\frac{2\bar{n}_i}{N_B} - 1 \right) - 2\bar{n}_i + 2N_B \right]$	5.0 Units
RWSLF	Locate one value of likelihood function in an array of 100 numbers.	0.15 Units

of four detectors. Taking the case of AOR as in Figure 4, solving equation (31) for Z_{io} and calculating one likelihood function in equation (30) have to be performed (6×10^6) times per minute. For four detectors, therefore, the computing power needed is $4(6 \times 10^6) \times (100 + 19)$ (see Table II) or about 2.86×10^9. For the purpose of comparison, similar calculations can be done for the ohter receivers and after rescaling 2.86×10^9 as 100 units, the relevant values are given in Table III.

From Table III, the following conclusions can be drawn. AOR requires the maximum computing power and hence is the costliest to build. This is followed by SOR I, SOR II and ATR in order. However, the least computing power is needed when AOR, SOR I or SOR II are built under RWSLF configuration. In the latter case, the computing power needed is almost the same whether the receiver is AOR, SOR I or SOR II.

Measurement of the Parameters (σ_I^2, N_S, N_B)

All the receiver structures mentioned above, with the exception of ATR, need external measurement of the parameters σ_I^2, N_S and N_B. The ATR needs only N_B. This is a major advantage of ATR over the rest of the receivers.

The parameter N_B can be measured in the receiver itself, without the need for a separate device. For example, if N_B is independent of time, N_B can be measured by the receiver at the beginning, with the

TABLE III

RELATIVE COMPLEXITY OF RECEIVER STRUCTURES IN TERMS OF NECESSARY COMPUTING POWER FOR A COMMUNICATION SYSTEM USING FOUR DETECTORS AND 6×10^6/MIN. BIT RATE

Receiver	Necessary Computing Power			
	No Storing of L.F.		L.F. Stored	
AOR	(Fig. 4)	100 Units	(Fig. 8)	0.13 Units
SOR I	(Fig. 5)	88 Units	(Fig. 8)	0.13 Units
SOR II	(Fig. 6)	4.6 Units	(Fig. 8)	0.13 Units
ATR	(Fig. 7)	4.2 Units	---	

laser off, and used throughout the operation. Alternatively, the laser, and hence the reception, may be shut off and new values of N_B measured periodically as necessary. If intermittent operation of the receiver is not permissible, N_B may be measured by a separate detector with a telescope focused to a point close to, but not including the laser at the transmitter. With N_B known, N_S can be calculated from the relationship

$$N_S = 2(\bar{n}_i - N_B) \tag{38}$$

where $\bar{n}_i$ is the average photoelectron count per bit.

The value of σ_I^2 can be assumed to be the saturation value (≈ 2.8) if the path length is long enough to ensure saturation. Otherwise σ_I^2 can be calculated from the measurement of C_n^2. These methods can be unsatisfactory for one or more of the following reasons:

1) The theoretical equation (6b) used for calculating σ_I^2 from C_n^2 is good only for small values of σ_I^2 ($\lesssim 1$).

2) C_n^2 can in most cases be measured only at a few points (usually only one) along the path of the beam. It would be reasonable to expect that the path of the beam will not be homogeneous in general, especially due to variations in the terrain and the height of the beam from the ground.

3) Very often a large mirror or lens may be used to collect enough energy of the laser beam. This will inevitably result in some

aperture averaging of irradiance which in turn will result in a lower effective value for σ_I^2 which will be different from the calculated or saturation value for σ_I^2 .

All this would suggest a need for calculating σ_I^2 directly from the photon counting done by the receiver. Below we show that such a calculation is indeed possible.

Let I be the irradiance at a detector, which may be the focal point of a large mirror or lens, where I would still obey a lognormal distribution.[27] If n is the number of photons counted during any bit interval, it can be shown that[30]

$$\frac{\langle I^m \rangle}{\langle I \rangle^m} = \frac{\langle n(n-1) \cdots (n-m+1) \rangle}{\langle n \rangle^m} \tag{39}$$

Considering only the receiver defined on page 13, we have

$$n = \begin{cases} n_S + n_B & \text{for } H_1 \\ n_B & \text{for } H_0 \end{cases}$$

where n_S is the number of photoelectrons due to laser radiation and n_B that due to background light, where $\langle n_S \rangle = N_S$ and $\langle n_B \rangle = N_B$. The irradiance at the detector due to the laser alone and σ_I^2, the variance of log-intensity, are related by the equation

$$\exp(\sigma_I^2) = \frac{\langle I_S^2 \rangle}{\langle I_S \rangle^2}$$

$$= \frac{\langle n_S (n_S - 1) \rangle}{\langle n_S \rangle^2}$$

$$= \frac{\langle n_S (n_S - 1) \rangle}{N_S^2} \tag{41}$$

By equation (40)

$$\frac{\langle n(n-1) \rangle}{N_S^2} = \frac{\frac{1}{2}[\langle (n_S + n_B)(n_S + n_B - 1) + n_B(n_B - 1) \rangle]}{N_S^2} \tag{42}$$

Noting that $\langle n_S n_B \rangle = N_S N_B$ and that $\langle n_B^2 \rangle = N_B^2 + N_B$, since n obeys a Poisson distribution, solving equation (42) for $\frac{\langle n_S (n_S - 1) \rangle}{N_S^2}$ and substituting in equation (41) gives

$$\exp(\sigma_I^2) = \frac{\langle n_S (n_S - 1) \rangle}{N_S^2}$$

$$= \frac{2\langle n(n - 1) \rangle}{N_S^2} - \frac{2N_B(N_S + N_B)}{N_S^2} \tag{43}$$

or,
$$(\sigma_I^2) = \ell n \, 2\left[\frac{\langle n(n - 1) \rangle - N_B(N_S + N_B)}{N_S^2}\right] \tag{44}$$

Since $\langle n(n-1)\rangle$ can be calculated from the photon counting readings, σ_I^2 can be calculated within the receiver. Hence the structure of RWSLF can be modified and made complete as shown in Figure 9. Other receivers (Figures 4-6) can be modified in the same way. The above equation holds for the case when the received intensity is low enough to be counting photons. If, however, the intensity at the receiver plane is strong enough to be in the Gaussian regime (superposed with log-normal turbulence), then it is not difficult to show that

$$\sigma_I^2 = \ln 2\left[\frac{\langle I^2\rangle - I_B^2 - I_B I - I_B}{I_S^2}\right] \tag{45}$$

where I is the detected signal for any bit, I_S is the average current due to the laser light alone and I_B is the average current due to background light alone.

Effect of Approximating the Likelihood Function on the Performance of Multi-Detector Receivers

In the last few sections we have been considering some approximations in the likelihood function. This was done because the complexity of the likelihood function is directly related to the complexity of the receiver structures. Any approximation leading to a simpler likelihood function can also lead to simpler receiver structures. These approximations also affect the performance of multi-detector receivers.

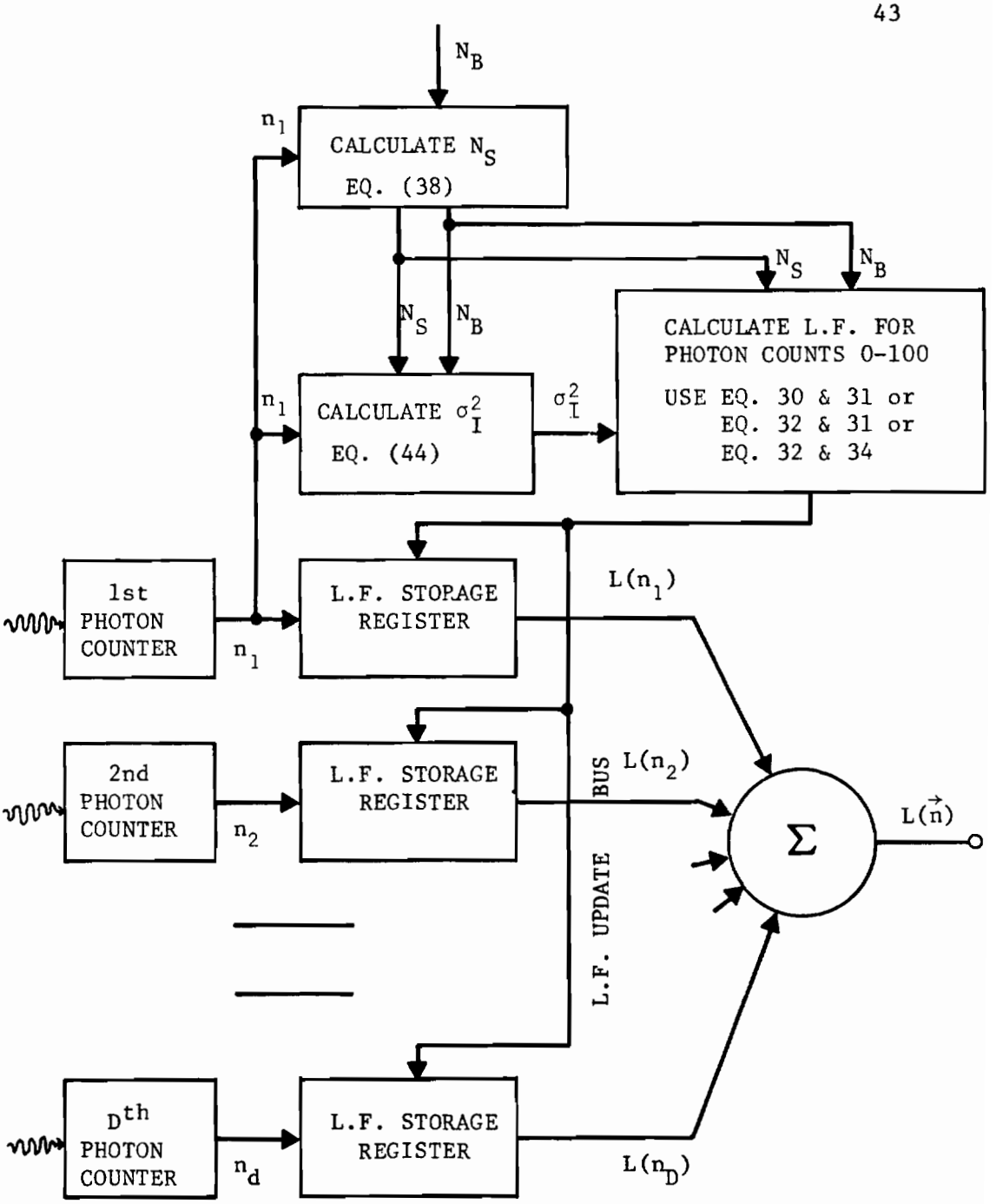

Figure 9. Receiver structure with stored likelihood function and calculation of N_S and σ_I^2.

Consider the communication system defined on page 13. When hypothesis H_1 is sent, the probability that a detector in the receiver array detects n photoelectron counts is given by the probability density function $p_1(a, b, c, d, n)$ where a, b, c and d are the parameters characterizing the channel and the signal strength. The corresponding density function for the hypothesis H_0 is $p_0(a, b, c, d, n)$. If the system uses an array of D independent detectors, the probability that the array detects $\vec{n}$ is

$$P_1(\vec{n}|H_1) = \prod_{i=1}^{D} p_1(a, b, c, d, n_i) \tag{46}$$

and

$$P_0(\vec{n}|H_0) = \prod_{i=1}^{D} p_0(a, b, c, d, n_i) \tag{47}$$

The likelihood ratio is

$$\underline{\Lambda}(\vec{n}) = \frac{\prod_{i=1}^{D} p_1(a, b, c, d, n_i)}{\prod_{i=1}^{D} p_0(a, b, c, d, n_i)} = \frac{\prod_{i=1}^{D} p_1(n_i)}{\prod_{i=1}^{D} p_0(n_i)} \quad \text{suppressing the dependence on a, b, c, d.} \tag{48}$$

Let $U(\underline{\Lambda})$ be a unit step function defined as

$$U(\underline{\Lambda}) = \begin{cases} 1 \text{ if } \underline{\Lambda} > 1 \\ 0.5 \text{ if } \underline{\Lambda} = 1 \\ 0 \text{ if } \underline{\Lambda} < 1 \end{cases} \tag{48a}$$

Therefore for a given bit with detection of $\vec{n}$, the probability of false alarm is

$$P_F(\vec{n}) = \tfrac{1}{2} \left[\prod_{i=1}^{D} p_0(n_i) \right] U(\underline{\Lambda}) \tag{49}$$

The probability of false alarm for the system will then be

$$P_F = \sum_{\vec{n}} P_F(\vec{n}) = \tfrac{1}{2} \sum_{\vec{n}} \left\{ \left[\prod_{i=1}^{D} p_0(\vec{n}) \right] U(\underline{\Lambda}) \right\} \tag{50}$$

where the summation is done over all the possible values for $\vec{n}$. In a similar way the probabilities for a miss are given by

$$P_M(\vec{n}) = \tfrac{1}{2} \left[\prod_{i=1}^{D} p_1(n_i) \right] \left[1 - U(\underline{\Lambda}) \right] \tag{51}$$

$$P_M = \tfrac{1}{2} \sum_{\vec{n}} \left\{ \left[\prod_{i=1}^{D} p_1(n_i) \right] \left[1 - U(\underline{\Lambda}) \right] \right\} \tag{52}$$

This leads to a total probability of error for the system

$$P_E = P_F + P_M$$

$$= \tfrac{1}{2} \sum_{\vec{n}} \left\{ \prod_{i=1}^{D} p_0(n_i)\, U(\underline{\Lambda}) + \prod_{i=1}^{D} p_1(n_i) \left[1 - U(\underline{\Lambda}) \right] \right\} \tag{53}$$

In writing the above equation for the error probability of the system, we have assumed an exact knowledge of the forms of the

functions $p_1(n_i)$ and $p_0(n_i)$ to determine the likelihood ration as given in equation (27). This is obviously the ideal case and the receiver using this likelihood function gives the least error probability possible for the given channel and signal parameters. This receiver may therefore be called the "Exact Receiver." In a real case the exact forms or values of $p_1(n_i)$ and $p_0(n_i)$ are not available and are usually substituted by the approximate forms or values $p_1'(n_i)$ and $p'(n_i)$. This may be due to various causes such as imperfect modeling of the channel, errors in the estimation of the relevant parameters and deliberate approximations as in section III of this chapter.

Using $p_0'(n_i)$ and $p_1'(n_i)$ we write the counterpart of equations (48) - (53).

$$\underline{\Lambda}'(\vec{n}) = \frac{\prod_{i=1}^{D} p_1'(n_i)}{\prod_{i=1}^{D} p_0'(n_i)} \tag{54}$$

$$P_F'(\vec{n}) = \tfrac{1}{2}\left[\prod_{i=1}^{D} p_0(n_i)\right] U(\underline{\Lambda}') \tag{55}$$

$$P_F' = \tfrac{1}{2} \sum_{\vec{n}} \left\{ \left[\prod_{i=1}^{D} p_0(n_i)\right] U(\underline{\Lambda}') \right\} \tag{56}$$

$$P_M'(\vec{n}) = \tfrac{1}{2}\left[\prod_{i=1}^{D} p_1(n_i)\right] \left[1 - U(\underline{\Lambda}')\right] \tag{57}$$

$$P_M' = \tfrac{1}{2} \sum_{\vec{n}} \left\{ \left[\prod_{i=1}^{D} p_1(n_i)\right] \left[1 - U(\underline{\Lambda}')\right] \right\} \tag{58}$$

$$P'_E = \tfrac{1}{2} \sum_{\vec{n}} \left\{ \prod_{i=1}^{D} p_0(n_i)\, U(\underline{\Lambda}') + \prod_{i=1}^{D} p_1(n_i) \left[1 - U(\underline{\Lambda}') \right] \right\} \qquad (59)$$

Equations (53) and (59) are of primary interest. In Appendix A it is shown that P_E as in equation (53) is a monotonically decreasing function of the number of detectors D. This should not be surprising, since this only means that the performance of the receiver improves with increasing number of detectors. However, the same cannot be said of P'_E as given in equation (59), and P'_E may sometimes increase with increasing D. This is proved below by a counter example. To make the example easier and hand verifiable, only a simplest case is presented.

Consider the receiver system defined on page 13 and using an array of independent detectors where the functions p_0, p_1, p'_0 and p'_1 are defined in Table IV.

Using equations (48), (53), (54) and (59) and Table IV we calculate P_E and P'_E for various values of D. The results are as shown in Table V.

TABLE IV

PROBABILITY DENSITY FUNCTION FOR A SIMPLE CASE OF "EXACT" AND REAL PHOTON COUNTING RECEIVER SYSTEMS

n	$p_o(n)$	$p_1(n)$	$p_o'(n)$	$p_1'(n)$
0	0.30	0.10	0.38	0.17
1	0.70	0.90	0.62	0.83
$\geqslant 2$	0.00	0.00	0.00	0.00

TABLE V

ERROR PROBABILITIES FOR THE "EXACT" AND REAL RECEIVERS OF TABLE IV

D	P_E	P_E'
1	0.399999	0.399999
2	0.339999	0.339999
3	0.306999	0.306999
4	0.291999	0.351999
5	0.288789	0.304839
6	0.267219	0.267219
7	0.239555	0.239555
8	0.221096	0.294931
9	0.210579	0.257900

It is evident that while the performance of an Exact Receiver using multiple detectors should get better with an increase in the number of detectors, that of the Real Receiver can deteriorate sometimes with an increase in the number of detectors. Though here we have considered only quantum signals, the extension to continuous signals should be obvious when letting the number of possible counts tend to ∞. While the result may be surprising, it appears that this reversal of performance is noticeable only in the case of channels with inherently high error rates and when the values of p_0' and p_1' are very poor approximations to p_0 and p_1 respectively.

A second point of interest as seen from Table V is the fact that P_E and P_E' are identical for the first three detectors. This shows that in some cases the performance of a Real System can be indistinguishable from that of an Exact System. This, of course, is a consequence of the quantum nature of the signals. This fact is very easy to see in the case of a single detector receiver. For example, in a certain case, the Exact Receiver may use a threshold count of 3.6 while that of a Real Receiver may be using 3.4. Since there can be no fractional counts, both receivers make identical decisions for H_0 or H_1 for all bits.

Conclusion

In this chapter we first considered the theoretical basis and the assumptions involved in deriving the approximate optimum receiver structure for the photon counting receiver using a laser beam as the carrier, and the atmosphere as the channel. Since these structures are complex, simpler structures were sought in order that a better trade off between complexity and performance might be obtained. This was done by approximating the likelihood functions and the equations for stationary fading, and by using an adpative threshold. The relative complexity of these receivers was estimated in terms of the computing power that each receiver may require during operation, for a communication system operating at 10^5 bits/sec and using an array of four detectors. Since the likelihood functions in a photon counting receiver system have only a finite number (about 100) of values, a receiver structure which could store these values and use them over again may need the least computing power and hence be the least costly. Also, the receiver structures were modified to include the measurement of N_S and σ_I^2 from the photon counting readings. Finally it was pointed out that gross approximations in the likelihood function can sometimes lead to an increased error rate for increased number of detectors.

A final evaluation of these receiver structures leading to definite choices is not possible until the actual performances of

these receivers are also known. An experimental investigation of the error rates for the receiver structures discussed above is the subject for the next chapter.

CHAPTER 4

EXPERIMENTAL INVESTIGATION OF ERROR RATES OF PHOTON COUNTING RECEIVERS

In Chapter 3 we considered the theoretical work of Teich and Rosenberg[3] leading to the optimum receiver structure for the case of a photon counting receiver using a laser beam as the carrier, the clear atmosphere as the channel and an array of detectors at the receiver plane. For the case of partially correlated fading at the detectors the receiver structure was too unwieldy, especially due to the covariance terms. The assumption of independent fading at each detector led to an approximate optimum receiver that was considerably simpler in structure. Additional receiver structures were considered in an attempt to find even simpler structures with a better trade off between complexity and performance. In this chapter we consider the experimentally investigated performances of the receiver structures considered in the earlier chapter. Error rates are experimentally measured for the following receiver structures:

1) AOR - The Approximate Optimum Receiver developed by Teich and Rosenberg for independent fading at each detector. (It is called "approximate" because a lognormal distribution for irradiance is assumed and because its development involved certain approximations involving the evaluation of integrals by the method of steepest descent.)

2) EER - The "Exact" Experimental Receiver is a hypothetical receiver without any of the approximations in AOR. (Because Teich and Rosenberg predict relatively high error probabilities for AOR,[31] part of the aim of the experiment was to find out how much the performance of AOR is affected by the above mentioned approximations.)

3) SOR I, SOR II - Suboptimum Receivers derived directly from AOR. (The simplicity of these receiver structures compared to AOR is very appealing.)

4) ATR - The Adaptive Threshold Receiver. (This receiver as described in the last chapter is both simple and performs better than the AOR.)

Also, probability density functions for the photon counts for log-normally faded irradiance have been reported by Diament, Teich and Rosenberg.[3, 32] In the present effort the probability distribution for the photon counts is determined experimentally and is compared with the theoretically predicted distribution.[3] The experimentally determined distribution functions are then used to calculate the error rate for the EER.

Finally, the error rates of the above receivers as a function of the number of detectors in the array are determined up to four detectors. For the case of the ATR, the error rates are also determined as a function of the averaging for the adaptive threshold.

Experimental Approach

It was judged to be impractical to measure the error rates for all of the different receiver structures (each with 1, 2, 3, and 4 detectors) under identical atmospheric conditions in order to compare their performance. The variability of the weather is one reason. It has been observed by others[27] and also in the preliminary experiments of the present effort that the structure parameter C_n^2 and the variance of log-intensity σ_I^2 can vary considerably in a few tens of minutes. The cost and complexity of the experiment is another reason. Consequently a different approach, as outlined below, was used.

An amplitude modulated photon counting signal was transmitted and received under measured conditions of the atmosphere. For each bit period, a step voltage of height proportional to the number of photoelectrons counted in the bit interval was generated by pulse integration. The resulting wave form, as shown in Figure 10, was recorded in an instrument tape recorder. These voltages, and hence the data regarding the photoelectron counts, for the measured atmospheric conditions could be reproduced any number of times in the laboratory. The reproduced data was given as the input for the processors of the various receivers considered above. Thus the performance of these receivers could be compared under identical atmospheric conditions.

In the last chapter it was explained that digital processing of the data for the purpose of decision making is possible in the case of the photon counting receiver system. For this reason, it was thought to be appropriate to use an existing digital computer for the processing in the present experiment. This way, the costly hardware and labor for circuit-building was exchanged for the relatively easy and more flexible software preparation, without sacrificing the truthfulness and usefulness of the results.

Determination of the error rate for an array of D detectors would need the data for the photoelectron counts from D different detectors distributed spatially. However, in the present effort we are interested only in the case where one can assume independent fading for each detector. This makes it possible to use the data from only one detector exchanging spatial diversity for time diversity. In exchanging spatial diversity for time diversity, we take the data from a single detector and displace it in time by T_1 seconds to obtain a sequence of data for the second detector, displace it by $2T_1$ seconds to obtain the sequence of data for the third detector and so on (see Figure 11) If T_1 is large enough, the statistical independence of any one sequence from all others can be assured. In the experiment, it was found that in all cases, the autocorrelation of the irradiance was zero (within experimental errors) if the temporal displacement was greater than about 50 msec. Three of the

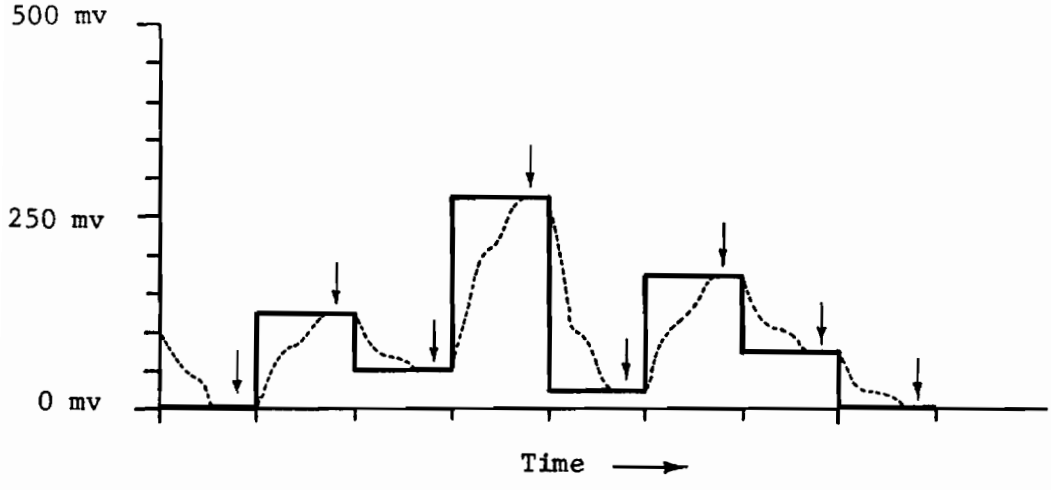

Figure 10. Recorded (solid line) and reproduced (dotted line) voltages during data collection and reproduction, respectively.

Sequence of data from a single detector:

$n_1, n_2, n_3 \cdots n_{2049}, \quad n_{2050} \cdots\cdots n_{4097}, \quad n_{4098} \cdots\cdots n_{6145}, \quad n_{6146} \cdots$

$t_1, t_2, t_3 \cdots (t_1 + T_1), (t_2 + T_1) \cdots (t_1 + 2T_1), (t_2 + 2T_1) \cdots (t_1 + 3T_1), (t_2 + 3T_1) \cdots$

Sequence of data for an array of four detectors using time diversity:

Detector 1 → $n_1, \quad n_2, \quad n_3, \quad n_4 \quad \cdots$

Detector 2 → $n_{2049}, n_{2050}, n_{2051}, n_{2052} \cdots$

Detector 3 → $n_{4097}, n_{4098}, n_{4099}, n_{4100} \cdots$

Detector 4 → $n_{6145}, n_{6146}, n_{6147}, n_{6148} \cdots$

Figure 11. Time diversity.

extreme cases of autocorrelation curves are shown in Figure 12. In the actual experiment a displacement of 222 msec was used to obtain the data for the second detector, a displacement of 444 msec for the third detector, and so on.

The Experiment

The schematic of the transmitter is shown in Figure 13. The transmitter consisted of an argon ion laser with vertical polarization and operated at 0.4880 μm wavelength, with a chopper modulator. The beam was focused to a spot of about 0.02 mm on the wheel. The chopper wheel had 150 rectangular slots (1 mm × 6 mm) with approximately 27 per cent duty cycle and was driven by a synchronous motor.[33, 34] The beam pointing error discussed in reference 33 did not arise in this case because of the focusing of the beam on the wheel. So, 4500 pulses/sec of nearly rectangular shape, 60 μ sec duration and 222 μ sec period were transmitted through the atmosphere. The middle 40 μsec of this 60 μ sec pulse duration was treated as the bit interval corresponding to a hypothesis H_1. Another 40 μ sec interval in between the 60 μ sec pulses was that corresponding to the hypothesis H_0 (see Figure 14). This results in a bit rate of 9 kHz.

The beam travels horizontally at a height of about 2.2 meters above extremely flat farm land. The distance between transmitter and the receiver was about 1.25 kms. The $1/e^2$ intensity of the beam at the receiver plane was adjusted to a diameter of about 3 meters with

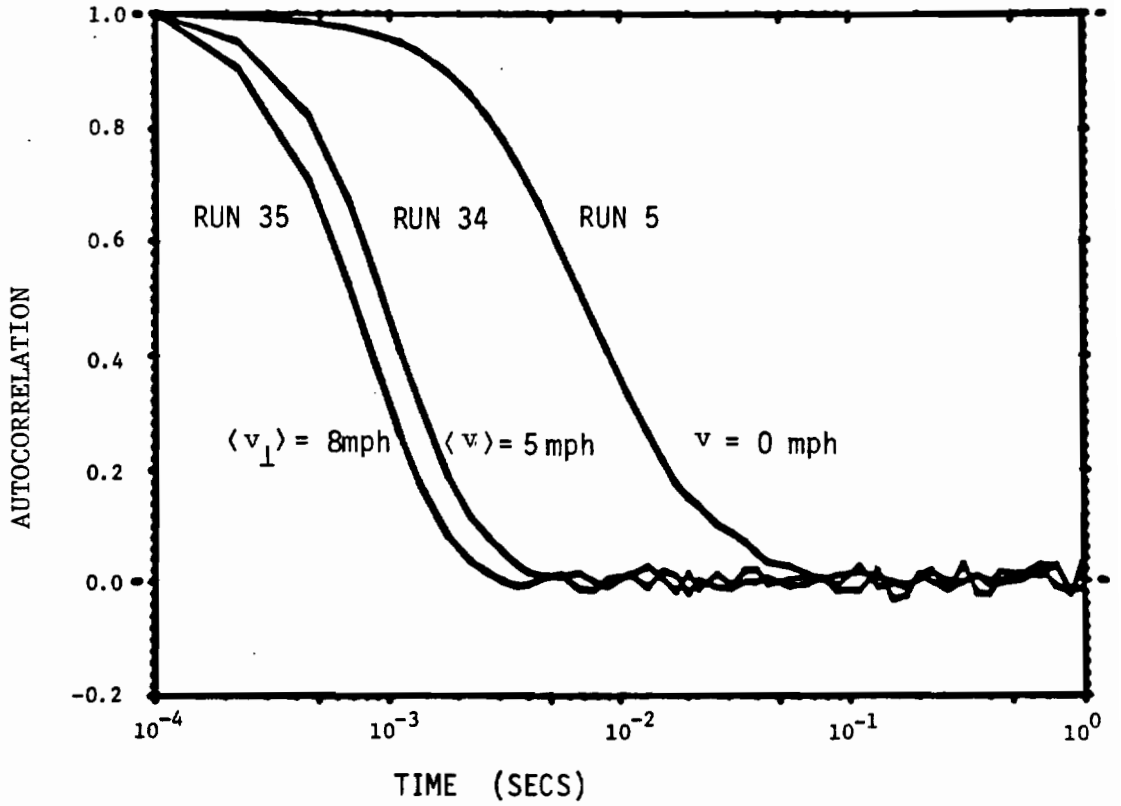

Figure 12. Autocorrelation curves for irradiance

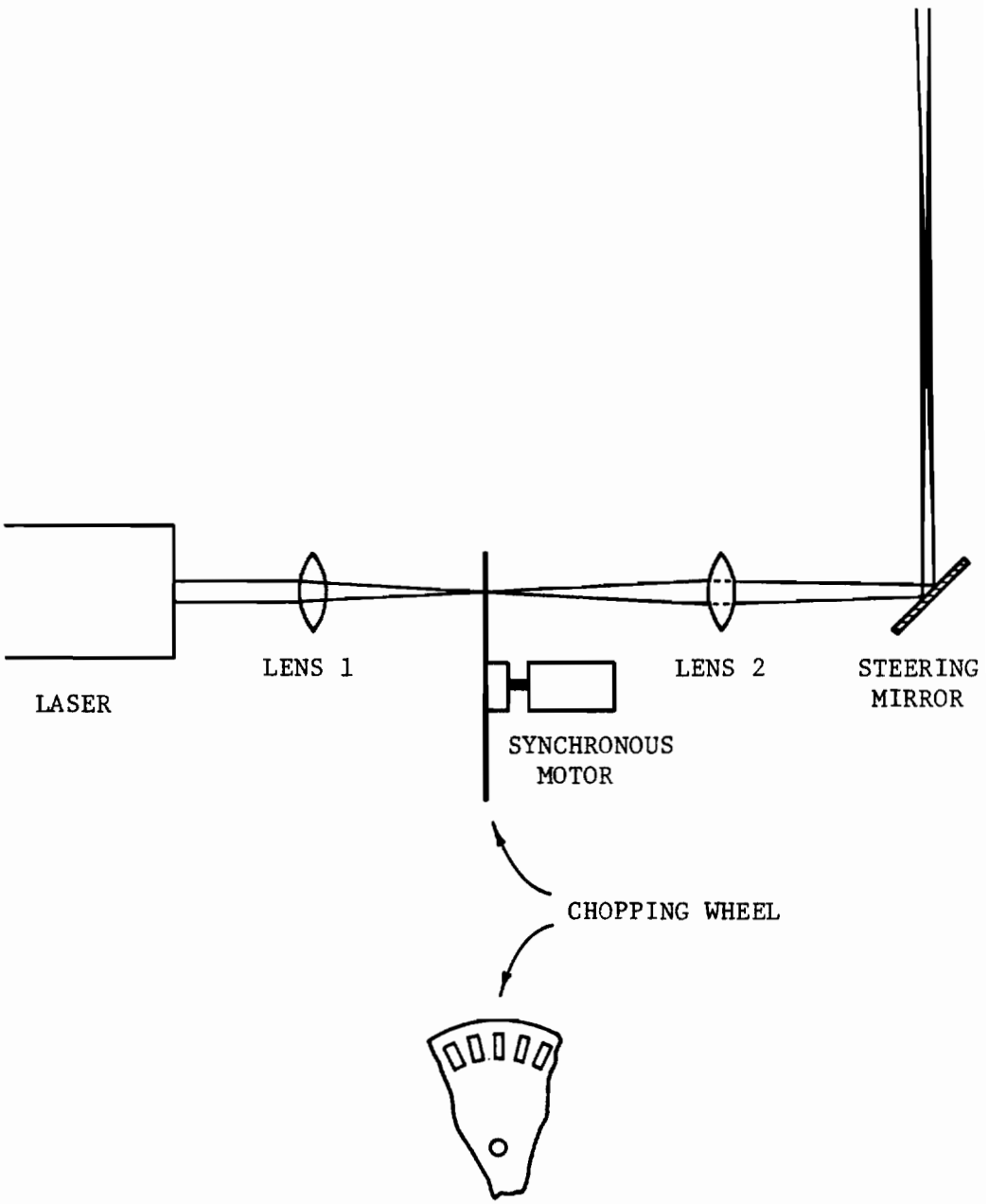

Figure 13. Transmitter using chopper modulation.

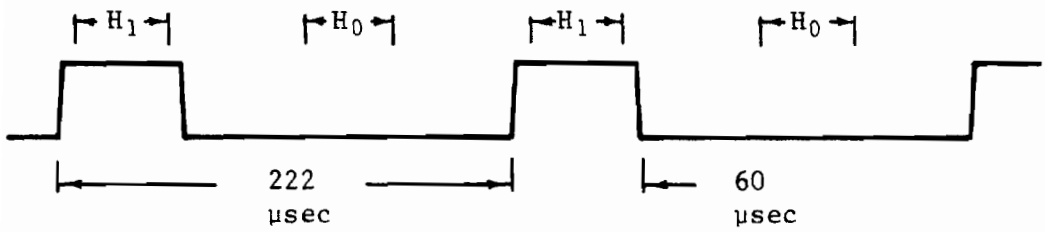

Figure 14. Chopper modulated laser pulses.

detectors being at the center. The laser was operated at a power level of about 200 mW. All experiments were done between 11 a.m. and 3 p.m. The turbulence could be expected to be well developed during this time of the day. In all cases, the strength of scintillations was almost in saturation.[35] As will be seen later, the assumption of lognornal statistics even in saturation gives a good agreement between experimental and theoretical results.

At the receiver end, there were three detectors, each for a specific purpose. The one of primary interest here is the photon counter. This consisted of a photomultiplier tube with a telescope at the front to collect the laser beam. A schematic of the optics making the telescope is shown in Figure 15. The signal to noise ratio was increased by the use of a narrow band filter at the front of telescope. The neutral density filters reduce the intensity of both the laser and the background light. In this way the laser beam intensity was adjusted to a mean photoelectron counting rate on the order of 50/bit interval while the background intensity was reduced to a very insignificant level of less than about 0.2/bit interval. Such a reduction of the actual background intensity was done purposely to help minimize any abrupt and unexpected changes in the background light (due to a passing cloud, for example), thereby rendering the parameters uncontrolled. Our preliminary experiments showed that such abrupt

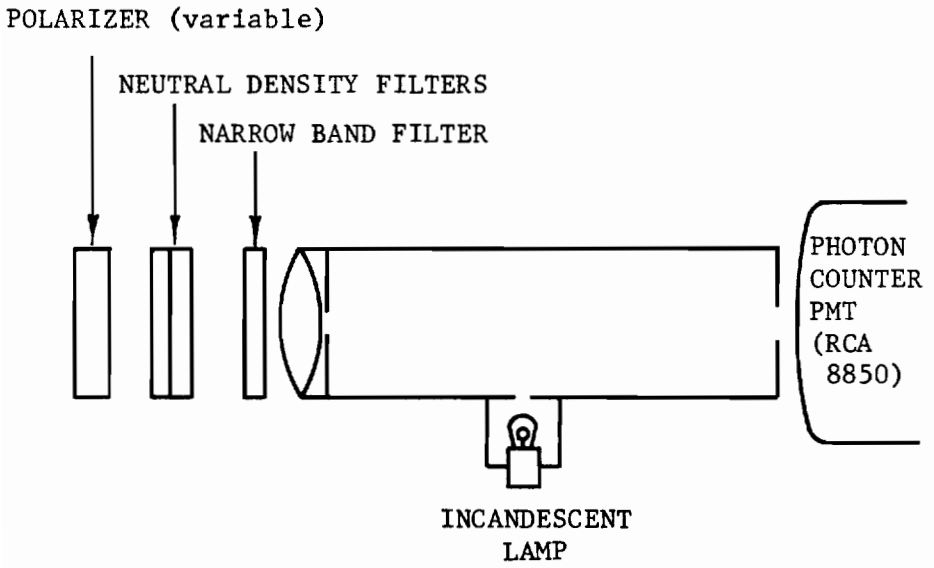

Figure 15. Control optics for photon counter.

variations in the background light can occur. Additional background intensity, when desired for reduced signal to noise ratio, was provided through a translucent window at the side of the telescope. The window was illuminated by a small incandescent lamp whose intensity could be controlled by adjusting the d.c. current for the lamp. This way, any desired value of N_B, the mean background photoelectron count/bit interval could be set. A polarizer at the front of the neutral density filters provides a finer control over the intensity of the laser beam. This provides a control on N_S the mean photoelectron count/bit interval due to laser light.

Careful consideration was given to choosing the field of view for the telescope. Due to turbulence the angle of arrival of the signal wave varies randomly.[36-38] Choosing too small a field of view can therefore result in the loss of the beam sometimes. On the other hand, too large a field of view will unnecessarily increase the background light. It must be expected that the range of variation of the angle of arrival of the wave can be considerably higher for small apertures than for larger ones. This is because, for a small aperture, the angle of arrival can vary not only due to the variation in the general direction of the wave front but also due to the local distortions in the wave front. For a larger aperture, the later tend to average out and hence play a negligible role (Figure 16). In the present case the aperture was chosen to be 2mm

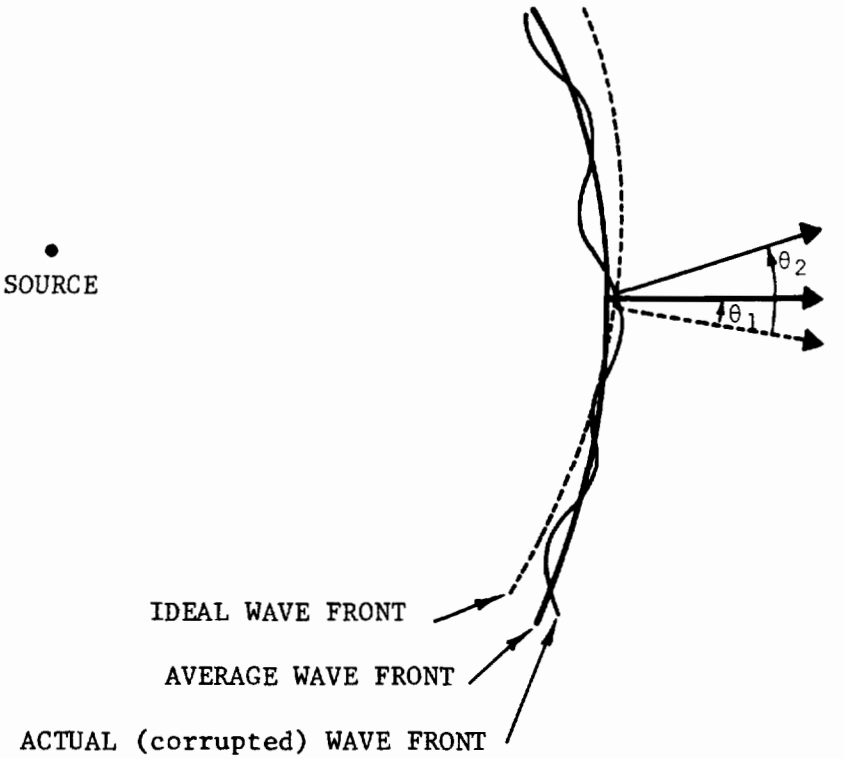

Figure 16. Angles of arrival for a corrupted wave front.

θ_1 - average angle of arrival for large section of wave front.

θ_2 - angle of arrival at a local point.

diameter. Since the Fresnel zone size ($\sqrt{\lambda L}$) is 25 mm, 2 mm is small enough to assume complete first order coherence over the aperture. The probability of the angle of arrival of the signal was experimentally measured by orienting a telescope of 4 mm diameter in different directions with respect to the laser beam, and measuring the photon counting rate. A typical result is shown in Figure 17. The full angle of arrival fluctuation is as high as 10 milliradians, or about one-half degree. The field of view for the receiver telescope was chosen to be about 40 milliradians to allow for a good margin of error in the alignment and drifts later on.

The photon counter used a photo-multiplier tube (RCA 8850) followed by an amplifier and discriminator unit (PAR 1121) which suppresses the noise pulses and generates a standard pulse of a constant height ($\approx$ -1 volt) and width ($\approx$ 15 nsec) for every photo-electron pulse from the PMT. These pulses are then integrated to obtain a voltage proportional to the number of photoelectron counts for each bit interval (Figure 10). These voltages are then recorded on an analog tape using an instrument tape recorder (Ampex 1300).

A second detector, almost identical to the above, except that there were no neutral density filters and that the PMT, RCA 931A (see Figure 18) was used to measure the irradiance (no photon counting). The detected signal was integrated over every bit interval and the

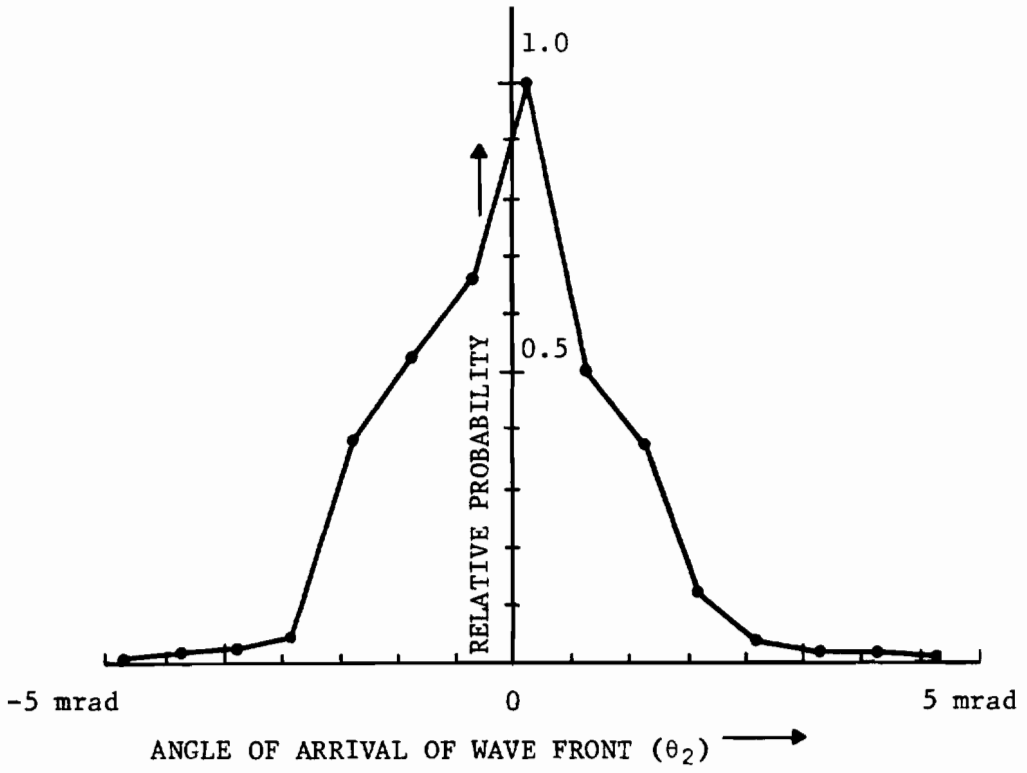

Figure 17. Probability distribution of arrival of wave front in turbulent atmosphere.

The wave front is Gaussian and has a diameter of 2.5 m. The path length is 1.25 km. Aperture diameter is 0.4 cm. $\sigma_I^2 = 1.9$.

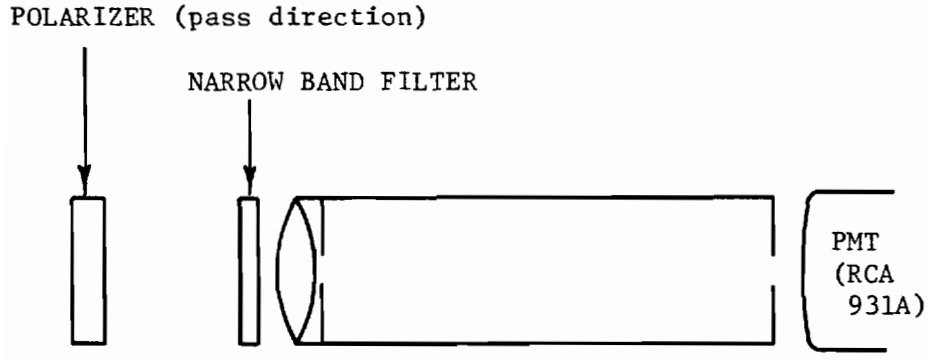

Figure 18. Control optics for PMT.

resulting wave form (similar to that in Figure 10) was simultaneously recorded on the analog tape in another channel.

The reference signal was obtained by using a large Fresnel lens (40 cm × 20 cm) to collect light from the laser beam. The large aperture reduced the turbulence fluctuations considerably. The light was then detected by a semiconductor diode. The resulting voltage signal was then processed to obtain the timing and gating pulses for the integration. The gating pulse was also recorded simultaneously on the analog tape in a third channel to provide the clock pulses for reproduction of the data. The block diagram of the three detectors is shown in Figure 19.

The block diagram for the reproduction of the data is shown in Figure 20. A faithful reproduction of the recorded voltages was achieved in the following way. The reproduced voltage wave form was passed through a carefully designed filter. The voltage levels of the resulting wave form were made to coincide with the voltage levels of the recorded wave over a small portion ($\approx$ 20%) of the period by adjusting the filter components. Voltage readings were taken over these portions of the wave form (see Figure 10). The measured voltages were then written on a digital tape. Recovering the data for photon counts or irradiance from these voltage readings was then straight forward.

Before doing the actual experiment, careful preliminary experiments were done at every stage with the aim of finding and weeding

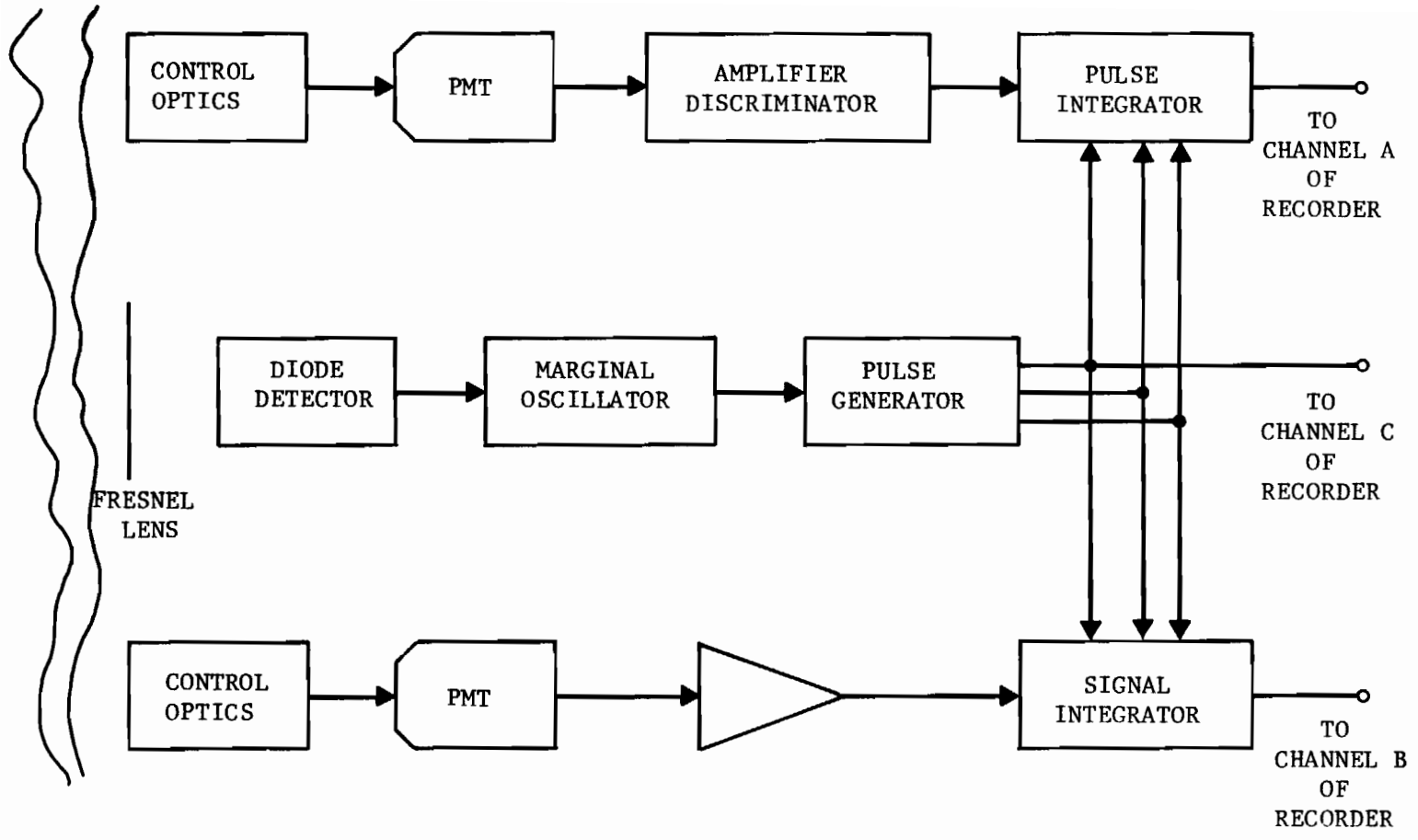

Figure 19. Block diagram of experimental photon counting receiver and data recording.

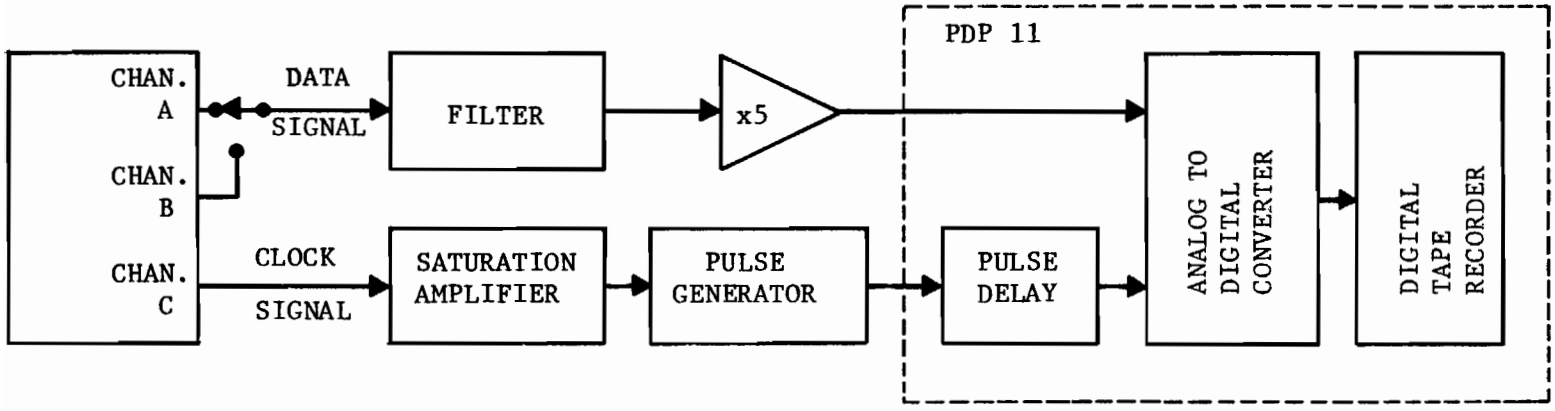

Figure 20. Block diagram for playback and data retrieval.

out any bugs. One such finding was that setting the voltages in the PMT to obtain maximum S/N ratio may not be the optimum thing to do in the case of a photon counting receiver. The reason for this is that in this operation there can be bursts of noise pulses which tend to increase the rate of false alarm of the receiver system. Further, it was found that this problem can be overcome by slightly increasing the "optimum" threshold voltage. Details of this effect are given in Appendix B.

When the experiments were done at the field site the values of N_S and N_B were set approximately to desired values. Observations were made for the wind velocity in the direction perpendicular to the path of the beam. Since the wind velocity was fluctuating only an average and approximate value was recorded. The value of C_n^2 at about the same height as the beam was measured using a Contel MT-2 meter.

Preliminary analyses of the data showed that in order to adequately and smoothly represent the distribution of the temporal fluctuations of irradiance, a minimum of 10 sec length of data would be needed. Therefore in all cases of data processing a minimum data size of 102,400 bits (11.3 secs) was used. A larger data size was used when it was deemed necessary. For each experimental run, the variance of log intensity and the autocorrelation for the temporal fluctuations (Figure 12) were determined from the data for irradiance.

The counterpart of the data from the tape for the photon counting was used to determine the probability distributions for photon counts for hypotheses H_1 as well as H_0. These curves are given in Appendix C. The same set of data for photon counting was then used to determine the probability of error for the EER, AOR, SOR I, SOR II and ATR. These probabilities were also determined as a function of the number of detectors up to four. For the case of the ATR the error probability was also determined as a function of the averaging. These results are listed in Appendix C. However, the relevant data needed for the discussion are presented in the subsequent pages.

Discussion of the Results

An inspection of the probability distribution curves for the photon counts (Figures 21-23) shows that on the whole there is good agreement between the experimentally measured and the theoretically calculated values using equations (30) and (31) in Chapter 3. The agreement is better in the region of low counts, which is the most important region as far as error rates are concerned. Because of the generally good agreement between the measured and calculated values of the probability distribution functions, one might expect the same for the error probabilities. As can be seen from Figures 24-26, this is indeed so. Curiously, in almost all cases experimentally measured values are slightly better.

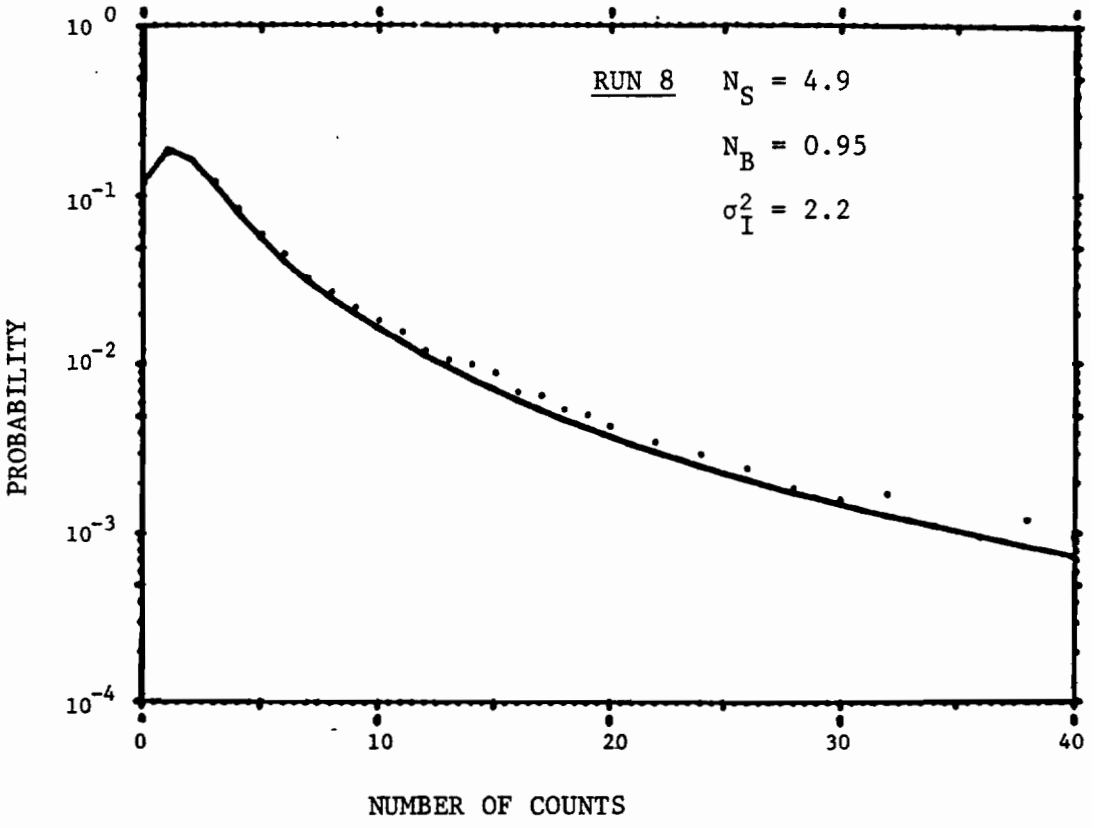

Figure 21. Probability density function for photoelectron counts.

Dots give the experimentally measured values.
Solid line gives the theoretical curve.

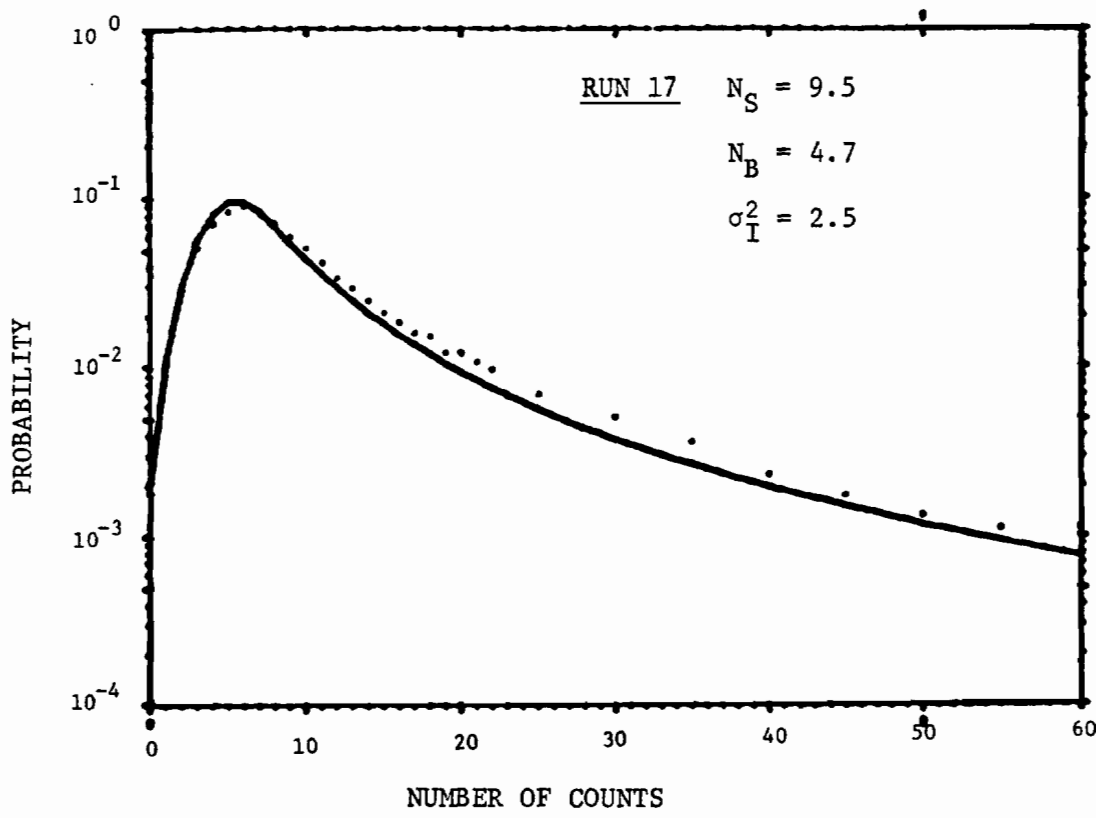

Figure 22. Probability density function for photoelectron counts.

. Dots give the experimentally measured values.
Solid line gives the theoretical curve.

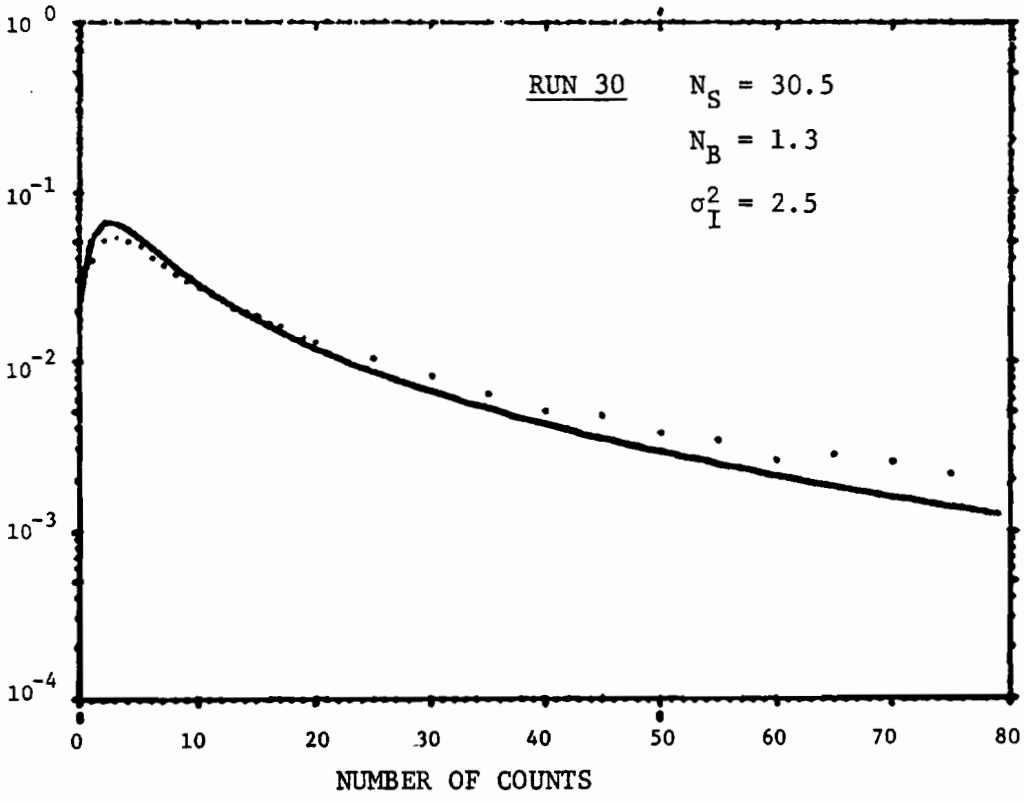

Figure 23. Probability density function for photoelectron counts.

Dots give the experimentally measured values.
Solid line gives the theoretical curve.

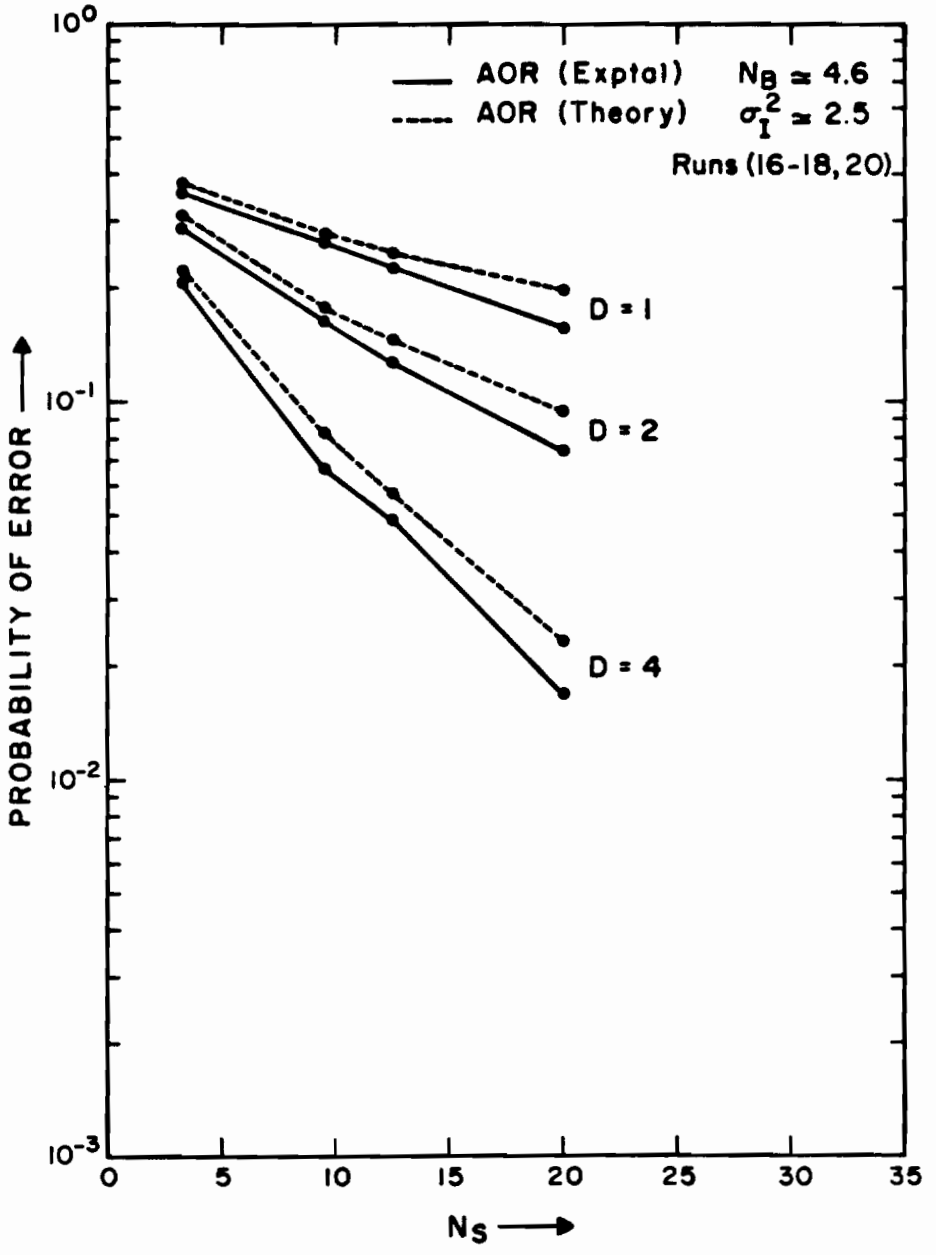

Figure 24. Probability of error as a function of average signal power at the detector.

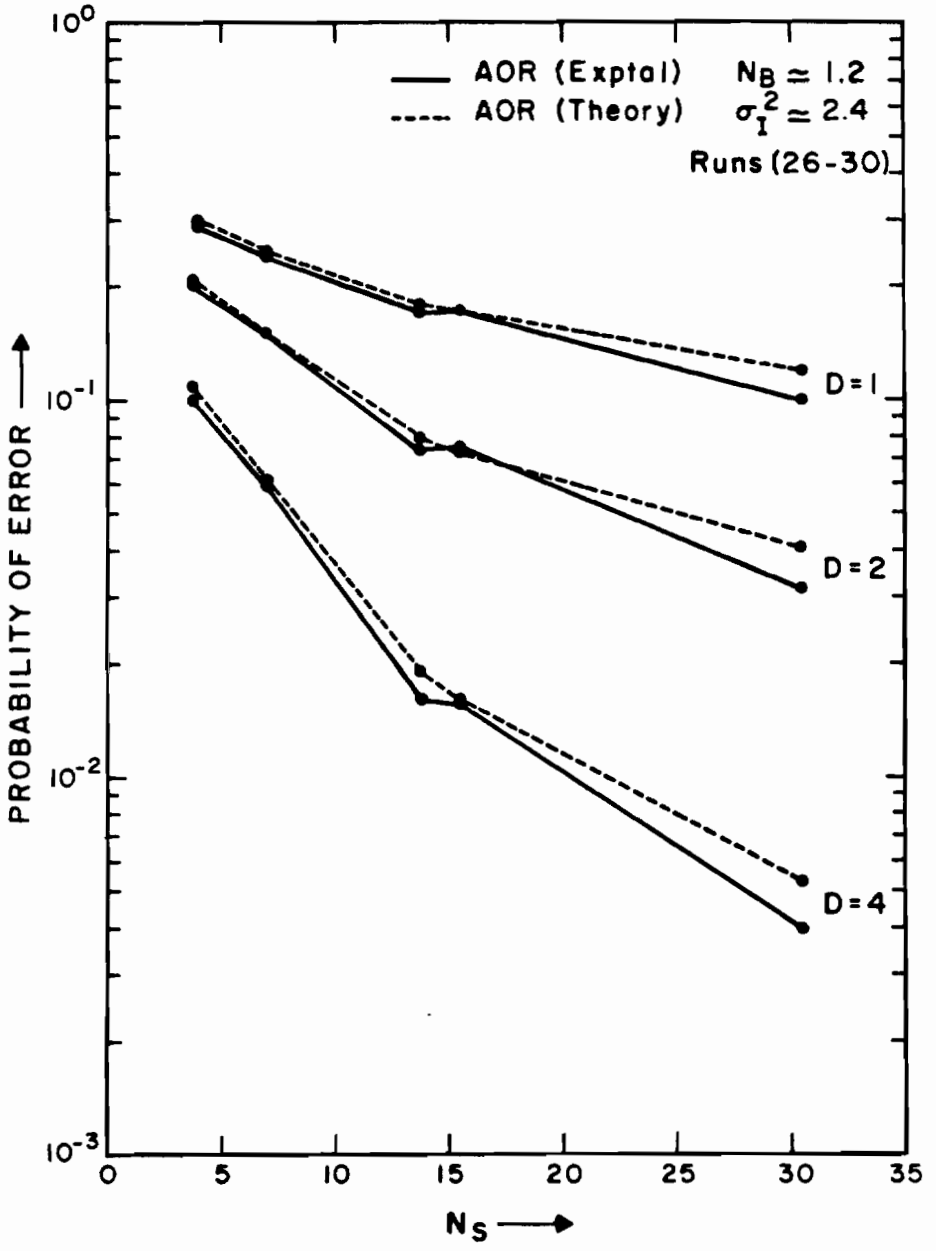

Figure 25. Probability of error as a function of average signal power at the detector.

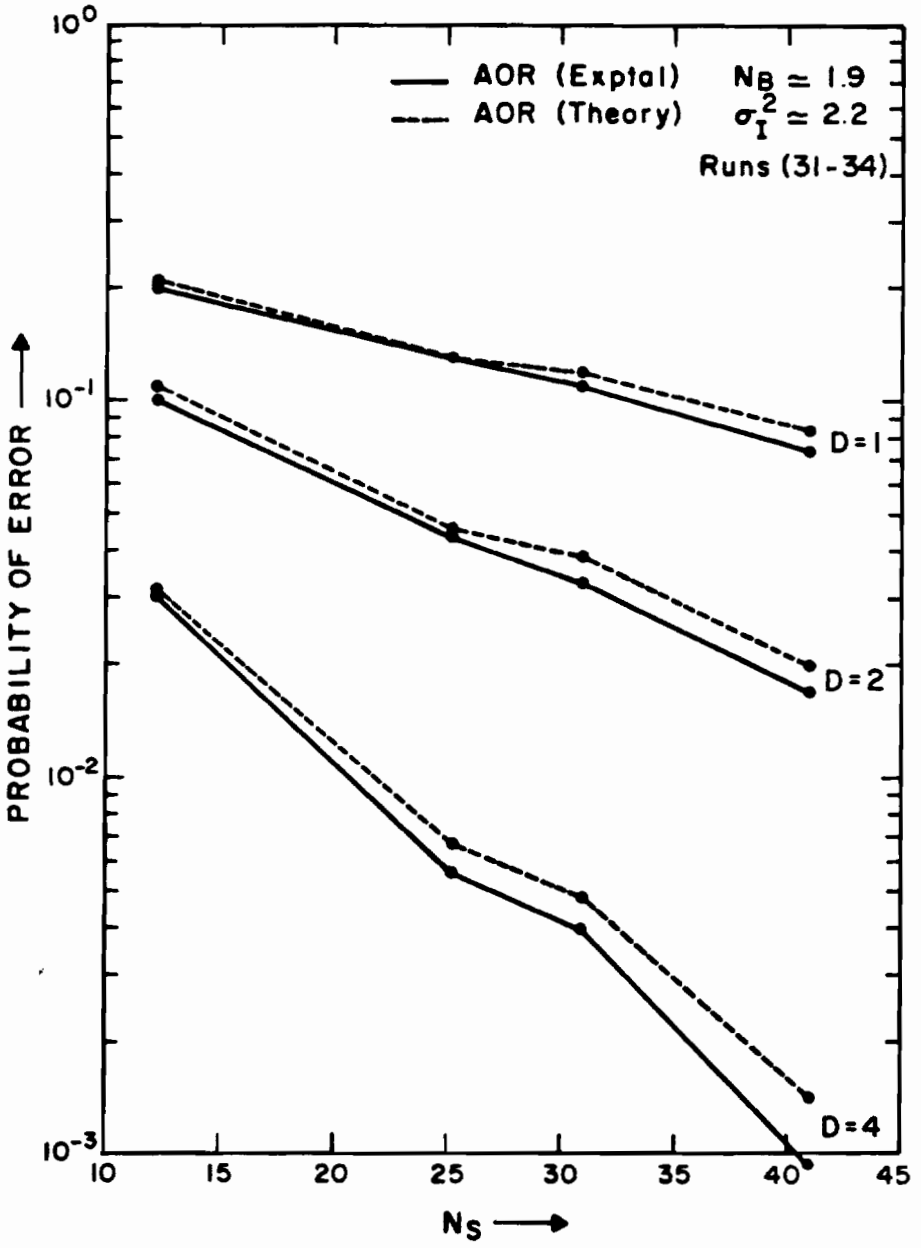

Figure 26. Probability of error as a function of average signal power at the detector.

Figures 27 and 28 illustrate the relative performances of the EER, AOR, SOR I, SOR II and ATR. First, consider the cases of the AOR and EER. In Figure 27 we note that the performances of the AOR and EER are indistinguishable. The reason for this is twofold. First, the approximations made in the development of the AOR are very good approximations and the difference between the AOR and EER is really very small. Secondly, these small differences could not show up in the error rates because of the discrete nature of the likelihood function. This fact was demonstrated in the last chapter, section V. However, when N_S and D are increased, the likelihood function tends to become "less discrete" in nature. In such cases the differences between the AOR and EER can show up. This point is clearly seen in Figure 28. In all, it appears that the thoery of Teich and Rosenberg is a valid theory and so could be used with confidence in designing the AOR system and predicting its performance.

Next let us compare the performance of the AOR and ATR. McIntyre and Churnside[29] predict that the ATR can perform better than the AOR if the bit rate is sifficiently higher than the scintillation frequencies. This, as we saw earlier, is because by averaging over a large number of bits over a period much smaller than the scintillation time, a very precise value of the fading can be obtained, which is better than that estimated from equation (31). Figure 27 shows that in such cases the ATR does perform better than the AOR (and EER, for that matter). This, combined with the fact that the ATR has also the

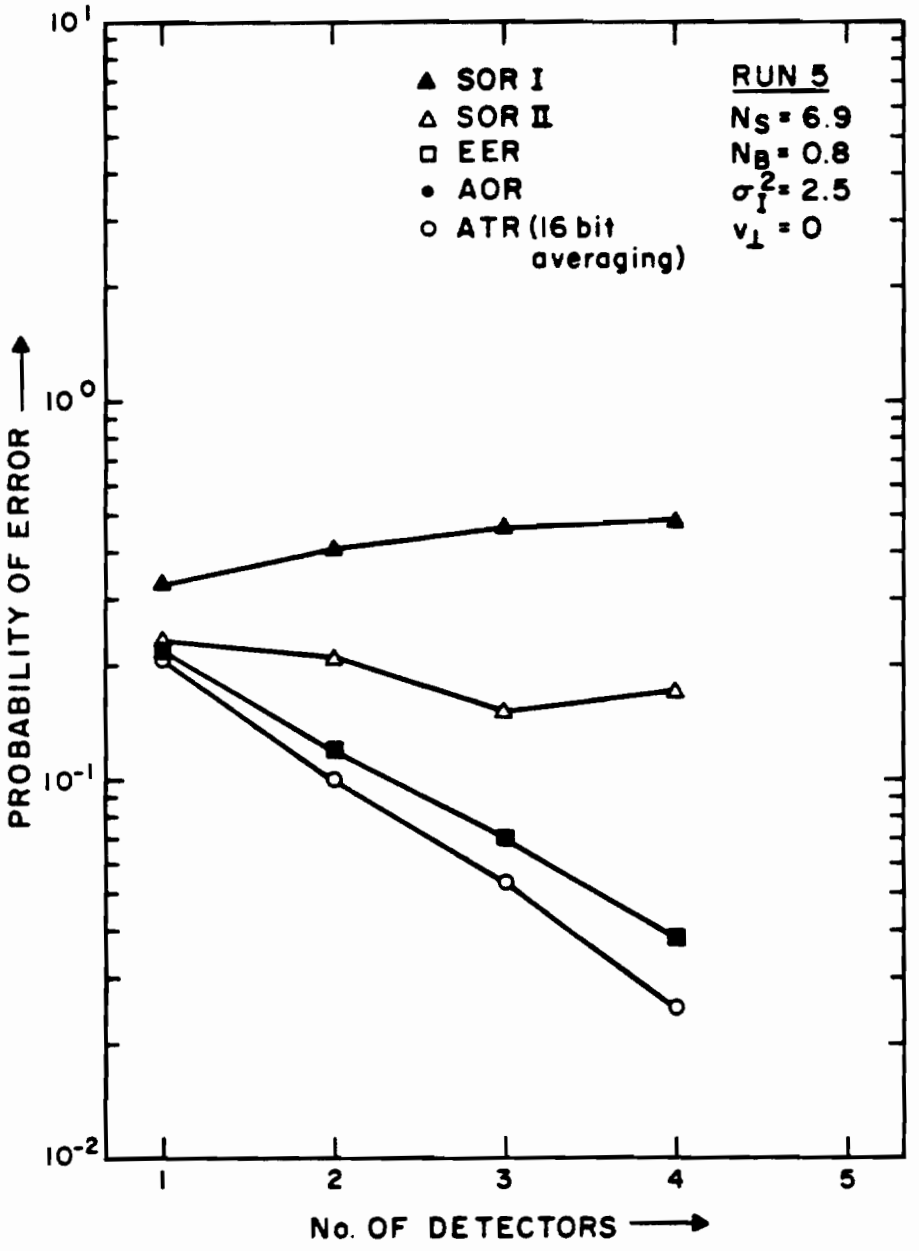

Figure 27. Probability of error vs. number of detectors.

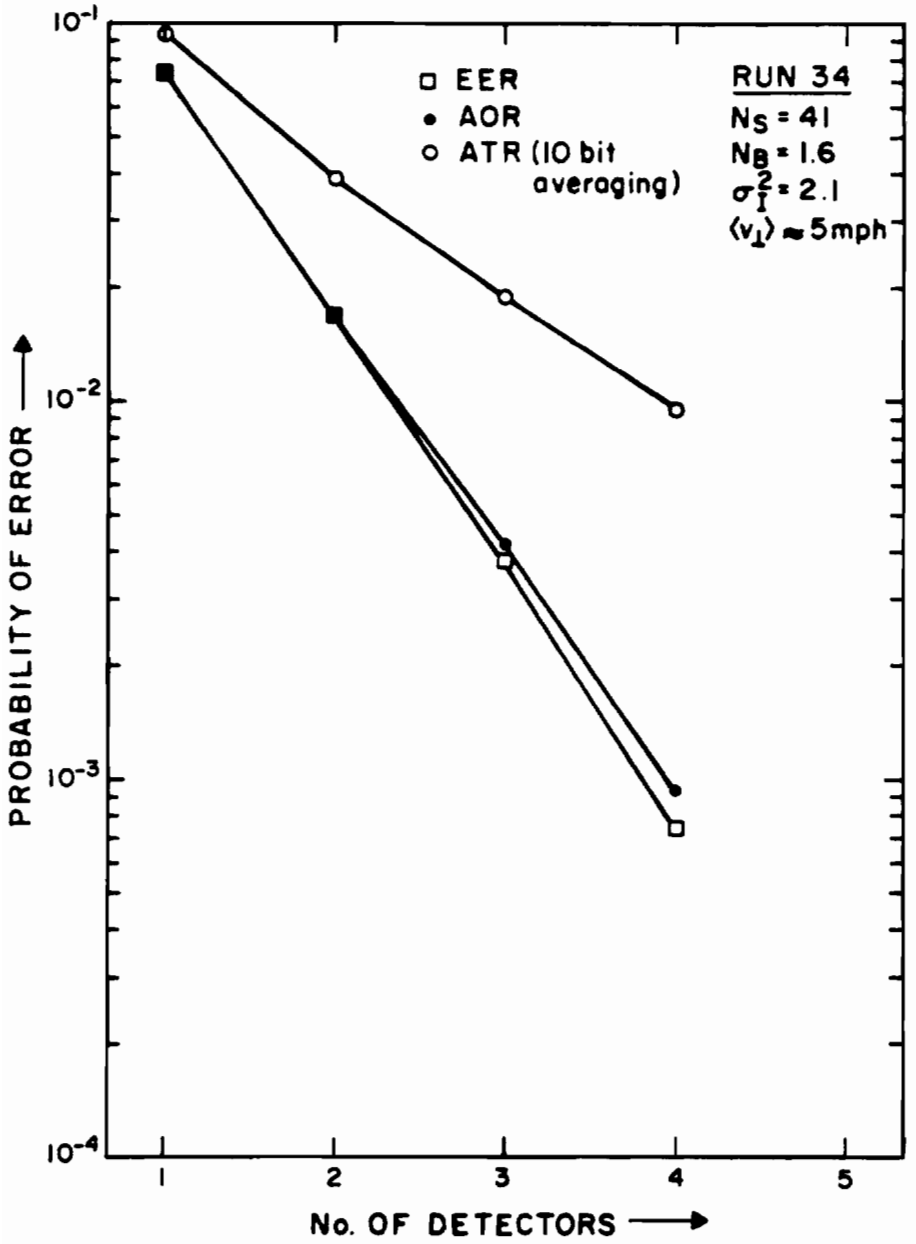

Figure 28. Probability of error vs. number of detectors.

simplest structure (see second column of Table III) and that the ATR does not need the values of σ_I^2 and N_S can very well make the ATR a very good choice. Figure 28 shows a case, however, where the ATR performs poorer than the AOR. The reason why this is so in this case is simply that due to winds perpendicular to the path of the laser beam there were high scintillation frequencies. This can be easily seen from Figure 12 which shows the autocorrelation function for the cases considered. Simple calculations using Figure 12 will show that the scintillation frequencies for the run 34 are roughly 10 times greater than that for the run 5. Therefore it would be reasonable to conclude that if a bit rate of 90 kHz (instead of 9 kHz) had been used in the experiment, the ATR could be shown to perform better than the AOR in the case of run 34 as well.

From the above considerations, we might expect that the ATR will perform very well provided the bit rate is large enough in any given practical situation. This is an easy condition to meet: One only needs to know how large is "large enough." To get some rough idea of this "largeness" of bit rate we look at Table VI. Table VI shows the performance of the ATR for different averaging for the runs 34 and 35. As can be seen, an approximate period for the optimum averaging is about 4/9000 sec ($\simeq$ 0.5 msec) for run 34 and less than 2/9000 sec ($\simeq$ 0.2 msec) for run 35. In the experiment about 10 to 20 bits averaged over during this period can give a good averaging. This is

TABLE VI

NUMBER OF BITS AVERAGED OVER VS. ERROR RATES FOR ATR

(In all cases the number of detectors is one.)

Run 12		Run 34		Run 35	
N	P_E	N	P_E	N	P_E
12	2.94 E-1	2	8.46 E-2	2	6.04 E-2
16	2.91 E-1	4	8.20 E-2	4	6.32 E-2
20	2.91 E-1	6	8.56 E-2	6	6.58 E-2
24	2.91 E-1	10	9.45 E-2	10	7.58 E-2
28	2.93 E-1	14	1.02 E-2	14	8.46 E-2

because in the experiment the H_1 bits and H_0 bits alternate regularly and equal number of H_1 and H_0 bits for the averaging is obtained by simply averaging over an even number of bits. But in a practical situation this condition is to be met by choosing "large enough" number of bits. It is easy to show that

$$N = 10^4 \frac{q_0}{g^2 q_1} \tag{60}$$

where N is the number of bits averaged over, q_1 and q_0 are the a priori probabilities for H_1 and H_0, and g is the percentage of RMS deviation of H_1 bits from the expected value Nq_1. It should be noted that in practical cases the error in the calculation of Z_{io} using equation (36) depends mainly on the deviation of the number of H_1 (or H_0) bits from the expected value. Assuming we allow a nominal value of 10 (%) for g and noting that q_1 and q_0 are equal we find that N is 100. Thus we arrive at a bit rate of a minimum of 200 K/sec for the case in run 34 and 500 K/sec for the case in run 35.

One other point we may note in connection with the AOR and ATR is that the curves in Figures 27 and 28 are approximately linear. This indicates an approximately exponential decrease in the error rates of AOR and ATR as the number of detectors is increased.

Finally, taking the cases of the SOR I and SOR II, we note they do not perform well. A reference to Table III may show that these

receiver structures are considerably simpler in comparison with the AOR and this was the motivation for us to consider these receiver structures. But, because of their poor performance these receiver structures will be ignored in the subsequent discussion.

Figures 29 and 30 show that as N_S increases, the error rates of both the AOR and ATR decrease in the same general manner. However, the error rates of the ATR are somewhat higher here, because of winds, resulting in high scintillation frequencies.

Finally we will briefly discuss the question, "What kind of error rates are possible in a photon counting communication system using a non-focused laser beam through a clear air turbulent atmosphere?". Figure 31 is indicative of the practical error rates using the AOR. In our experiment only point detectors were used, since point detectors are more fundamental than finite size detectors. Also, all experiments were done at turbulence levels close to saturation. Again this is because such levels of turbulence are more fundamental; in most practical cases if the path length is more than a few hundred meters, saturation is inevitable.[35] As such, the experimental results for P_E should be considered as worst case values. In real cases, however, the detectors can be of considerable size. This can reduce the effects of turbulence through aperture averaging, resulting in a smaller value for σ_I^2. Therefore, the practically possible receivers can have error rates better than what

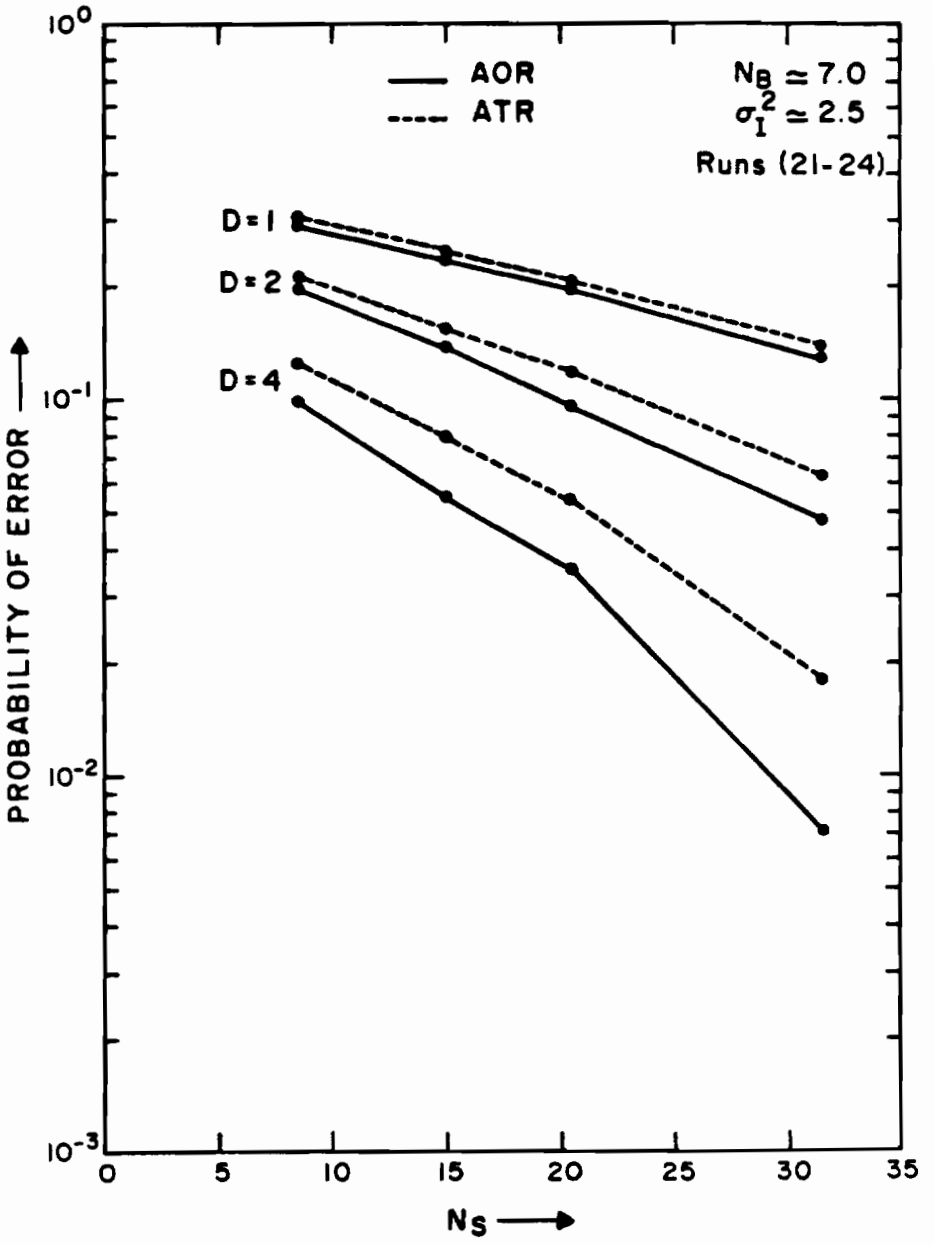

Figure 29. Probability of error as a function of average signal power at the detector.

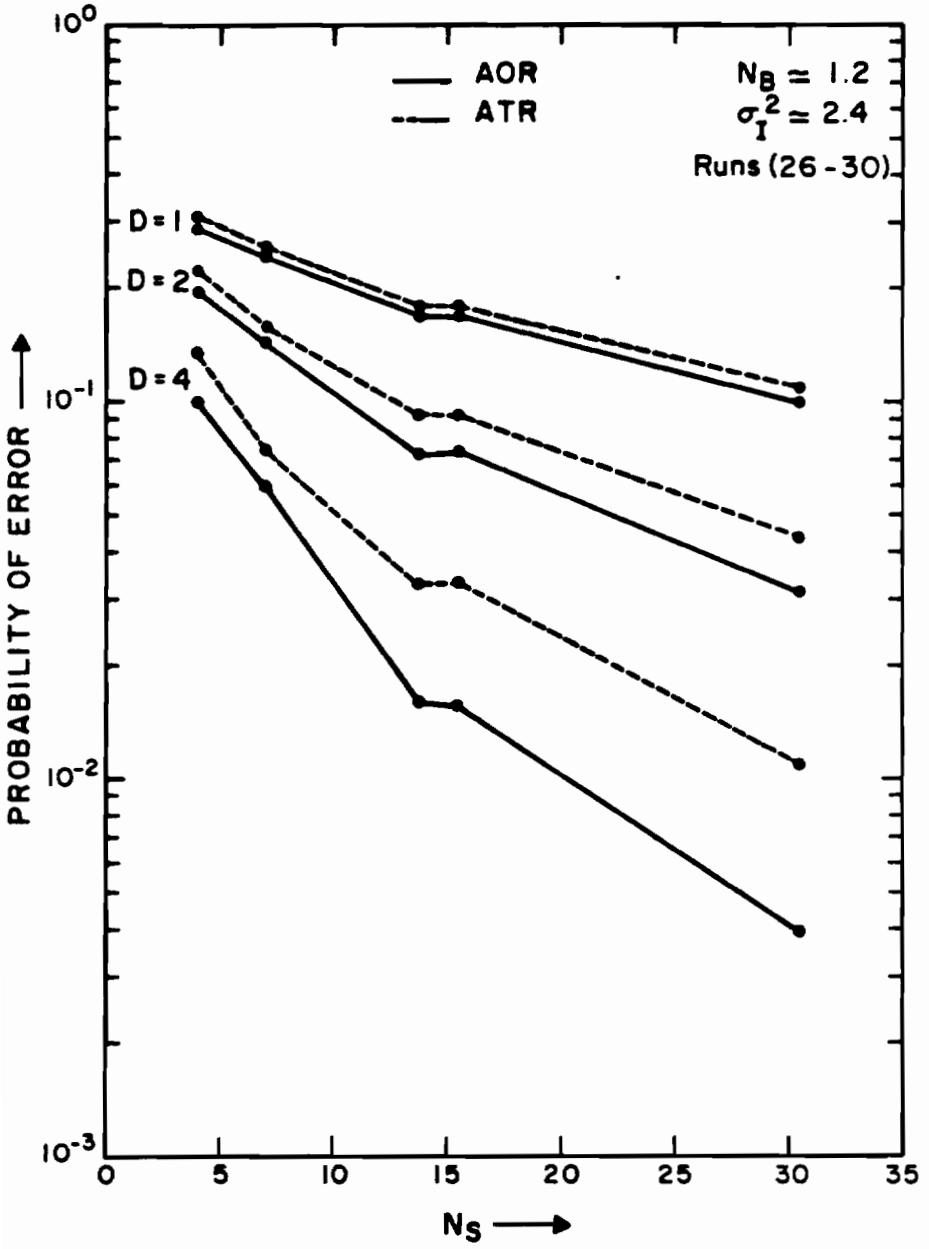

Figure 30. Probability of error as a function of average signal power at the detector.

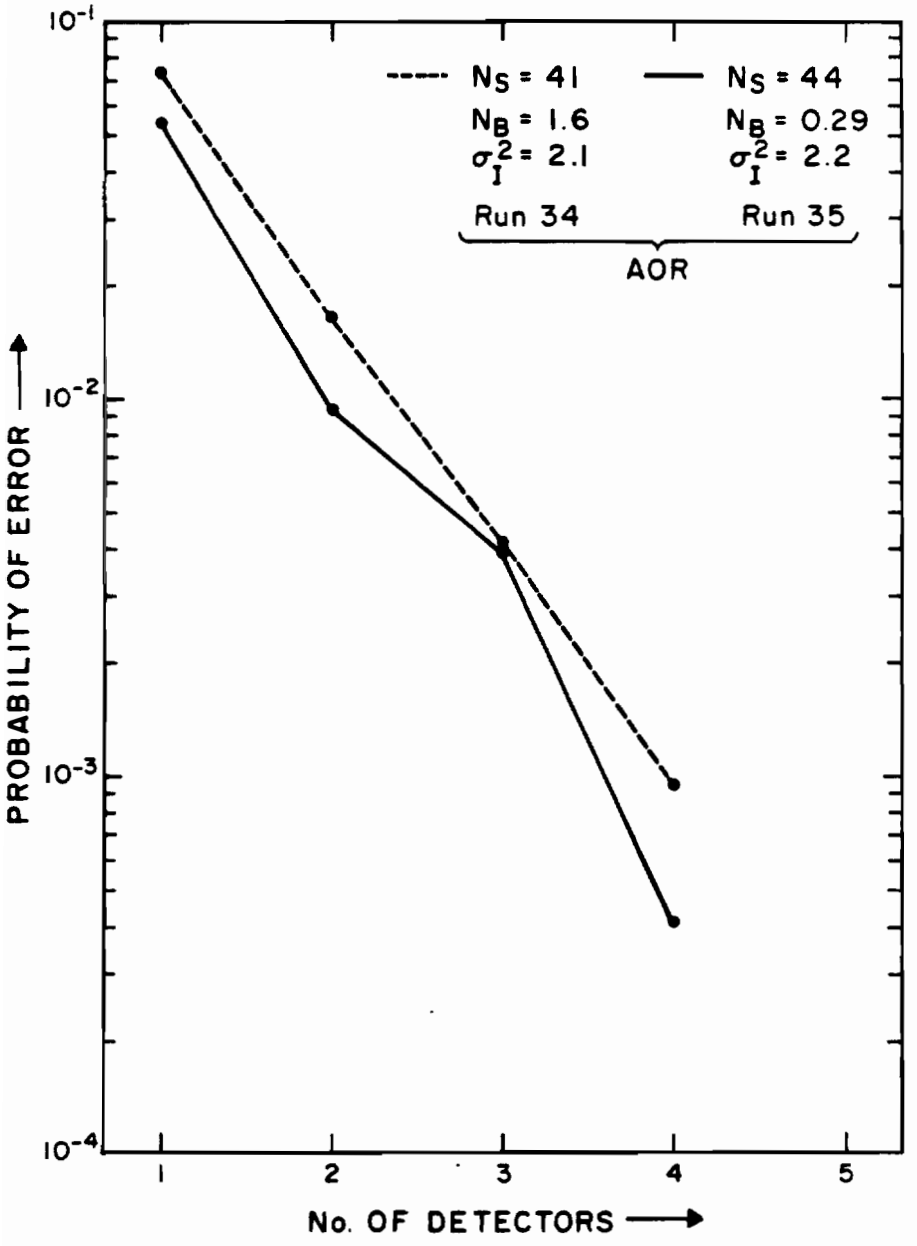

Figure 31. Probability of error vs. number of detectors.

Figure 31 shows. An investigation of the Photon Counting Receiver System using finite size detectors was beyond the scope of the present effort. However, we saw earlier that the results of this investigation confirm the validity of the theory by Teich and Rosenberg.[3] Therefore, we can now use the calculations from the theory to get some understanding of the performance of the system in areas not directly covered in this experiment.

The curves in Figures 32-34 were obtained from the theoretical calculations. An examination of these curves brings out two important facts.

1) When the turbulence is low ($\sigma_I^2 \leq 0.01$) all of the constant P_E curves are parallel to the σ_I^2 axis. This means that at these low turbulence levels, the P_E can be reduced only be increasing S/N ratio. This also means, as a corollary, that if $\sigma_I^2 \leq 0.01$, there is little to be gained by reducing σ_I^2 even further.

2) When the turbulence is in saturation ($\sigma_I^2 \leq 2$) all the constant P_E curves tend to be parallel to the N_S axis. This means that at these levels of turbulence, increasing N_S even by a large factor is not likely to improve the error rate very much. On the other hand, reductions in σ_I^2 even by a small factor can result in considerably lower values for P_E.

Tables VII-A and VII-B were prepared using theoretical calculations, to see the degree of improvement possible using finite

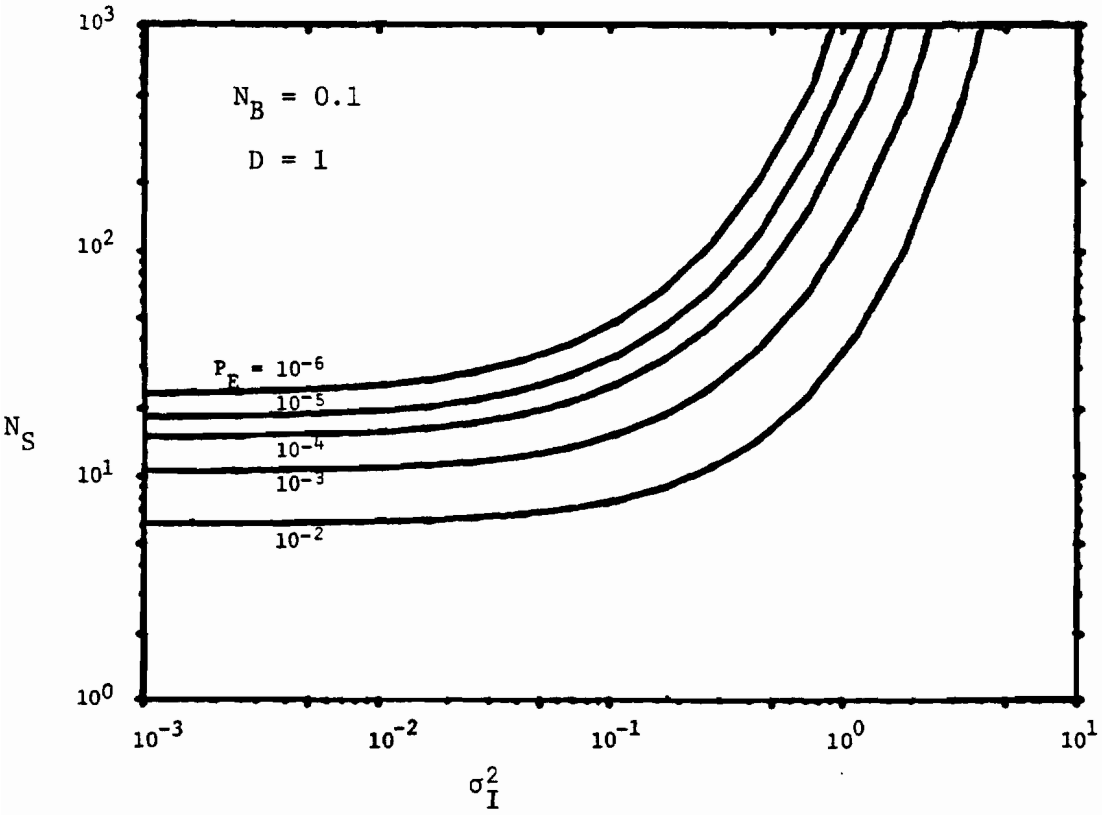

Figure 32. Theoretically calculated laser power in terms of N_S, for achieving a probability of error P_E, for $D = 1$, $N_B = 0.1$ and for any given value of σ_I^2.

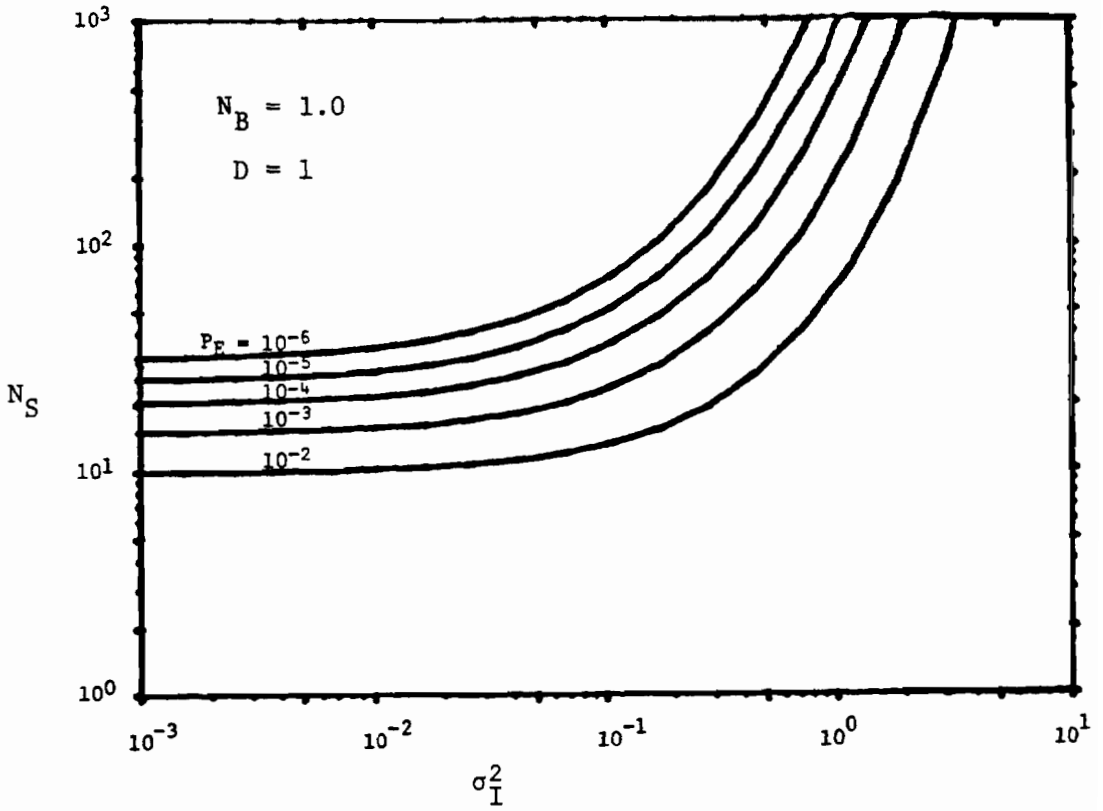

Figure 33. Theoretically calculated laser power in terms of N_S, for achieving a probability of error P_E, for $D = 1$, $N_B = 1.0$ and for any given value of σ_I^2.

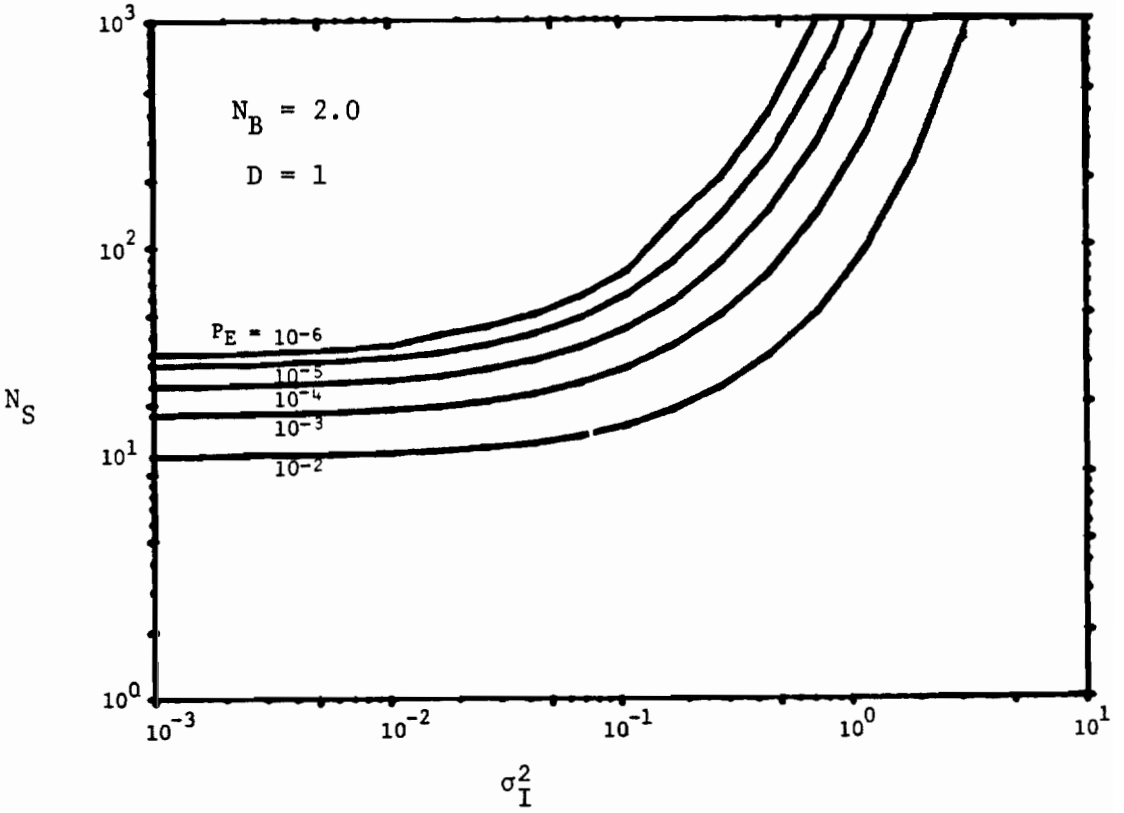

Figure 34. Theoretically calculated laser power in terms of N_S, for achieving a probability of error P_E, for D = 1, N_B = 2.0 and for any given value of σ_I^2.

TABLE VII-A

PROBABILITY OF ERROR AS A FUNCTION OF σ_I^2 AND D

(N_S = 30.5, N_B = 1.3)

σ_I^2		No. of Detectors			
		1	2	3	4
2.5	Experimental	1.0 E-1	3.2 E-2	1.1 E-2	4.0 E-3
	Theory	1.2 E-1	4.1 E-2	1.4 E-2	5.3 E-3
1.0	Theory	3.7 E-2	4.6 E-3	6.3 E-4	9.1 E-5
0.5	Theory	1.1 E-2	5.0 E-4	2.5 E-5	1.4 E-6
0.2	Theory	1.8 E-3	1.2 E-5	1.4 E-7	1.3 E-9
0.1	Theory	3.4 E-4	7.5 E-7	1.5 E-9	3.7 E-12

TABLE VII-B

PROBABILITY OF ERROR AS A FUNCTION OF σ_I^2 AND D

(N_S = 44.2, N_B = 0.29)

σ_I^2		No. of Detectors			
		1	2	3	4
2.2	Experimental	5.5 E-2	9.4 E-3	3.9 E-3	4.1 E-4
	Theory	5.4 E-2	8.9 E-3	1.7 E-3	3.2 E-4
1.0	Theory	1.0 E-2	4.4 E-4	2.1 E-5	9.9 E-7
0.5	Theory	1.7 E-3	1.3 E-5	1.1 E-7	9.7 E-10
0.2	Theory	6.5 E-5	2.4 E-8	1.2 E-11	6.8 E-15
0.1	Theory	4.2 E-6	9.9 E-11	3.1 E-15	1.1 E-19

size detectors and hence some aperture averaging. The tables show that even with good aperture averaging, the use of multiple detectors may be necessary to obtain low error rates of the order of 10^{-6} or less.

As one final point it must be mentioned that adding more detectors to improve the performance (it was mentioned that performance improves approximately exponentially with each additional detector) can be relatively an easy thing to do. This is because each additional detector costs proportionately less. The end of Section II and Section III of Chapter 3 discuss how the discrete nature of the likelihood function is useful in cutting down the digital processing costs after each detector.

To sum up, on the basis of the results of the present investigation as explained in Chapters 3 and 4, one may confirm the following conclusions.

1) The work of Teich and Rosenberg[3] provides a good theoretical basis for the receiver structure and for calculating the error rates for a photon counting receiver using a turbulent channel modeled by a lognormal distribution for irradiance.

2) Assuming independent fading for each detector, the approximate optimum receiver is very nearly as good as the exact receiver under the given channel and signal parameters.

3) The adaptive threshold receiver performs better and also is less complex when compared to the approximate optimum receiver. A

practical adaptive threshold receiver may require a bit rate that is greater than 500 K/sec.

4) The decrease in the error probability of both the adaptive threshold and approximate optimum receiver with the increase in the number of detectors is approximately exponential.

5) The suboptimum receivers derived from the approximate optimum receiver perform poorly.

6) Receiver structures other than the adaptive threshold receiver need the values of σ_I^2 and N_S for their operation. These values can be evaluated from the photon counting readings and do not require separate measurement.

7) The receiver structure configuration with stored likelihood function considerably reduces the computing power needed for digital processing. For this reason, this configuration may be very appropriate when large bit rates are used.

8) Error rates of the order of 10^{-6} or less can be obtained by the combined use of aperture averaging as well as multiple detectors.

9) The selection of the operating voltages for the photon counting PMT to achieve maximum S/N ratio may not always be the best. At least in come cases this may result in high rates of noise pulses causing false alarms. The situation may be remedied by simply increasing the threshold voltage slightly (about 25% - 50%).

CHAPTER 5

SOME GENERAL CONSIDERATIONS FOR PHOTON COUNTING RECEIVERS

In this chapter we briefly consider a few more aspects of a photon counting receiver, which were not part of the present thesis, but nevertheless are important in one way or the other. After overcoming the deleterious effects of the turbulence, the forbidding weather conditions would be a very major concern especially in those areas where clouds, fog, snow or rain may all too often interrupt the path of the laser beam.

There are two aspects to the above problem. One is that the prevailing weather conditions may cause a total or near total extinction of the beam. In such conditions the most reasonable thing to do might be to shut off the communication and wait for clearer weather. The possibility of boring a transparent hole through the fog, cloud, etc. by the laser beam was considered by Sutton[11] and Harney.[12] Their calculations indicate that no significant hole boring can happen at moderate power levels, especially if the fog or cloud is fairly thick.

In the case of satellite to earth communications the above problem may be overcome in a different way by setting up receiver stations in more than one place which may have a minimum of weather correlation.[6] So, if one station could not receive due to bad

weather conditions, the transmission may be directed to another station where conditions may be favorable.

The other aspect concerns the drift from the expected performance of the receiver. In all communication systems, one needs the assurance that the error rates of the system will not increase beyond a maximum prescribed value due to any inadvertent changes in the conditions under which the system may have to operate. Drifts and changes can occur in the uncontrollable parameters resulting in changes in the performance. A photon counting communication system designed and optimized for clear turbulent conditions may well be able to operate without serious interruption in a lightly rainy or mildly foggy condition. However, one should expect a drift from the expected error rates for the system. An understanding of the magnitude and nature of these drifts, and possible methods to predict and cope with them need to be investigated in order to "better optimize" the system and make it more usable under these mild conditions of weather. It might be possible that the error rate of the system could be monitored and displayed continuously, so that the operator could decide whether to go on or to shut off the system.

The use of high bit rates in the photon counting receiver system may be desirable on many occasions. For example, the adaptive threshold receiver requires a high bit rate of transmission. But

high bit rate makes certain other problems more severe. For example, a photon counting receiver system operating at 10^6 bits/sec and $N_s = 20$ will have to be able to count about 5×10^7 random events per second. This would require a resolution better than 1 nano second, which might be hard to obtain in discriminator circuits. The dead time of the PMT will also begin to play a significant role, unless more sophisticated crossed field versions of PMT are used. In such cases one possibility is to calculate the new probability distribution function for photon counts after taking the dead time effects into account, and use it to describe a new receiver structure. Such a calculation for the probability density function has been done for free space by Canton and Teich.[39] The effects of the dead time on the error rates of the receiver system as compared to without dead time has been numerically calculated by Stephens and Davidson.[40] From their calculations it appears that the degradation may not be very much ($\sim$ 1 db). This might be expected because dead time effects are serious only when there is a surge of photons coming due to high intensity of the received beam. But most of the errors occur only when there is a low intensity of the beam due to fading and the problem of dead time of the PMT is not likely to affect the error rates here. However, in a system in which the extreme variations in the intensity due to turbulence have been reduced to a minimum by a good aperture averaging, the dead time effects can more significantly affect the performance of the receiver.

At very high bit rates, since the photoelectron pulse counting could become extremely difficult (if not impossible), one may have to resort to passive R-C integration of pulses with no dumping between subsequent bits. This would mean the system would retain a memory of the previous bit. Fluchel et al. have calculated the resulting degradation in performance for such a case for the free space channel and pulse position modulation and report a typical degradation of an order of magnitude in error rates.[41] High bit rates can also give rise to a channel with memory due to pulse stretching. There has been at least one report that due to multiple scattering in clouds the pulse stretching can be reduced by narrowing the field of view so that only the direct beam is received.[15] But then, in situations where the beam intensity has been reduced by the presence of clouds, etc., the field of view may need to be increased to collect more energy from the scattered light.[16] This means an intelligent compromise will have to be made here.

Time synchronization is another problem which is more serious in the case of a photon counting system. Because of this a separate channel dedicated only to transmitting synchronization pulses may be needed. In practice, this can be done using a single laser, by using one polarization for sending the message, and using the other for sending the synchronization information. For the case in which a separate channel for the synchronization pulses is used,

Haney and Gagliardi have investigated the density function for the phase error of a phase locked loop following photon countin detection.[42] Gagliardi shows that the increase in the error probability of the system due to error in time synchronization is more for on-off keying than for a binary pulse position modulation system.[43] Interestingly, he also observes that for the OOK system, there is an irreducible minimum error rate which cannot be overcome by any other means except by switching to a different modulation. He further observes that increasing the signal strength, instead of improving the performance, may actually degrade it in such a case. However, it must be pointed out that his observations could be true only for an OOK system using no guard rings (i.e., no dead space between adjacent bit intervals). If the guard rings are wide enough to accomodate the error in time synchronization, the above observations for an OOK system need not be true. Titterton[44] has presented several graphs showing the degradation of performance of a system due to timing errors for several cases.

It must be noted that all of the above works on the timing errors and the resulting degradation assume a free space channel, i.e., no random fading due to turbulence. Naturally one should expect a more serious degradation for a turbulent channel and work in this area to date is minimal. For the present, however, it might be said that to reduce the effects of timing errors, it would be desirable to make use

of as short pulses as possible and to use a separate channel for sending the synchronization pulses. Also, using a separate channel for sending the synchronization pulses would be very helpful in case a continuous monitoring of the error rate of the system is needed.

APPENDIX A

APPENDIX A

To prove that P_E is a monotonically decreasing function of D we start with equations (48) and (53) of Chapter 3.

$$\underline{\Lambda}(\vec{n}) = \frac{\prod_{i=1}^{D} P_1(n_i)}{\prod_{i=1}^{D} P_0(n_i)} \tag{1A}$$

$$P_E = \tfrac{1}{2} \sum_{\vec{n}} \left\{ \prod_{i=1}^{D} P_0(n_i)\, U(\underline{\Lambda}) + \prod_{i=1}^{D} P_1(n_i) \left[1 - U(\underline{\Lambda}) \right] \right\} \tag{2A}$$

To save writing we may use the following substitutions.

$$\prod_{i=1}^{D} P_1(n_i) = a \tag{3A}$$

$$\prod_{i=1}^{D} P_0(n_i) = b \tag{4A}$$

Equation (2A) then becomes

$$P_E = \tfrac{1}{2} \sum_{\vec{n}} \left\{ b\, U\left(\frac{a}{b}\right) + a \left[1 - U\left(\frac{a}{b}\right) \right] \right\} \tag{5A}$$

P_E is the error probability for the exact receiver using D detectors. The summation is done over all possible D dimensional vectors $\vec{n}$. Let

P_{E1} be the probability of error for the same system using (D + 1) detectors. Then,

$$P_{E1} = \tfrac{1}{2} \sum_{\vec{n}} \left\{ \sum_{n_j=0}^{N_0} b\, P_0(n_j)\, U\left(\frac{a\, P_1(n_j)}{b\, P_0(n_j)} \right) \right. \tag{6A}$$

$$\left. + \sum_{n_j=0}^{N_0} a\, P_1(n_j) \left[1 - U\left(\frac{a\, P_1(n_j)}{b\, P_0(n_j)} \right) \right] \right\}$$

where N_0 is the maximum count per bit that is possible in practice.

$$P_E - P_{E1} = \tfrac{1}{2} \sum_{\vec{n}} \left\{ b\, U\left(\frac{a}{b}\right) - \sum_{n_j=0}^{N_0} b\, P_0(n_j)\, U\left(\frac{a\, P_1(n_j)}{b\, P_0(n_j)} \right) \right. \tag{7A}$$

$$\left. + a\left[1 - U\left(\frac{a}{b}\right) \right] - \sum_{n_j=0}^{N_0} a\, P_1(n_j) \left[1 - U\left(\frac{a\, P_1(n_j)}{b\, P_0(n_j)} \right) \right] \right\}$$

Noting that $\sum_{n_j=0}^{N_0} a\, P_1(n_j) = a$, and collecting terms together,

$$P_E - P_{E1} = \tfrac{1}{2} \sum_{\vec{n}} \left(\left[(b - a)\, U\left(\frac{a}{b}\right) \right] \right. \tag{8A}$$

$$\left. + \left\{ \sum_{n_j=0}^{N_0} \left[a\, P_1(n_j) - b\, P_0(n_j) \right] U\left(\frac{a\, P_1(n_j)}{b\, P_0(n_j)} \right) \right\} \right)$$

Say, $$P_E - P_{E1} = \tfrac{1}{2} \sum_{\vec{n}} [T_1 + T_2] \tag{9A}$$

We may note that $T_1 \leq 0$ and $T_2 \geq 0$. We may further note

$$\sum_{n_j=0}^{N_0} \left(a\, P_1(n_j) - b\, P_0(n_j) \right) = a - b \tag{10A}$$

and that

$$\sum_{n_j=0}^{N_0} \left[a\, P_1(n_j) - b\, P_0(n_j) \right] \tag{11A}$$

$$\leq \sum_{n_j=0}^{N_0} \left[a\, p_1(n_j) - b\, p_0(n_j) \right] U\left[\frac{a\, P_1(n_j)}{b\, P_0(n_j)} \right]$$

In view of equations (10A) and (11A) one could see that the RHS of (9A) is always positive or zero; i.e., $P_E - P_{E1} \geq 0$.

$\therefore$ P_E is always a decreasing function of the number of detectors D.

APPENDIX B

APPENDIX B

The output of a photon counting PMT would normally consist of pulses due to photo emitted electrons as well as noise electrons (due to thermal emission, etc.). Since the gain of the PMT is somewhat random, the height of both kinds of pulses would be distributed over a range of voltages. However, the noise pulses would be generally smaller in voltage since not all of them would originate at the cathode and so experience less gain. Therefore, most of the noise pulses can be stopped by setting a threshold voltage and suppressing all pulses below that voltage.

When the threshold voltage is low, any additional increase in the threshold voltage is likely to suppress more noise pulses than photoelectron pulses. But when the threshold voltage is high, most of the noise pulses would already have been suppressed and so any additional increase in threshold voltage would suppress more of the photoelectron than the noise pulses. Similarly, when the voltage between the cathode and anode is small, any increase in the same will produce more photoelectron pulses than noise pulses. But at higher values this is reversed. So for the best S/N operation of the PMT the threshold voltage and the anode voltage should be chosen properly. The methods for doing this can be found in any of the manufacturer's literature for photon counting instruments using a PMT.

In our experiment, we found that choosing the voltages to get maximum S/N may not always be the best. Our experiment is aimed at determining the error probability of a binary coded on-off keying photon counting receiver. The anode voltage and the threshold voltage for maximum S/N were found to be 1800 V and 2 mV respectively. With the PMT operating at these voltages the probability distribution for the pulse rates was determined. Figures 35-37 show the pulse (due to noise or photoelectron) rate distribution for 1) with no light falling on the cathode of the PMT; 2) a steady light falling on the cathode so that the average pulse rate was 2.6/bit interval; and 3) a steady light falling on the cathode so that the average pulse rate was 12.5/bit interval. The dots give the measured probabilities while the solid curves give the theoretically expected Poisson distribution. As can be seen, there are a few cases of unexpectedly high rates of pulses. The probability of observing these high pulse rates seems to increase with increasing photon rates. While the exact reason for this was not understood, on close examination it was found that the high pulse rates were due to bursts of noise pulses within the PMT.

While in other applications these bursts of pulses may not amount to much, they adversely affect the performance of the photon counting receiver. This is because these high rates of pulses will be interpreted as due to high rate of arrival of photons and thus cause an error (false alarm). As can be seen from Figures 35-37, this error can be of the order of 10^{-3}.

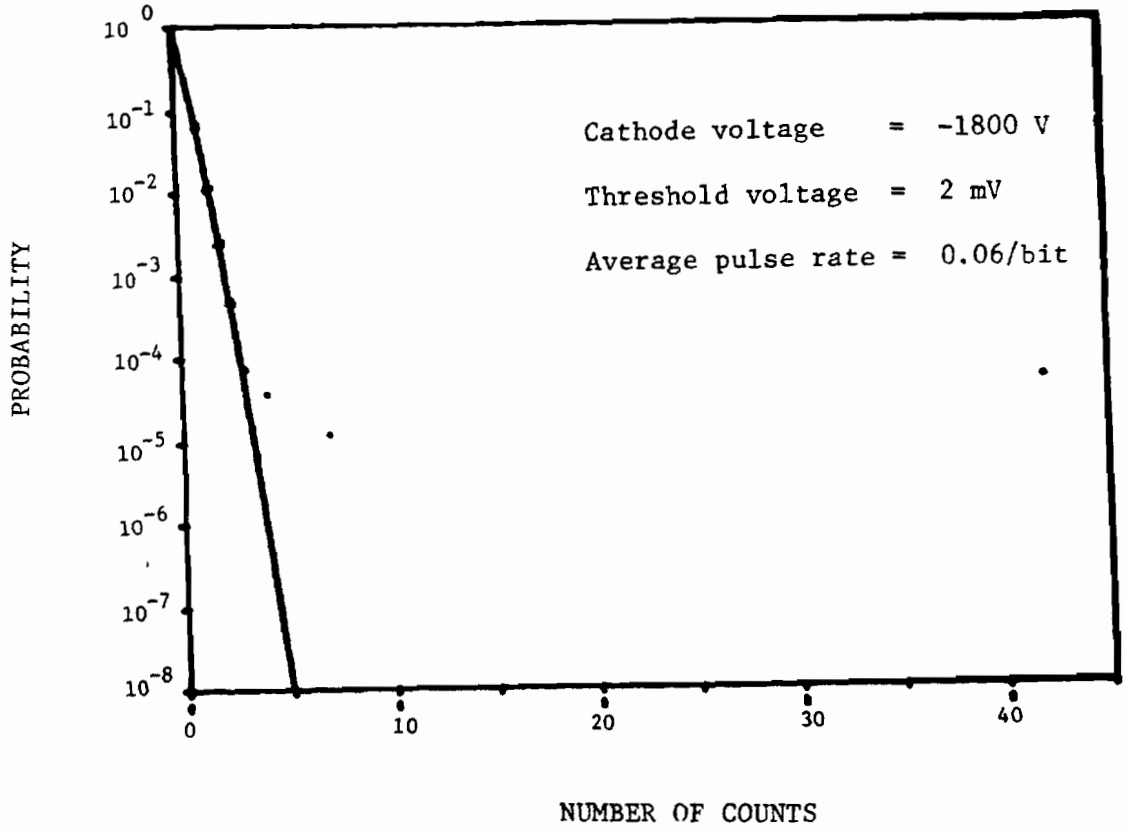

Fig. 35. Probability density function for output pulse (due to photo as well as noise electrons) rate when PMT voltages are optimized to obtain maximum S/N ratio for the PMT.

Dots give the experimentally measured values.
Solid line is the theoretically expected Poisson curve.

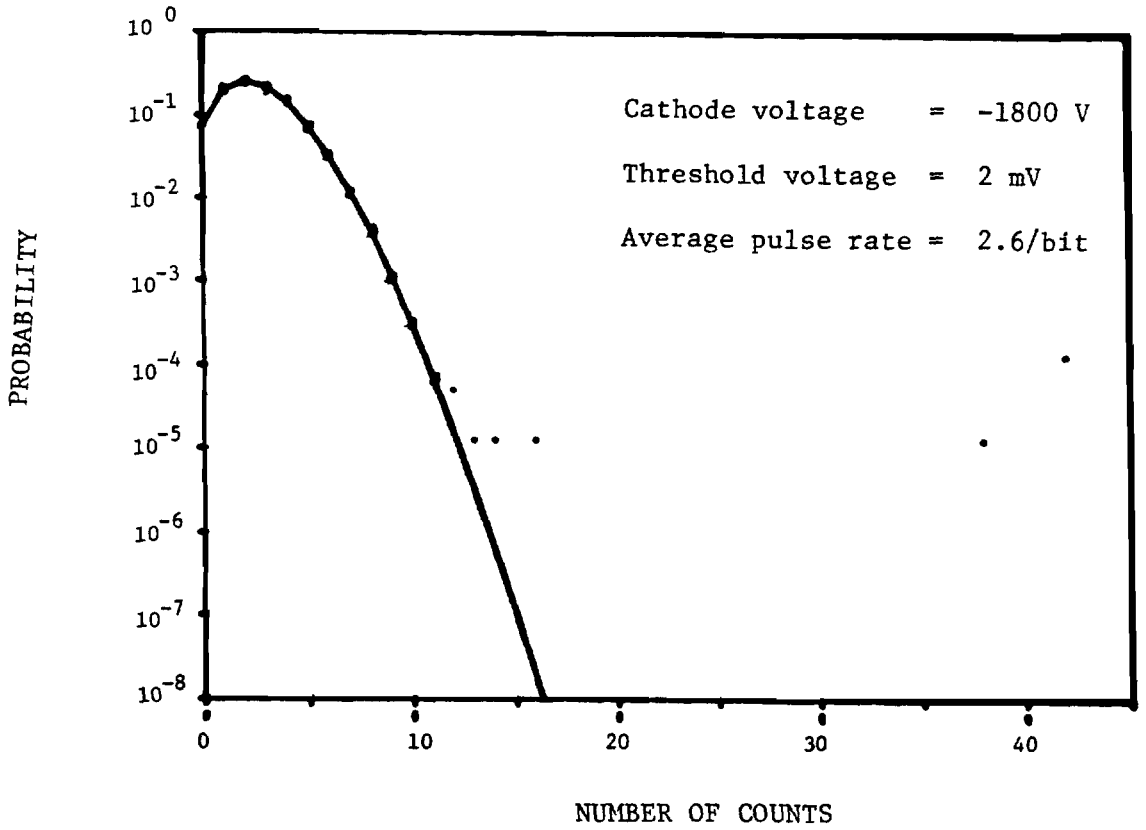

Fig. 36. Probability density function for the output pulse (due to photo as well as noise electrons) rate when PMT voltages are optimized to obtain maximum S/N ratio for the PMT.

Dots give the experimentally measured values.
Solid line is the theoretically expected Poisson curve.

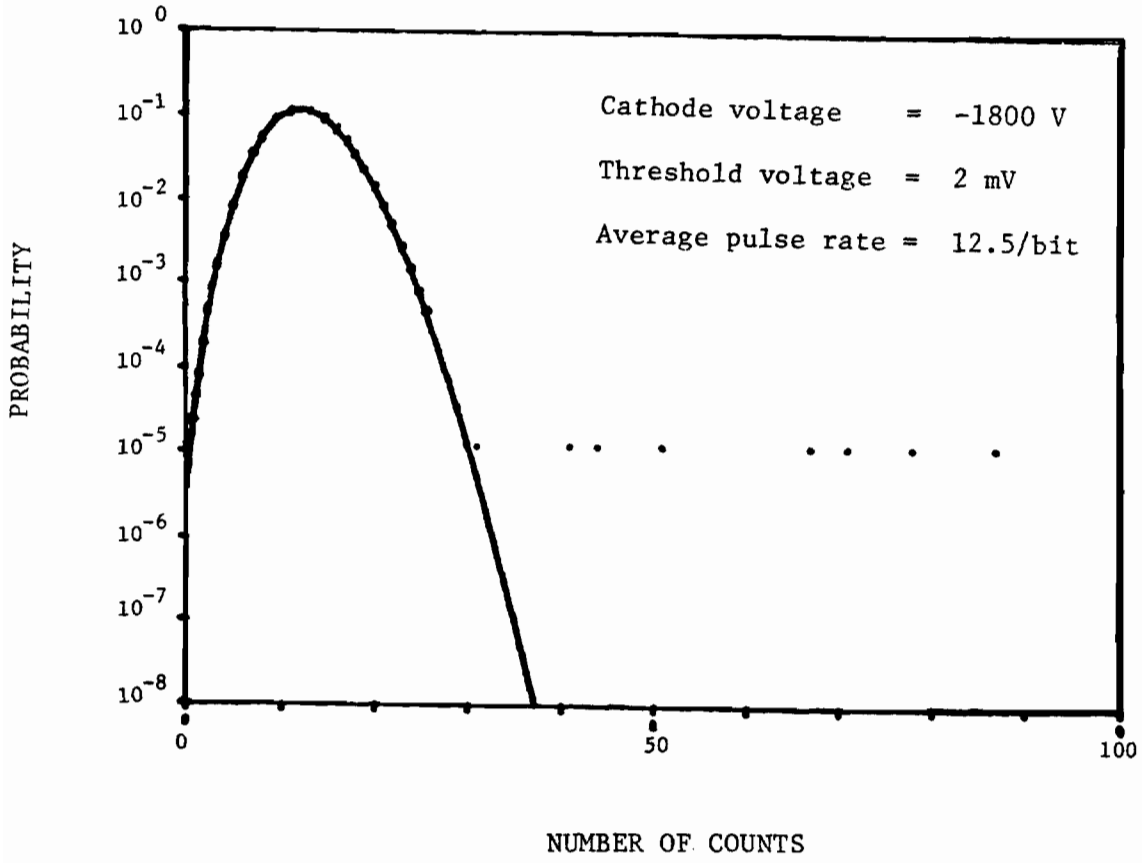

Fig. 37. Probability density function for the output pulse (due to photo as well as noise electrons) rate when PMT voltages are optimized to obtain maximum S/N ratio for the PMT.

Dots give the experimentally measured values.
Solid line is the theoretically expected Poisson curve.

It was further found that these bursts of pulses can be stopped by slightly increasing the threshold voltage. Figure 38 gives the probability distribution of pulse rates with PMT operating at 1800 V and 3 mV. This offset the "optimum conditions" for the PMT and resulted in about 10% less value for S/N, but completely stopped the bursts of noise pulses. It should be obvious that for a photon counting receiver system designed to operate with an error probability of 10^{-4} or less, a loss of 10% S/N ratio is worth suffering in order to reduce false alarm by 10^{-3}.

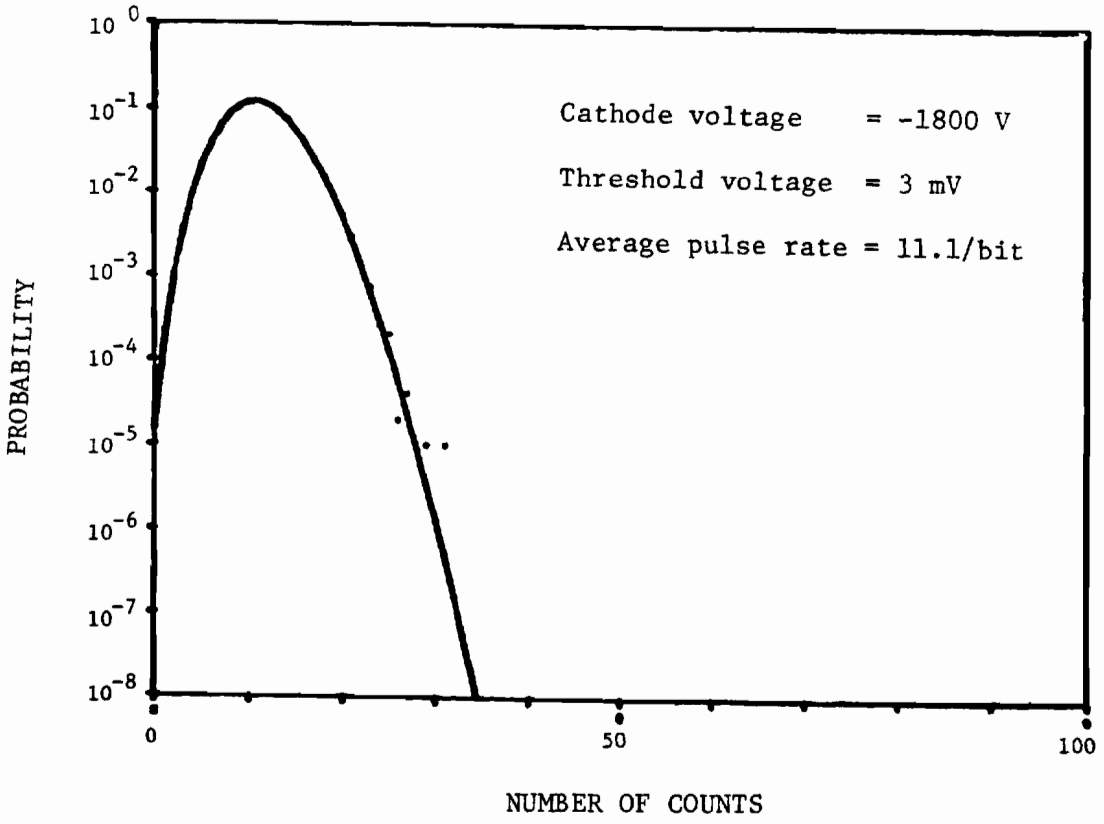

Fig. 38. Probability density function for the output pulse (due to photo as well as noise electrons) rate after the threshold voltage has been increased from its optimum value for maximum S/N of the PMT.

Dots give the experimentally measured values.
Solid Line is the theoretically expected Poisson curve.

APPENDIX C

APPENDIX C

Experimental results obtained in connection with the photon counting receiver system are presented in this Appendix. The probability density function for H_1 bits (see Figure 14) is shown for 35 different cases obtained by changing the parameters N_S and N_B. The normalized variance of irradiance, σ_I^2, was calculated from a direct measurement of the intensity fluctuations and used in the theoretical calculation of the density functions. For comparison, the theoretical value, $(\sigma_I^2)_T$, was calculated from a measurement of C_n^2. Relevant parameters (e.g., the transverse wind velocity, $\langle v_\perp \rangle$) were measured for each case and are presented along with the density functions. The density functions for runs 1-30 are shown in Figures 39-68, and the density functions for runs 31-35 are given in Tables VIII-A through VIII-E.

Experimentally measured error rates for the receivers EER, AOR, SOR I, SOR II and ATR with 1 through 4 detectors are presented in Tables IX-A to IX-G. Table X presents experimental as well as theoretical values of error rates for AOR for a single detector. Tables XI and XII do the same for a two detector and a four detector array respectively. The theoretical error rates for four detector arrays were calculated only for selected cases.

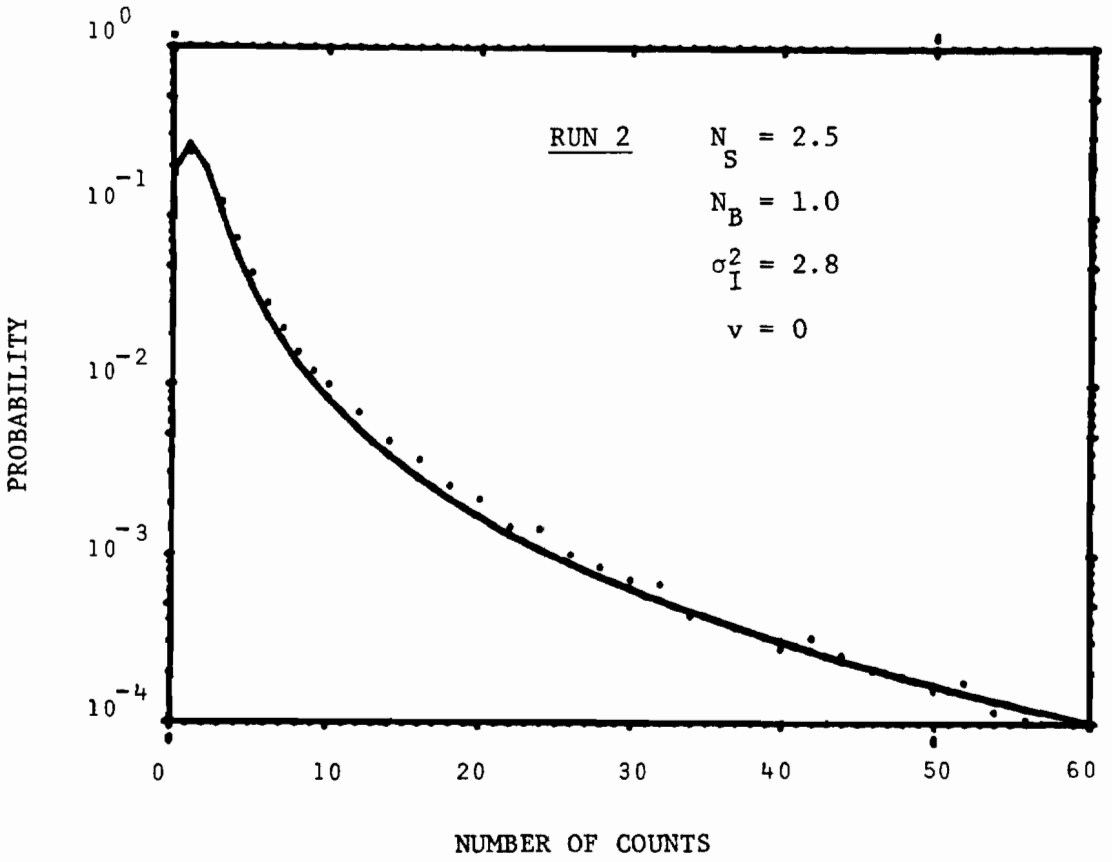

Figure 40. Probability density function for photoelectron counts.

Dots give the experimentally measured values.
Solid line gives the theoretical curve.

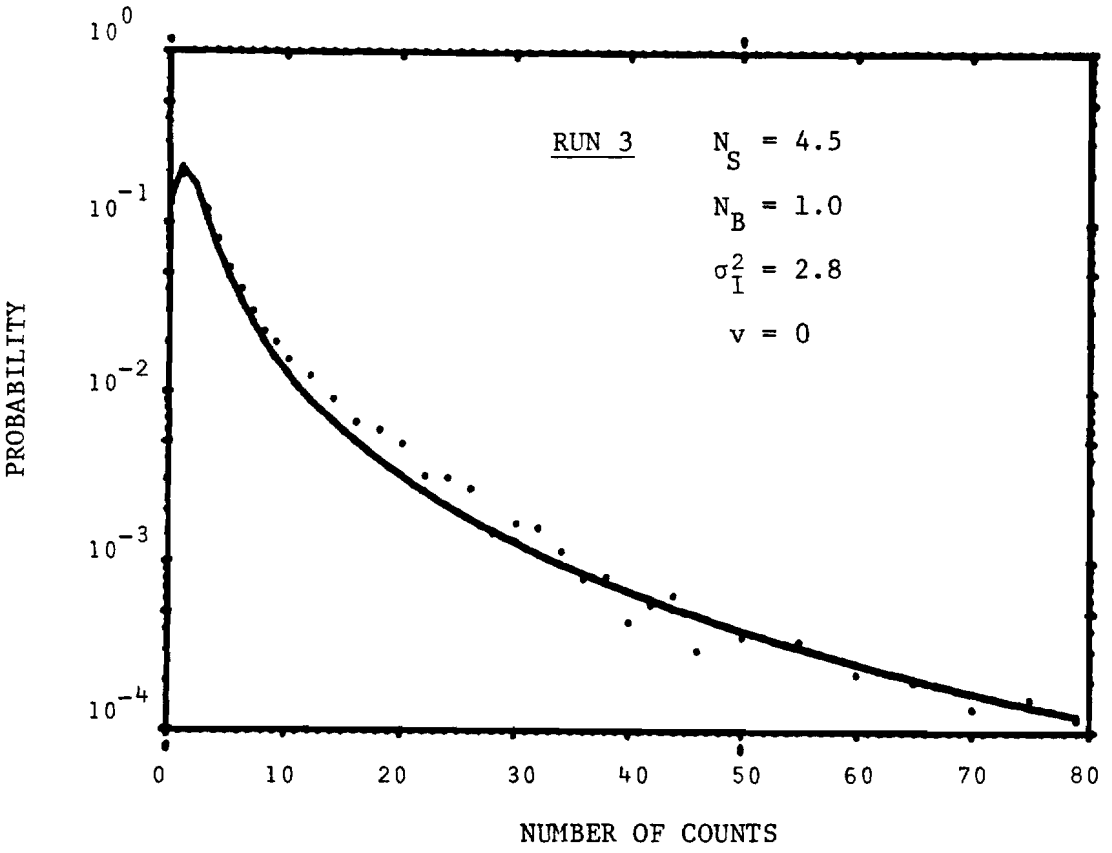

Figure 41. Probability density function for photoelectron counts.

Dots give the experimentally measured values.
Solid line gives the theoretical curve.

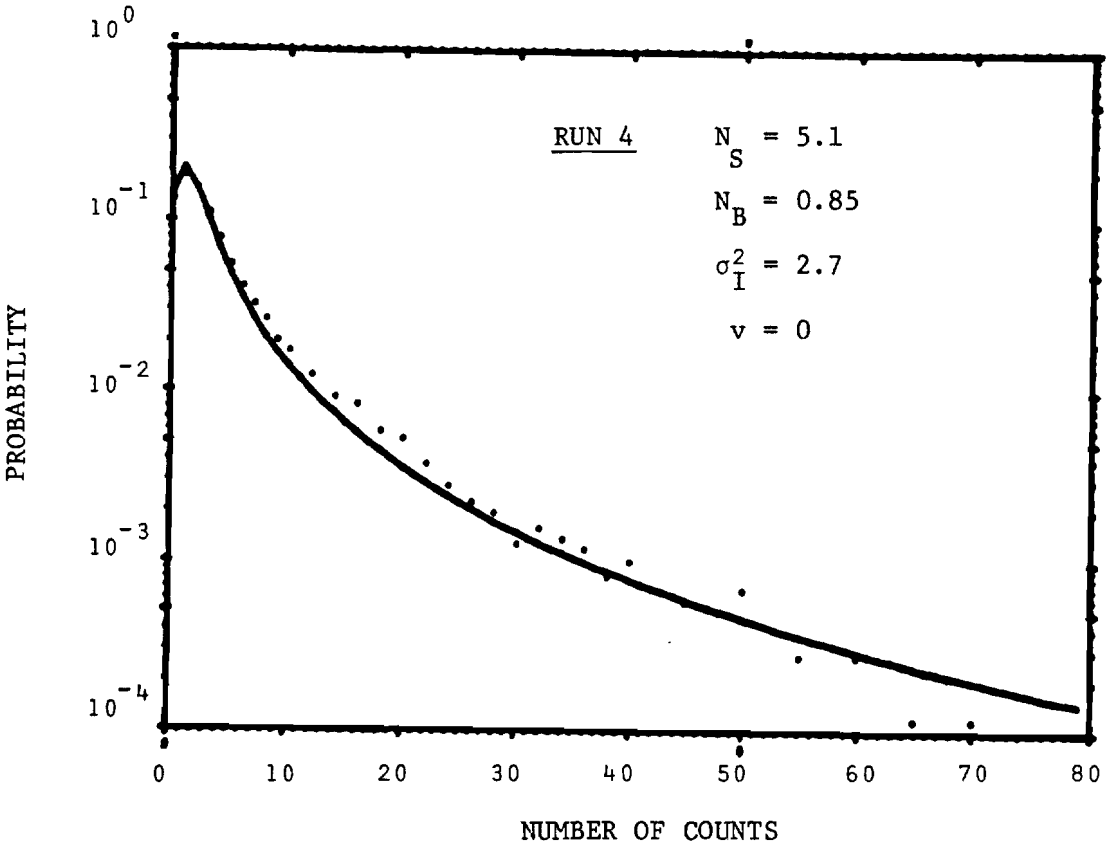

Figure 42. Probability density function for photoelectron counts.

Dots give the experimentally measured values.
Solid line gives the theoretical curve.

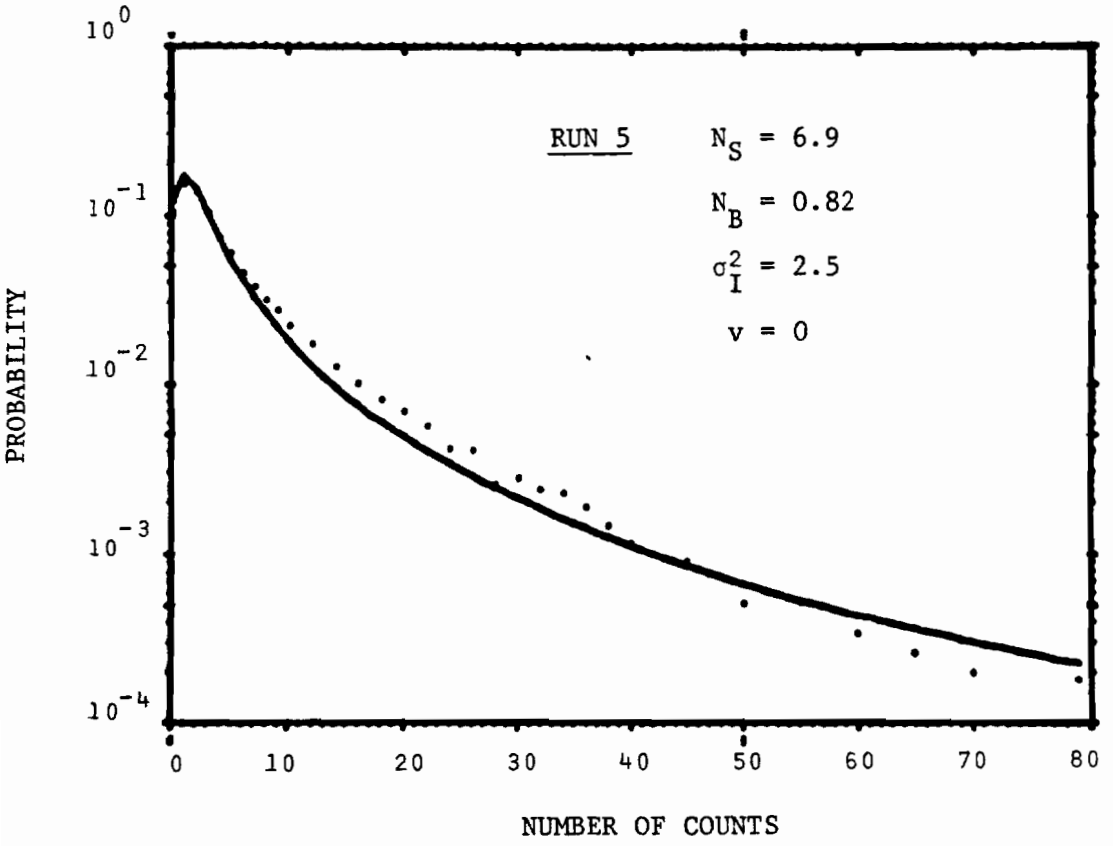

Figure 43. Probability density function for photoelectron counts.

Dots give the experimentally measured values.
Solid line gives the theoretical curve.

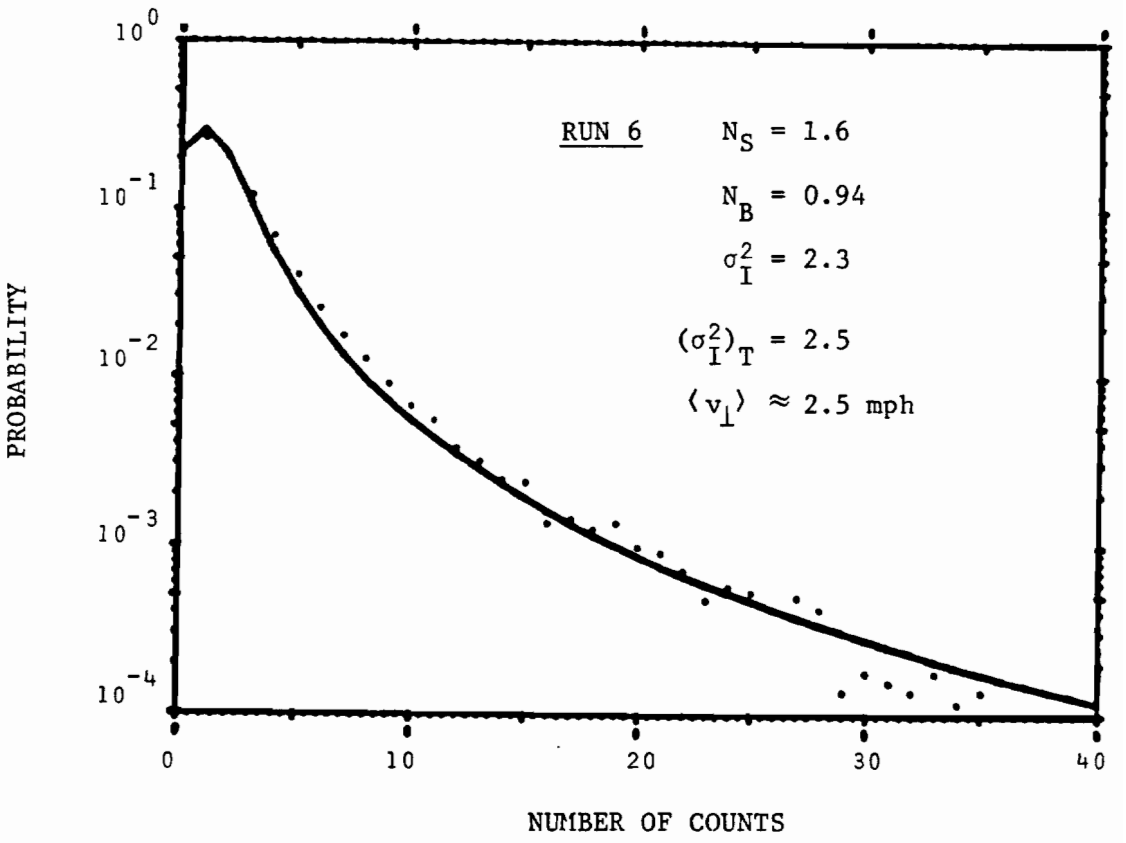

Figure 44. Probability density function for photoelectron counts.

Dots give the experimentally measured values.
Solid line gives the theoretical curve.

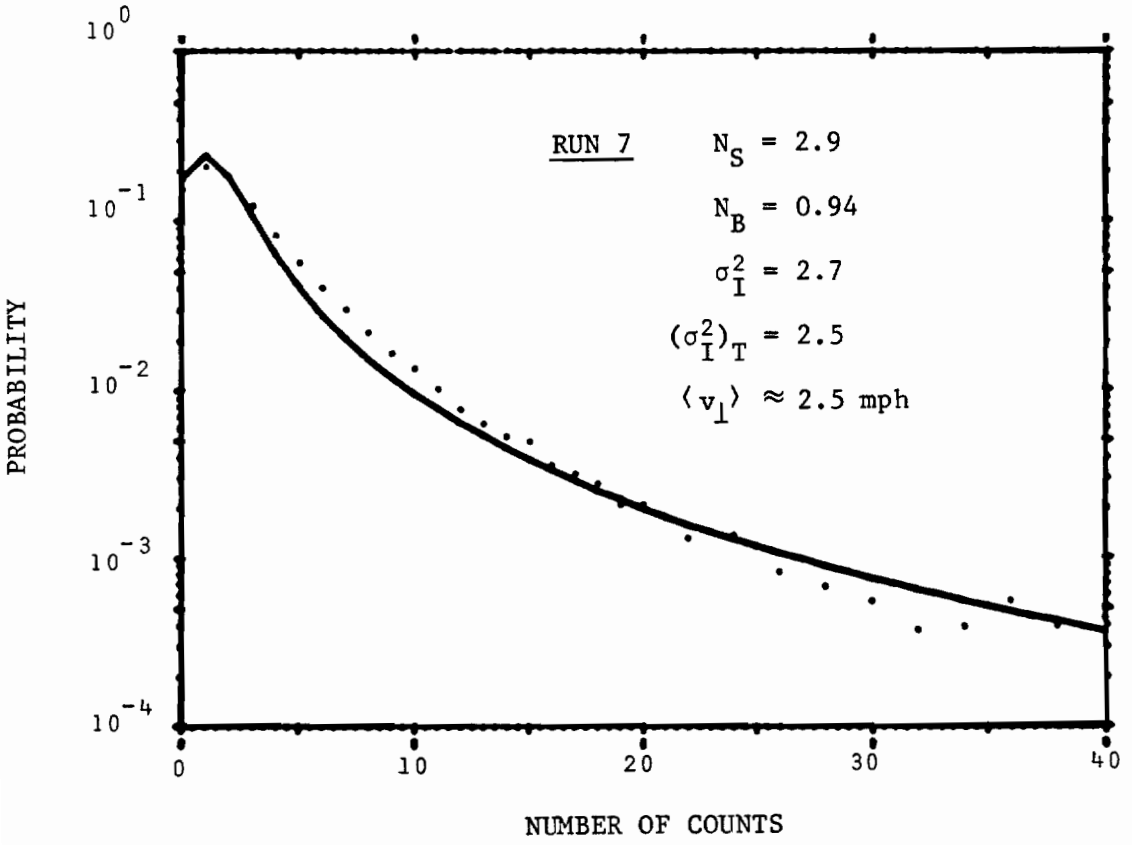

Figure 45. Probability density function for photoelectron counts.

Dots give the experimentally measured values.
Solid line gives the theoretical curve.

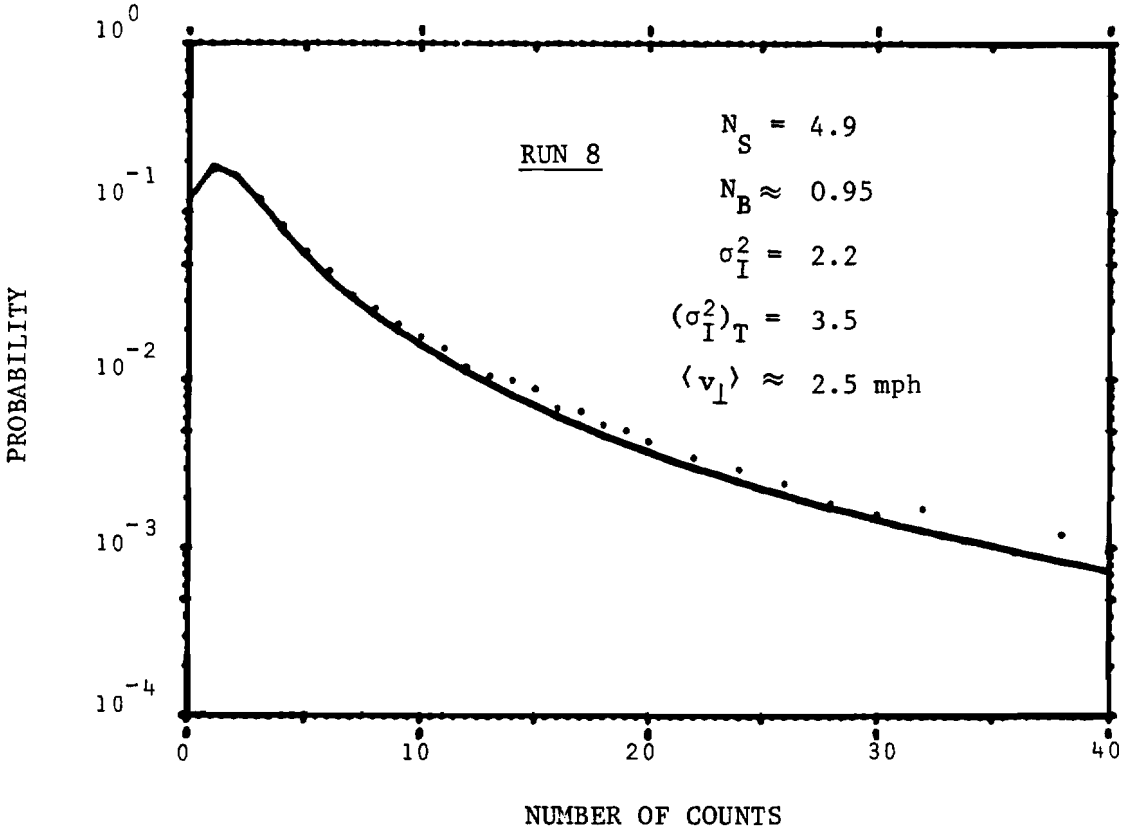

Figure 46. Probability density function for photoelectron counts.

Dots give the experimentally measured values.
Solid line gives the theoretical curve.

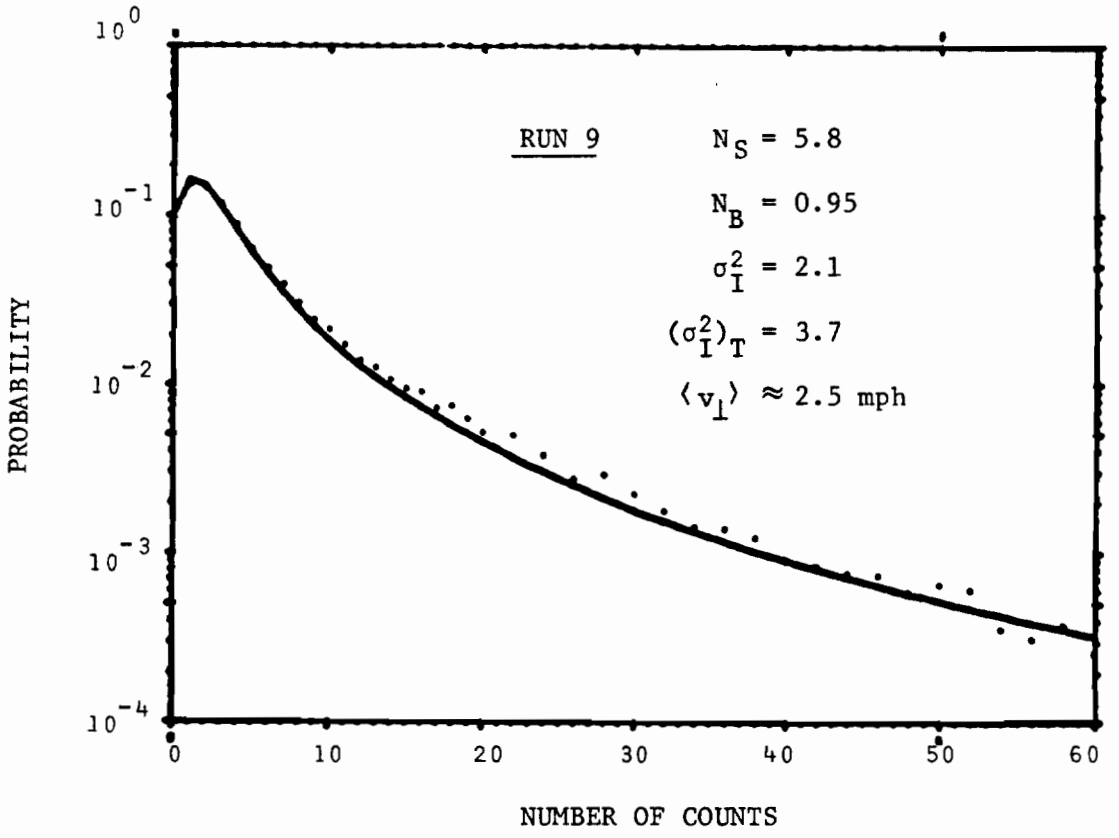

Figure 47. Probability density function for photoelectron counts.

Dots give the experimentally measured values.
Solid line gives the theoretical curve.

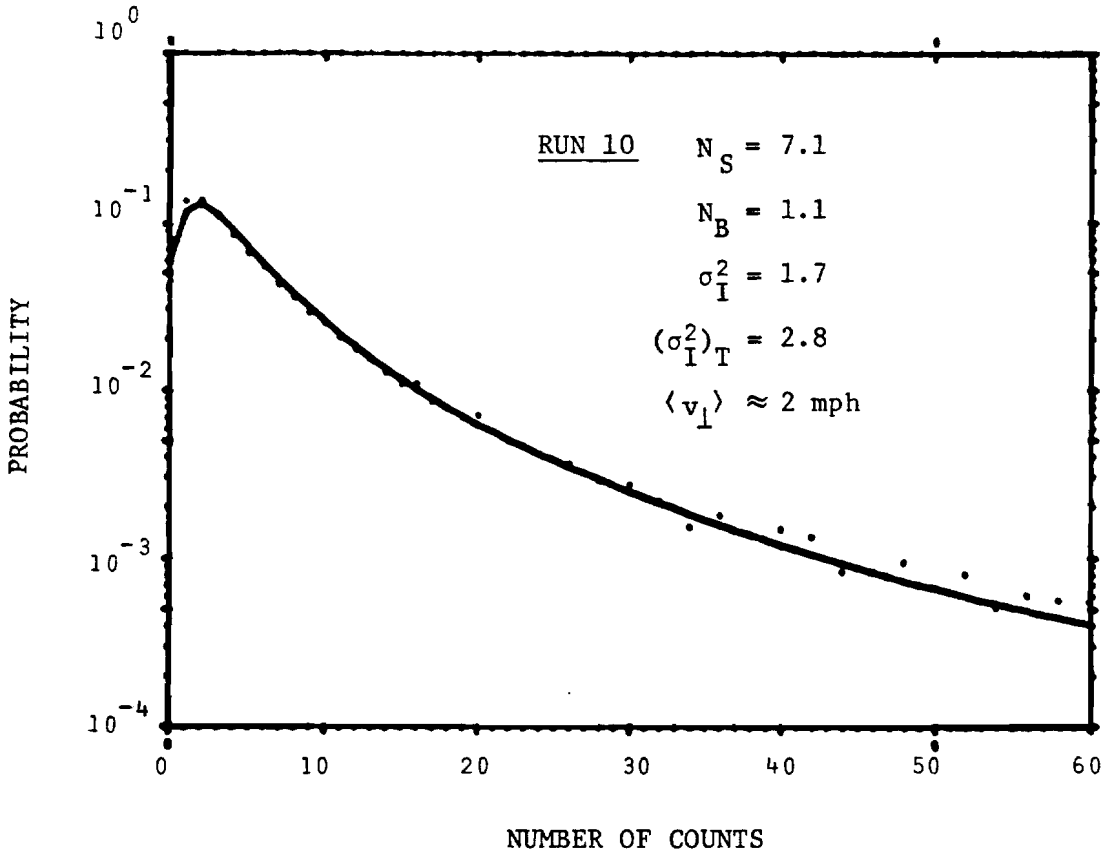

Figure 48. Probability density function for photoelectron counts.

Dots give the experimentally measured values.
Solid line gives the theoretical curve.

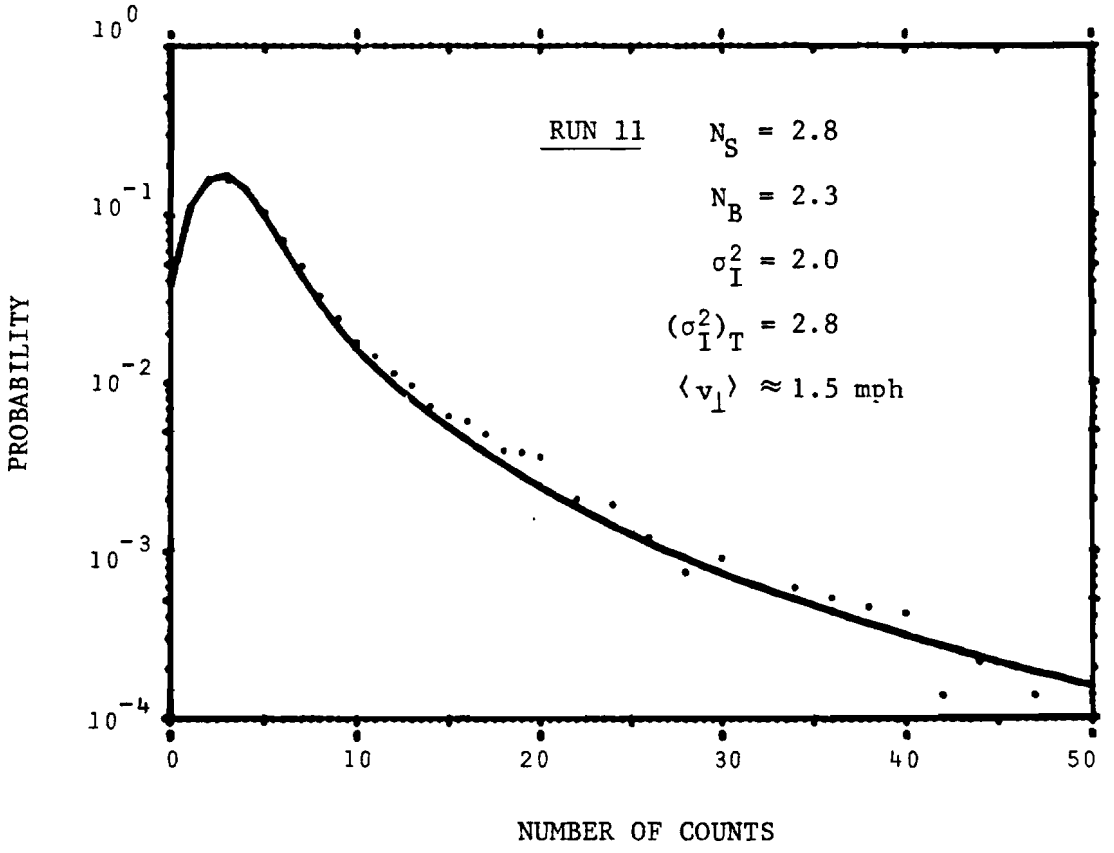

Figure 49. Probability density function for photoelectron counts.

Dots give the experimentally measured values.
Solid line gives the theoretical curve.

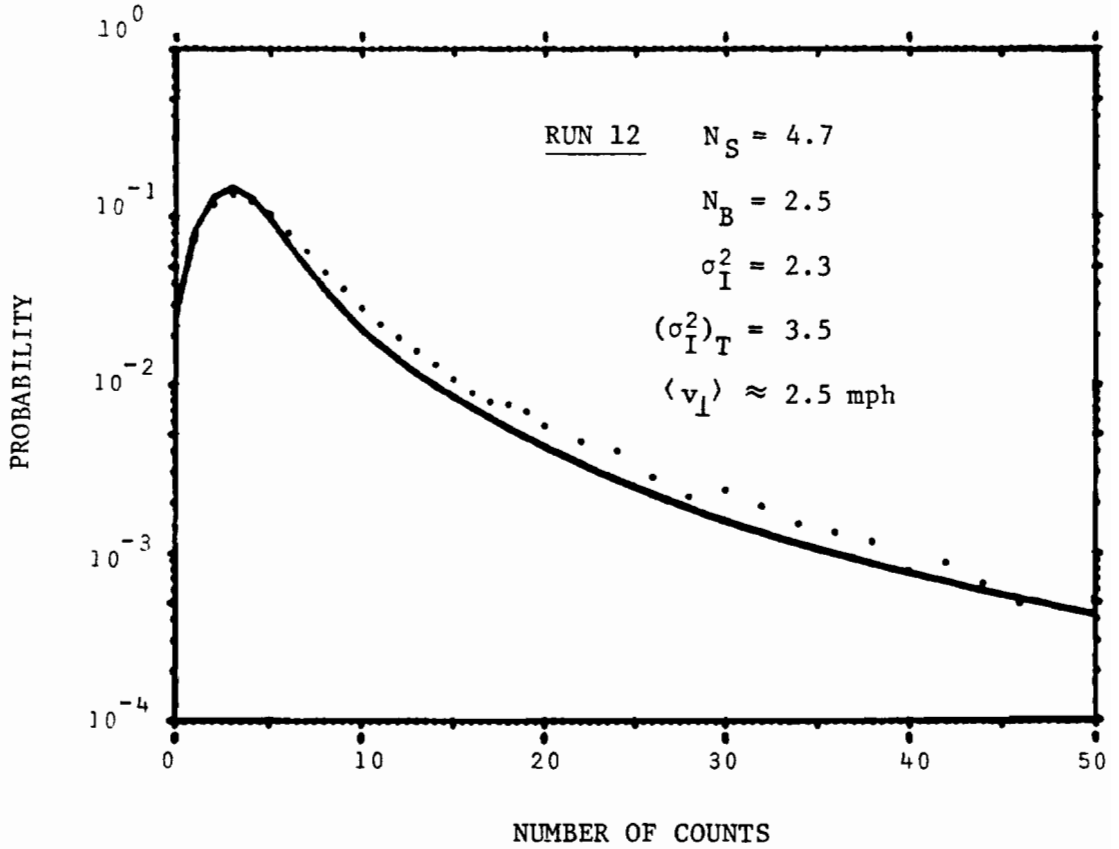

Figure 50. Probability density function for photoelectron counts.

Dots give the experimentally measured values.
Solid line gives the theoretical curve.

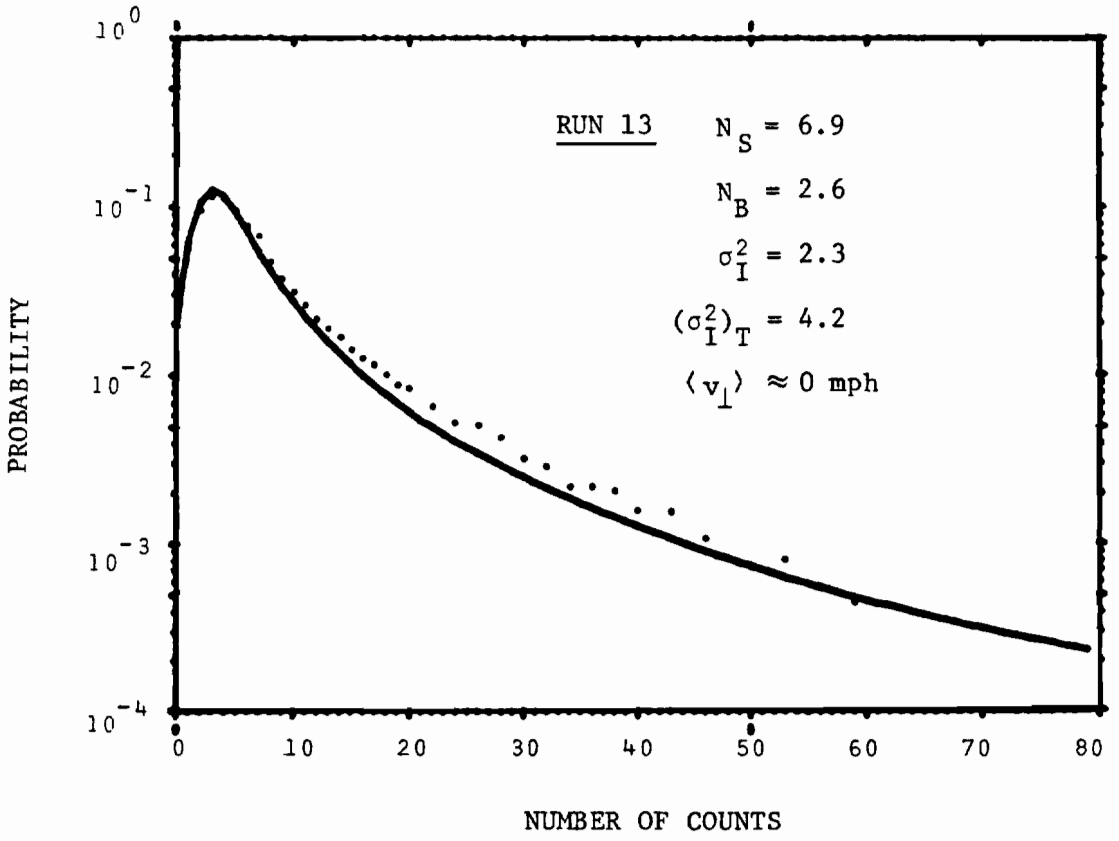

Figure 51. Probability density function for photoelectron counts.

Dots give the experimentally measured values.
Solid line gives the theoretical curve.

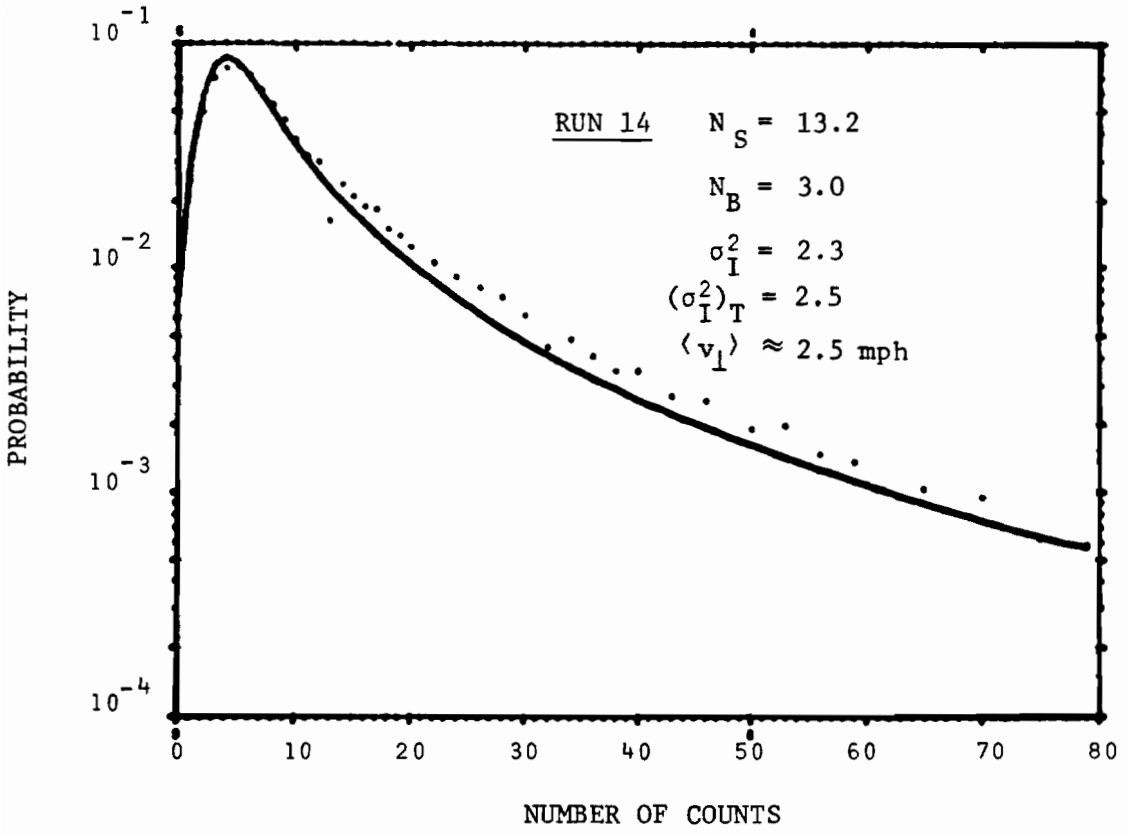

Figure 52. Probability density function for photoelectron counts.

Dots give the experimentally measured values.
Solid line gives the theoretical curve.

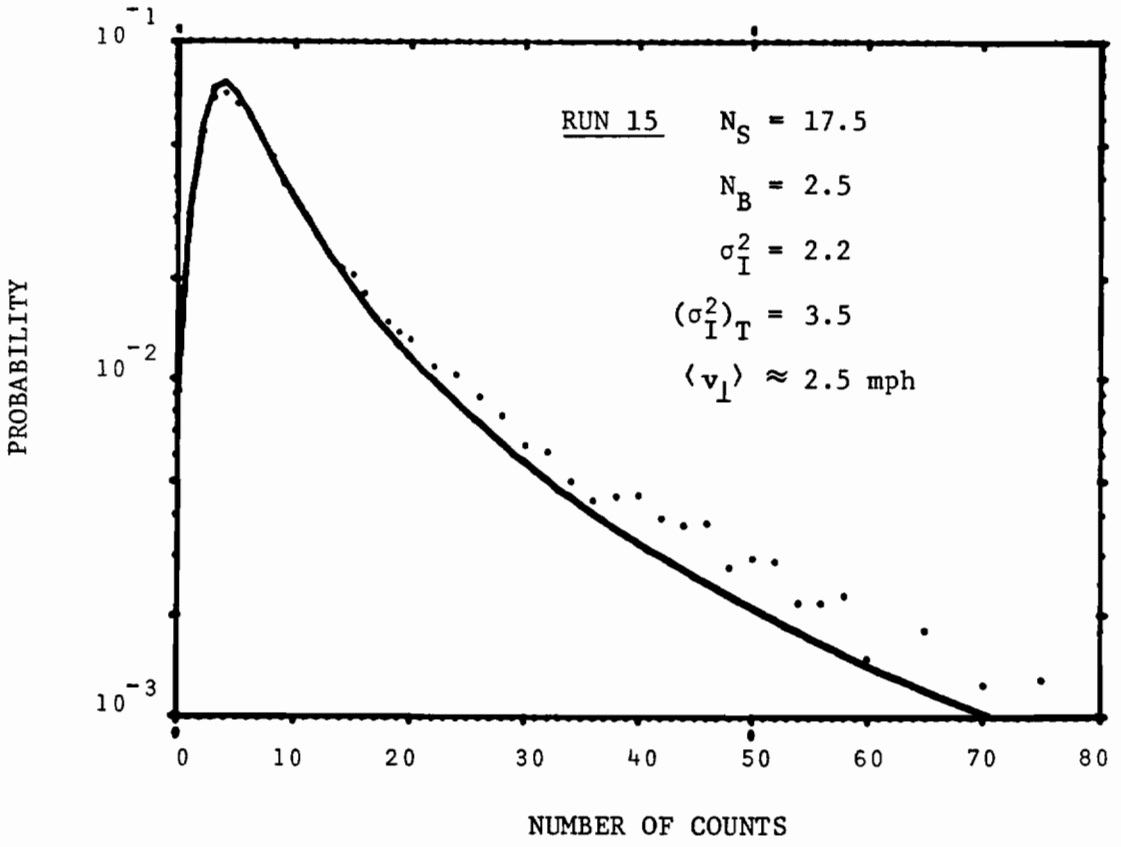

Figure 53. Probability density function for photoelectron counts.

Dots give the experimentally measured values.
Solid line gives the theoretical curve.

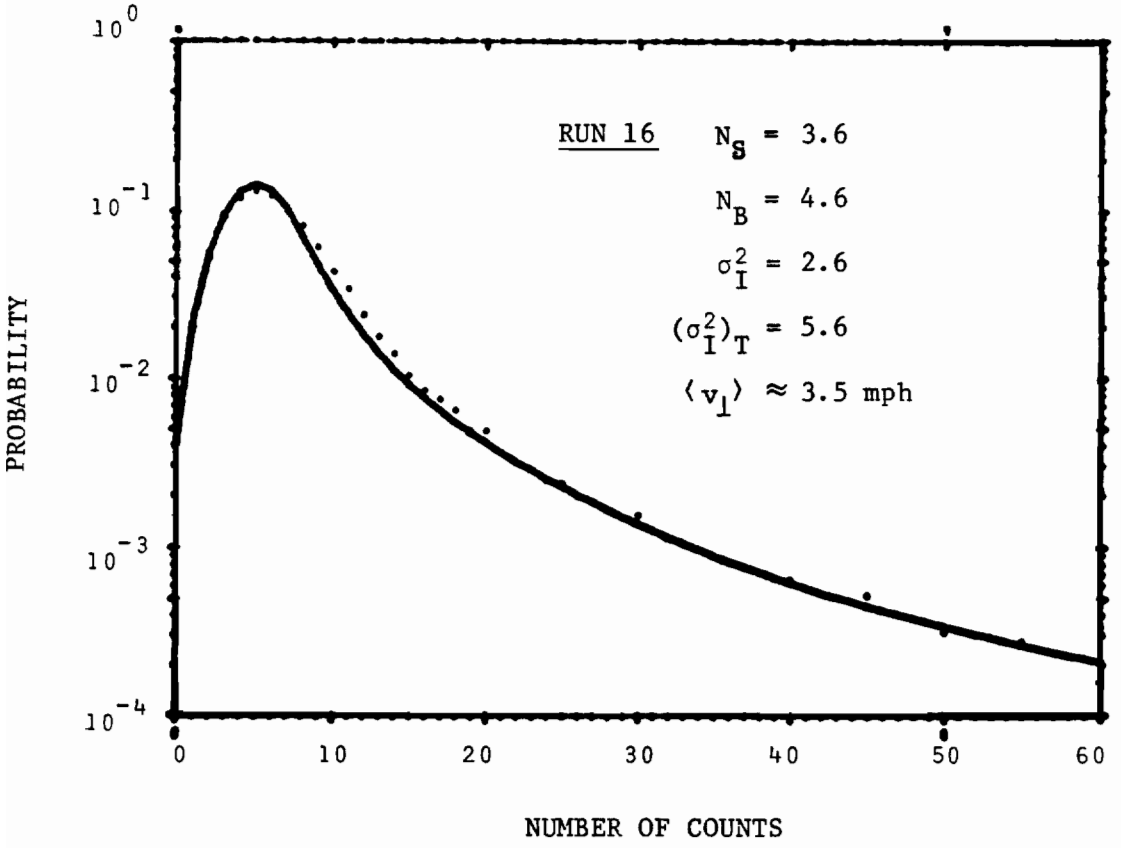

Figure 54. Probability density function for photoelectron counts.

Dots give the experimentally measured values.
Solid line gives the theoretical curve.

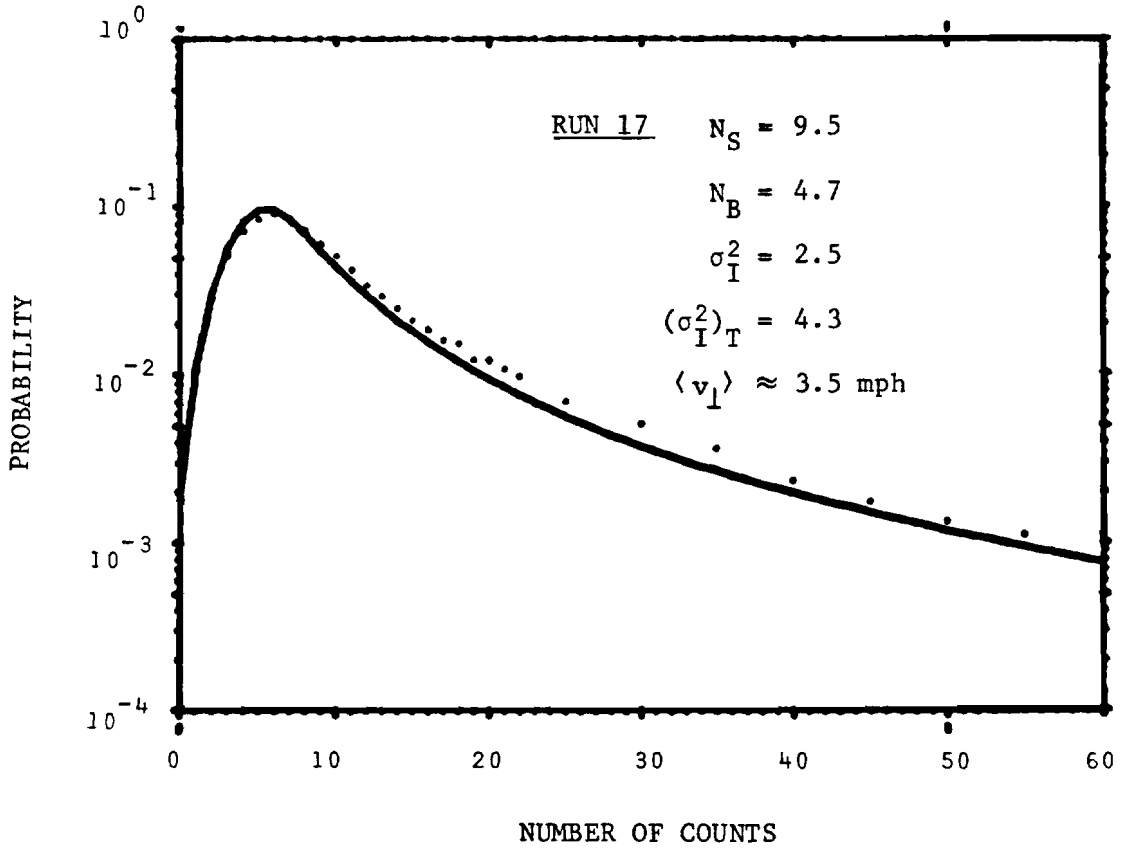

Figure 55. Probability density function for photoelectron counts.

Dots give the experimentally measured values.
Solid line gives the theoretical curve.

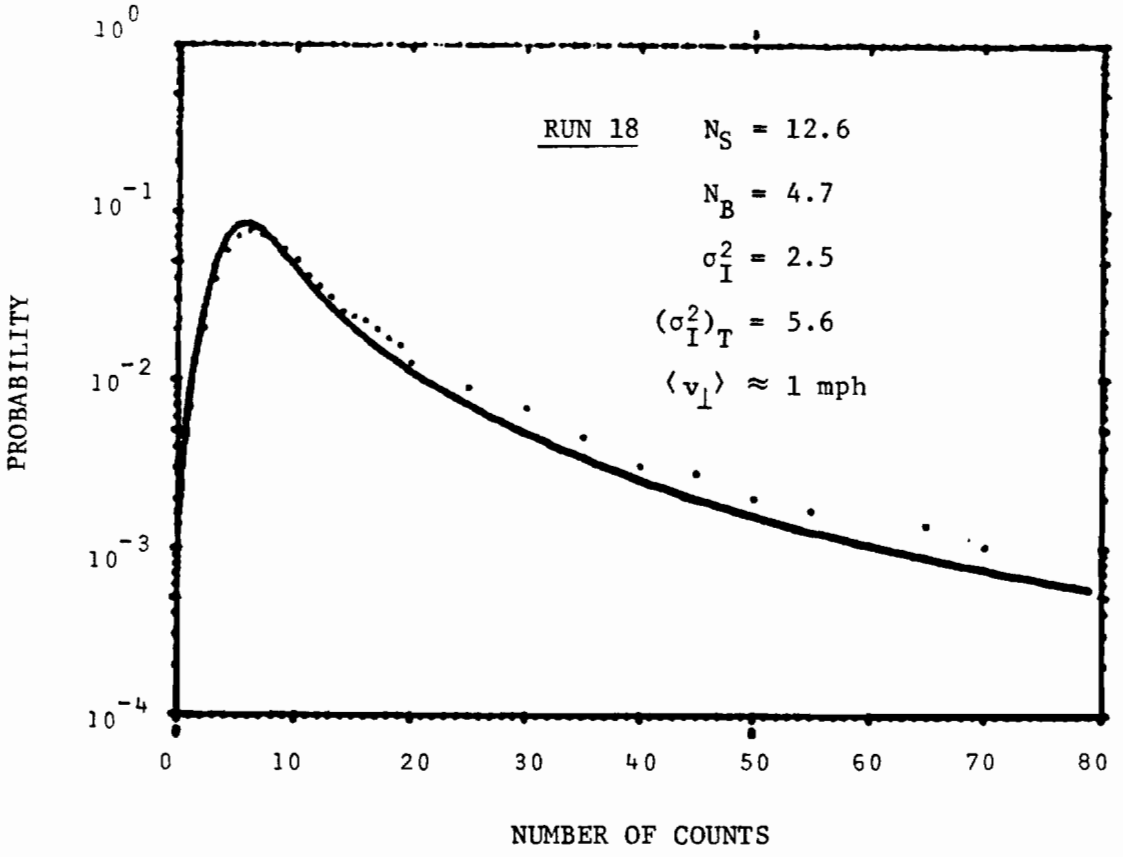

Figure 56. Probability density function for photoelectron counts.

Dots give the experimentally measured values.
Solid line gives the theoretical curve.

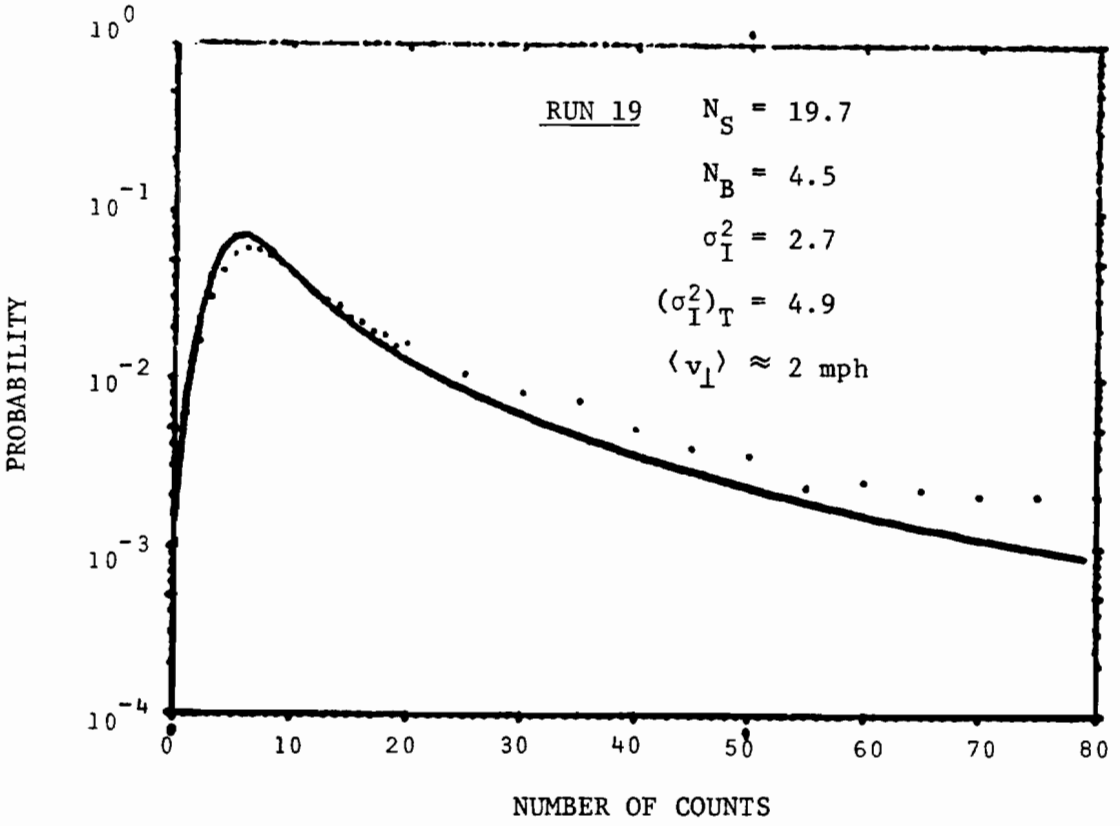

Figure 57. Probability density function for photoelectron counts.

Dots give the experimentally measured values.
Solid line gives the theoretical curve.

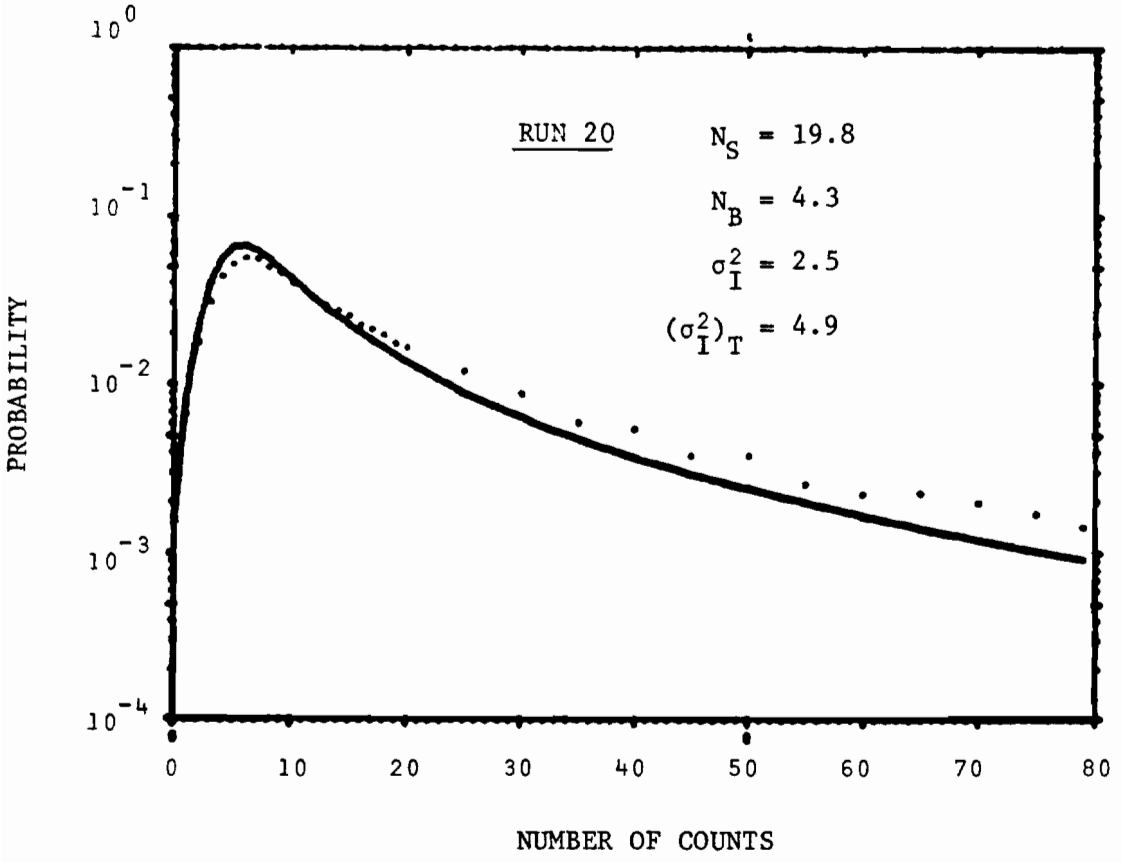

Figure 58. Probability density function for photoelectron counts.

Dots give the experimentally measured values.
Solid line gives the theoretical curve.

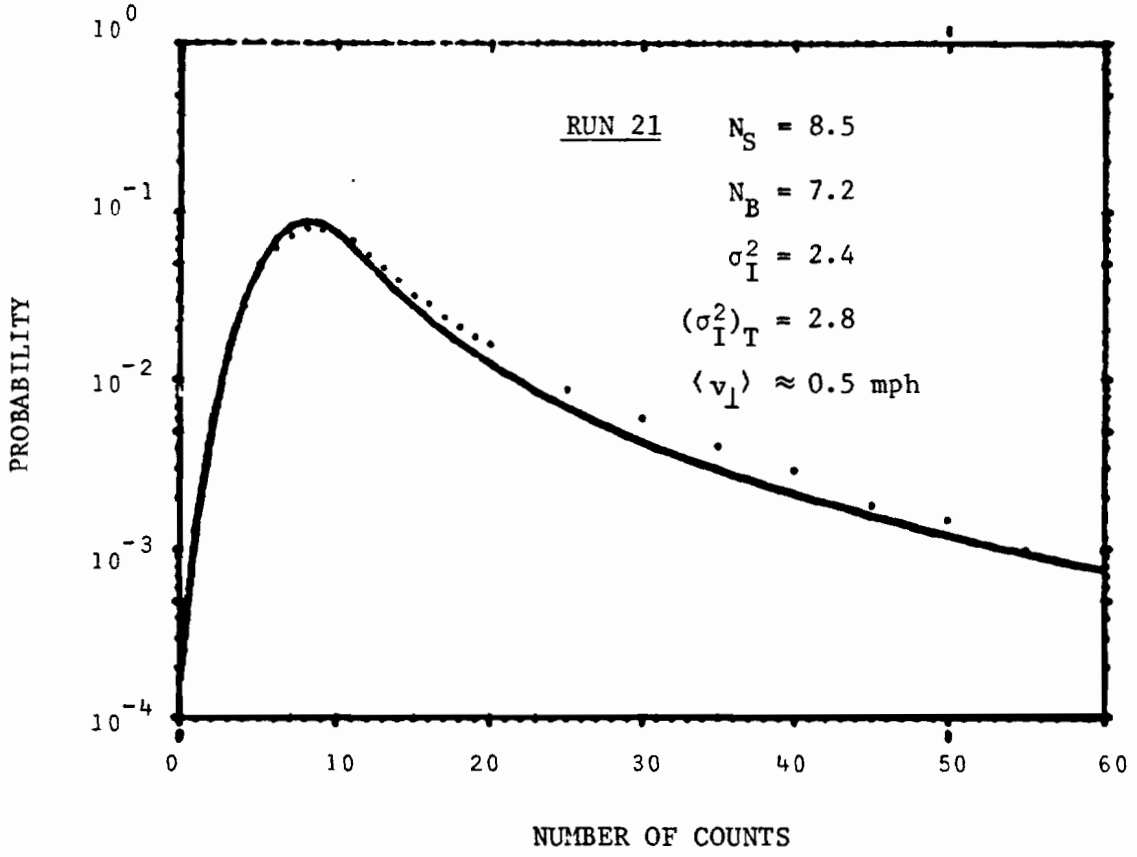

Figure 59. Probability density function for photoelectron counts.

Dots give the experimentally measured values.
Solid line gives the theoretical curve.

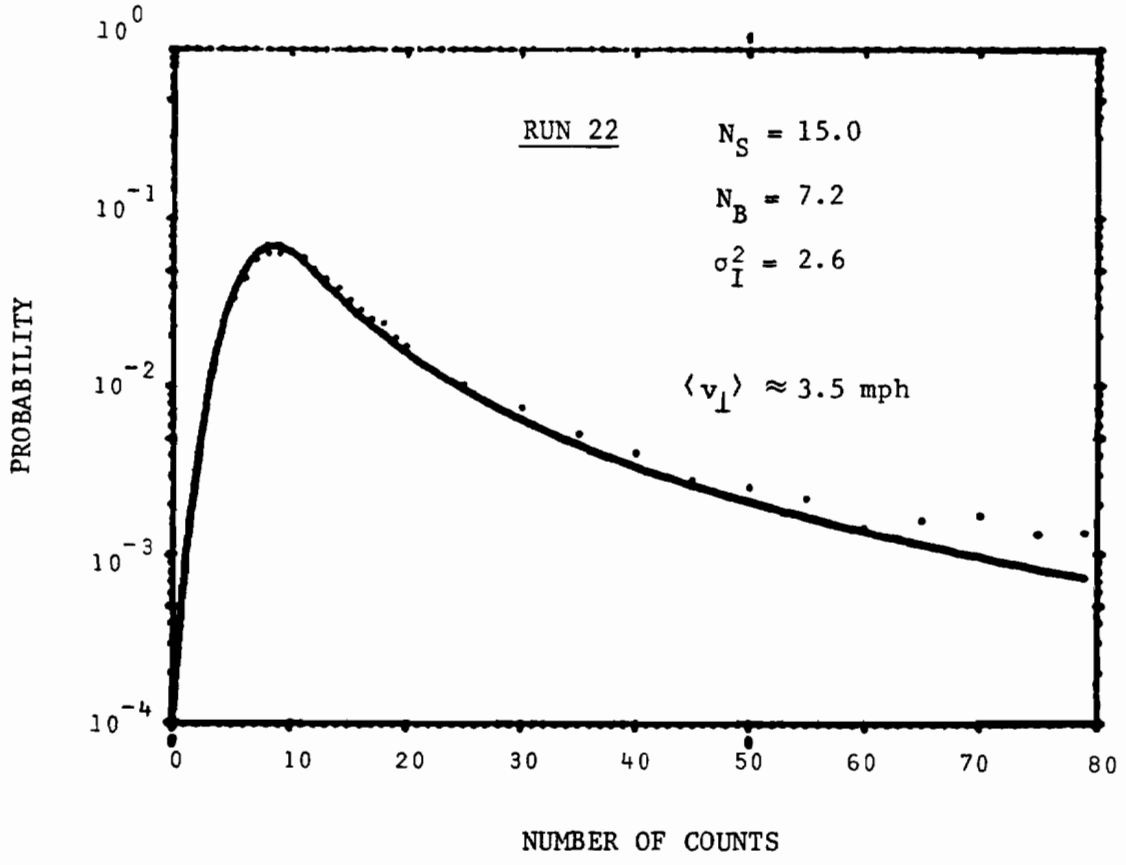

Figure 60. Probability density function for photoelectron counts.

Dots give the experimentally measured values.
Solid line gives the theoretical curve.

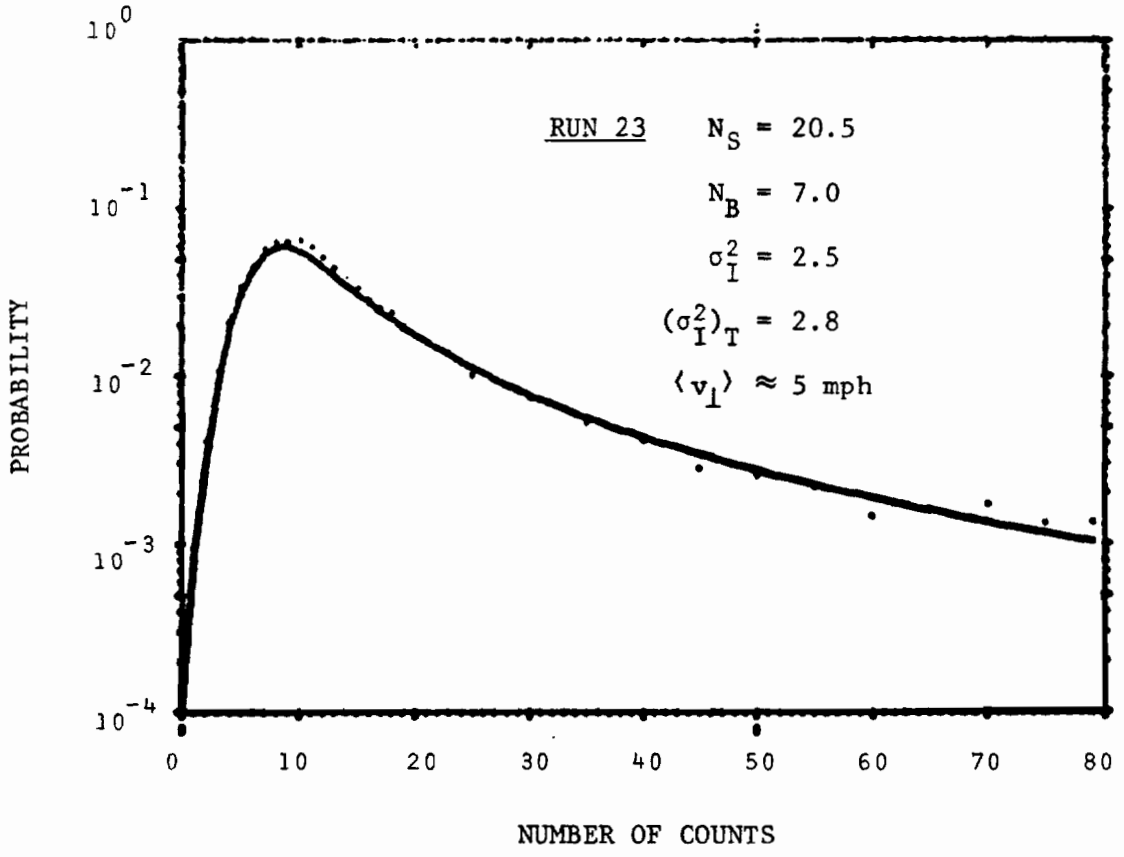

Figure 61. Probability density function for photoelectron counts.

Dots give the experimentally measured values.
Solid line gives the theoretical curve.

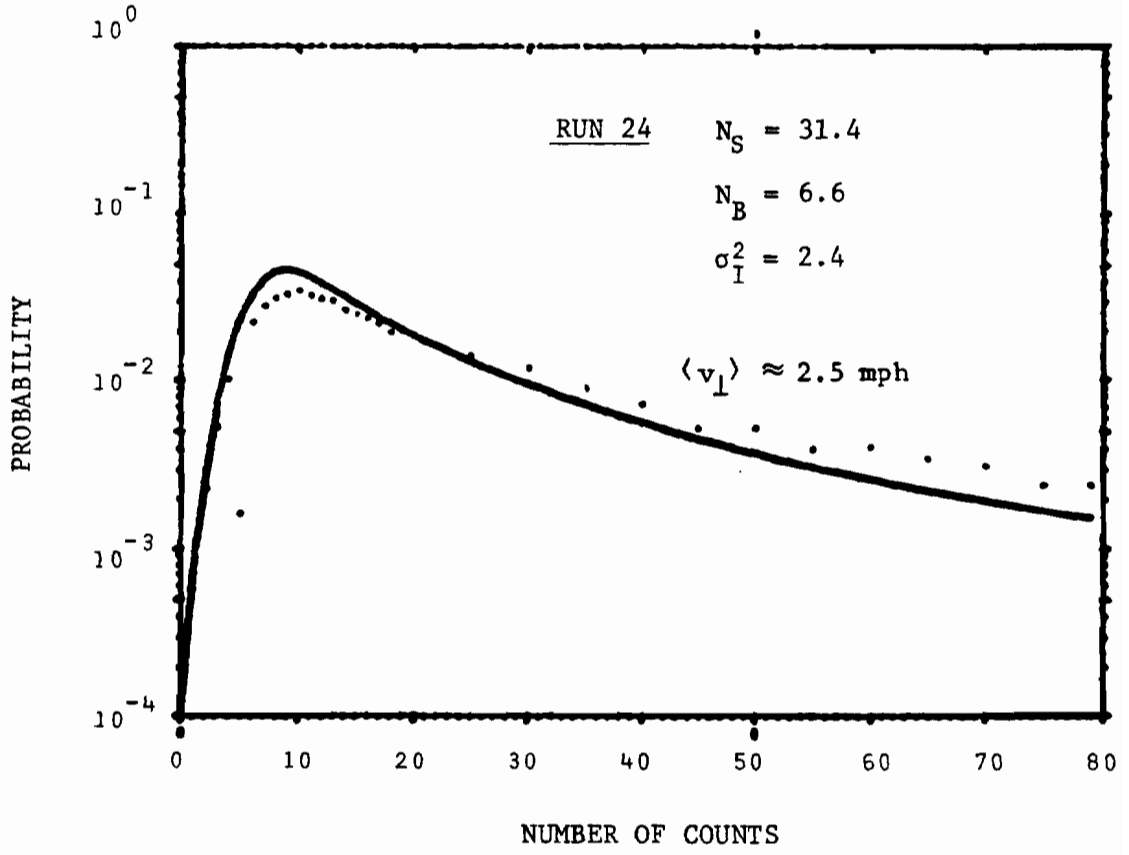

Figure 62. Probability density function for photoelectron counts.

Dots give the experimentally measured values.
Solid line gives the theoretical curve.

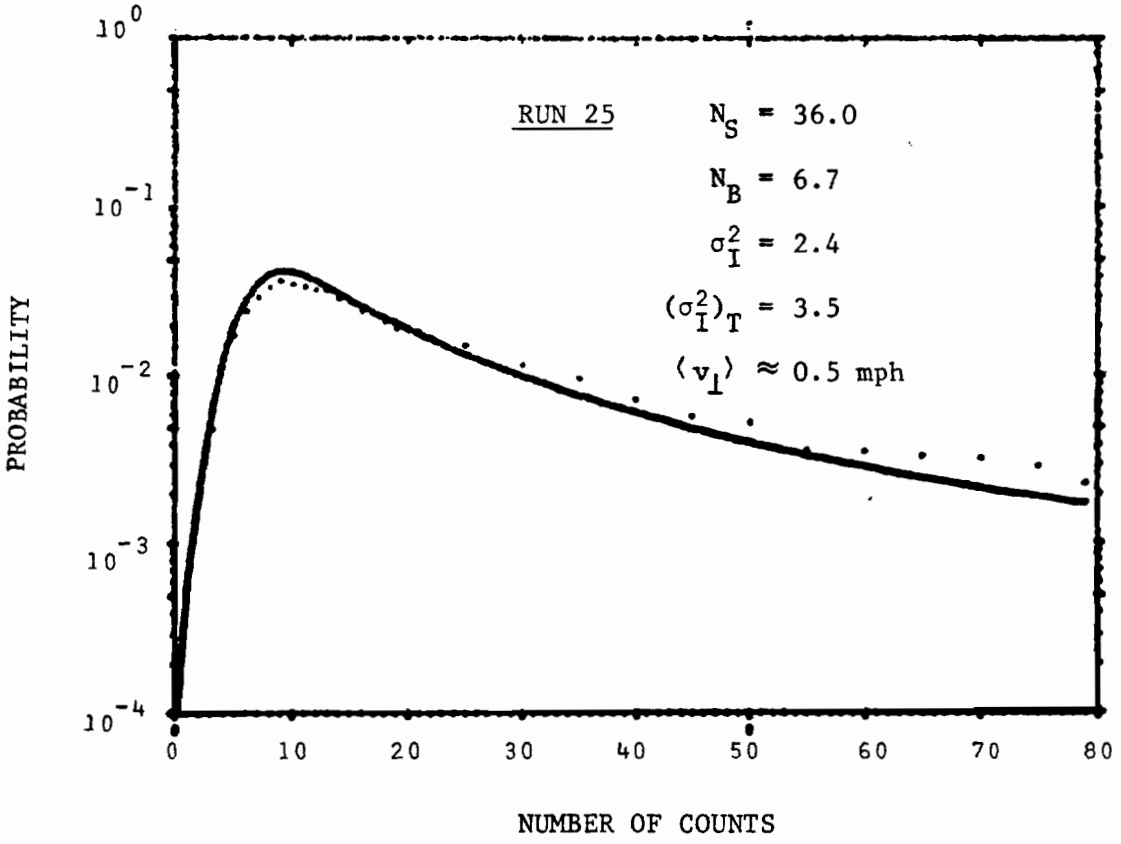

Figure 63. Probability density function for photoelectron counts.

Dots give the experimentally measured values.
Solid line gives the theoretical curve.

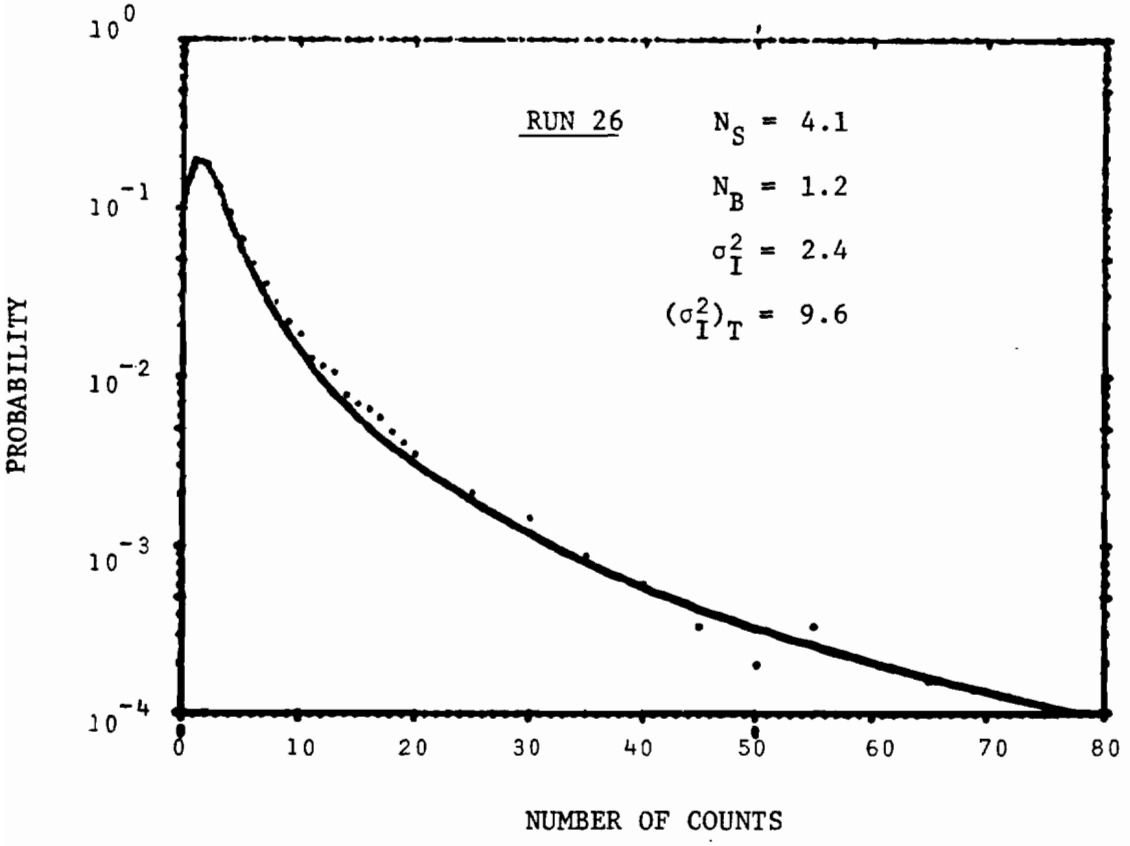

Figure 64. Probability density function for photoelectron counts.

Dots give the experimentally measured values.
Solid line gives the theoretical curve.

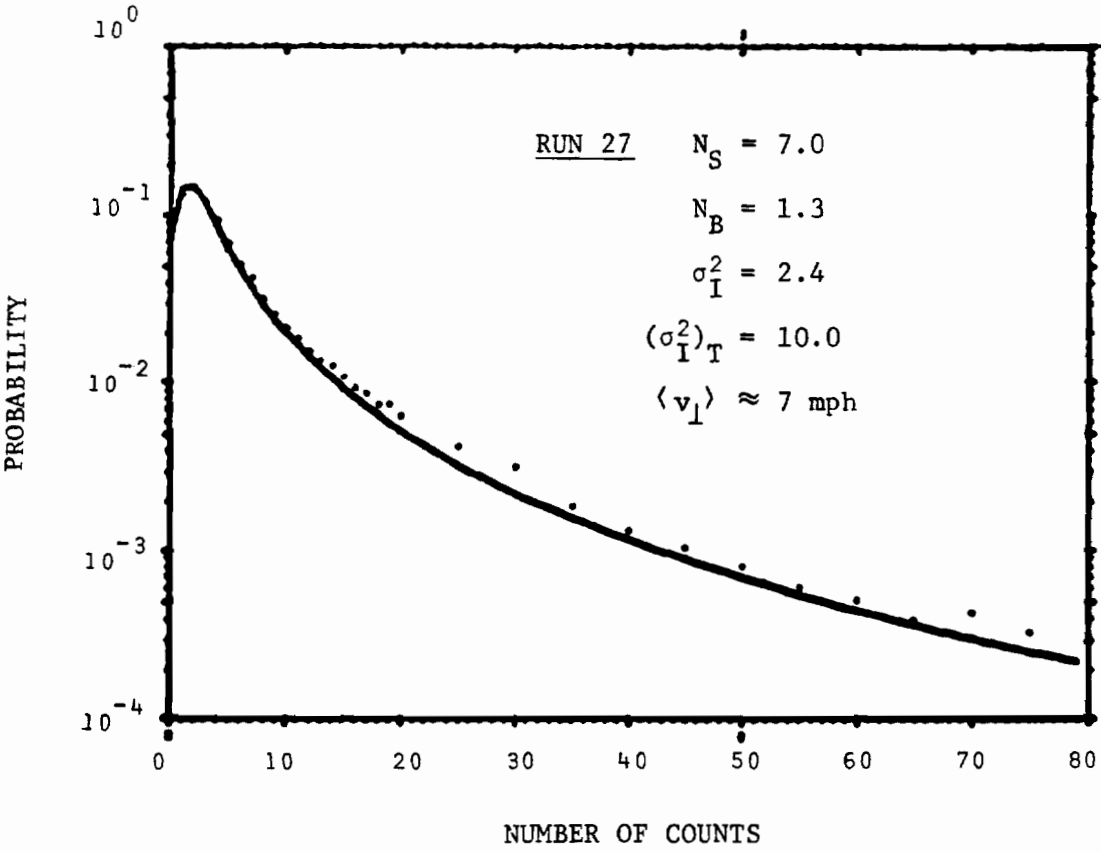

Figure 65. Probability density function for photoelectron counts.

Dots give the experimentally measured values.
Solid line gives the theoretical curve.

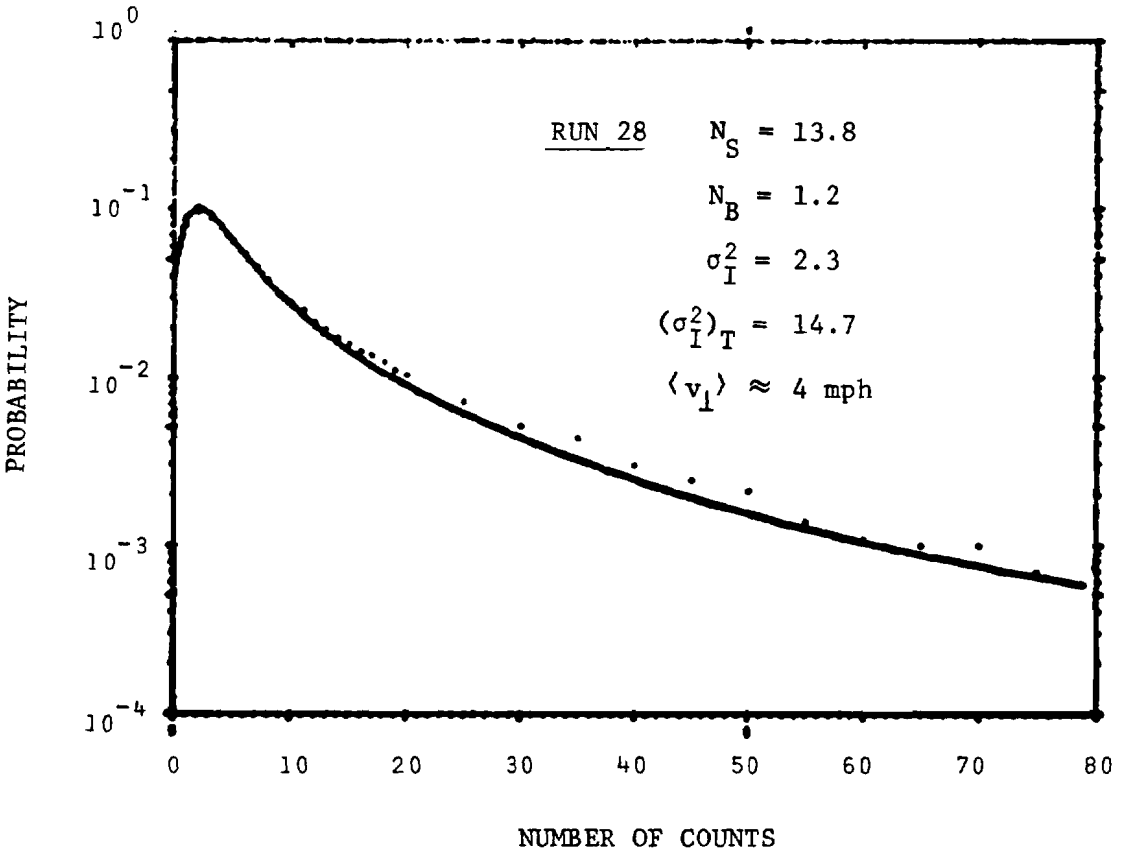

Figure 66. Probability density function for photoelectron counts.

Dots give the experimentally measured values.
Solid line gives the theoretical curve.

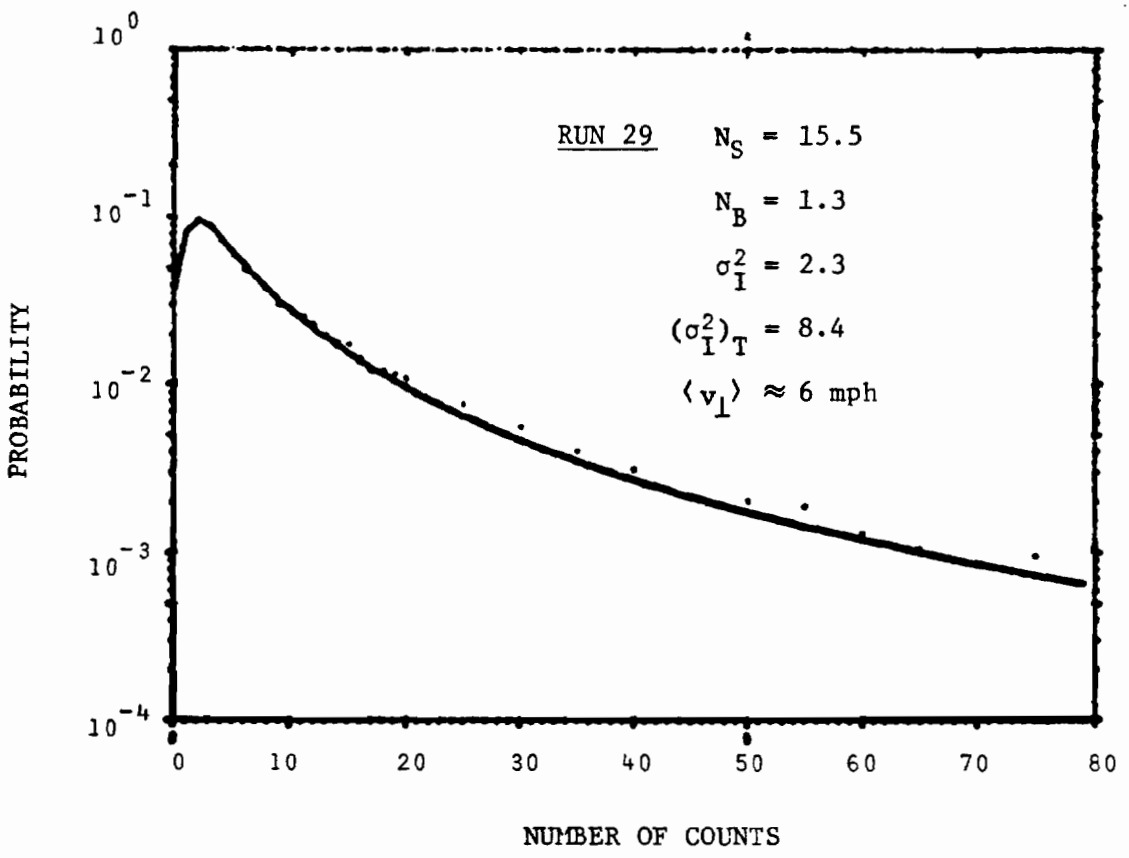

Figure 67. Probability density function for photoelectron counts.

Dots give the experimentally measured values.
Solid line gives the theoretical curve.

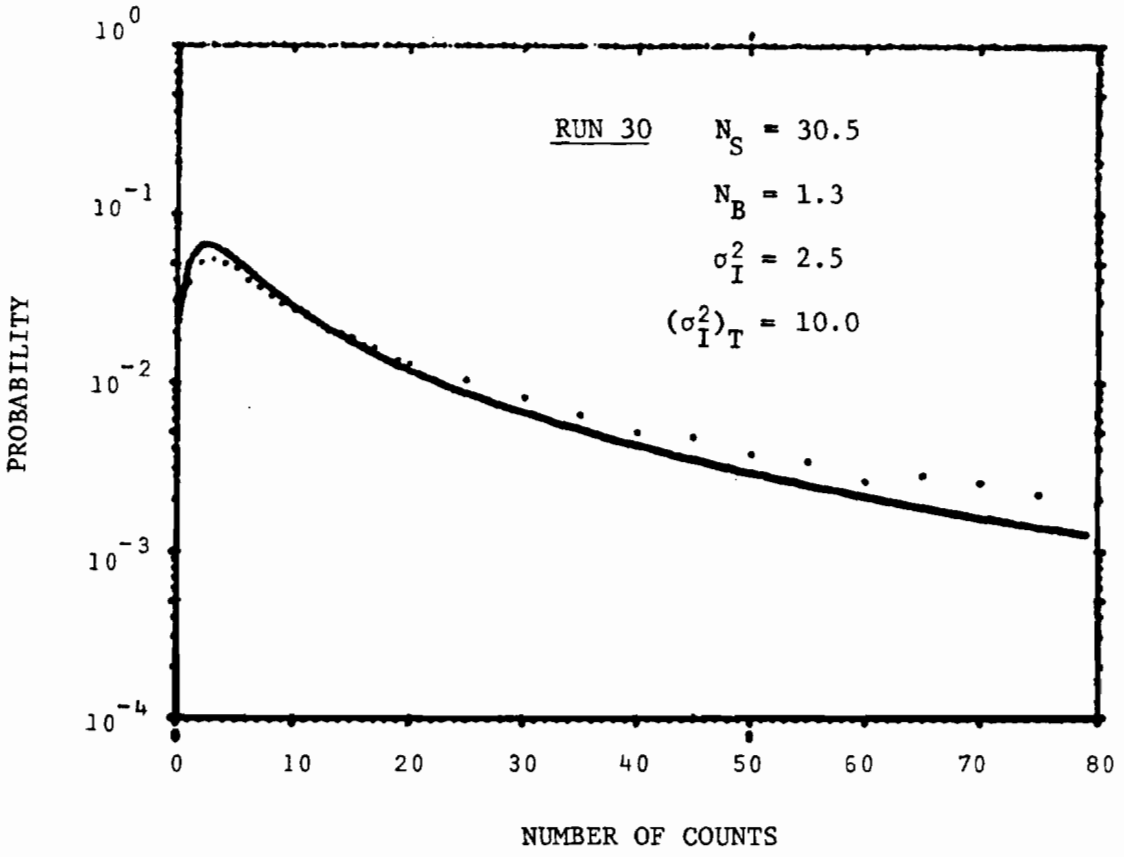

Figure 68. Probability density function for photoelectron counts.

Dots give the experimentally measured values.
Solid line gives the theoretical curve.

TABLE VIII-A

EXPERIMENTALLY DETERMINED PROBABILITIES FOR PHOTON COUNTS

RUN 31

(N_S = 12.4, N_B = 2.2, σ_I^2 = 2.3, $(\sigma_I^2)_T$ = 10.5, $\langle v_\perp \rangle \simeq$ 5 mph.)

Count	Probability	Count	Probability	Count	Probability
0	0.187 E-1	36	0.326 E-2	72	0.742 E-3
1	0.519 E-1	37	0.322 E-2	73	0.781 E-3
2	0.796 E-1	38	0.283 E-2	74	0.957 E-3
3	0.920 E-1	39	0.262 E-2	75	0.430 E-3
4	0.875 E-1	40	0.283 E-2	76	0.645 E-3
5	0.801 E-1	41	0.223 E-2	77	0.352 E-3
6	0.650 E-1	42	0.248 E-2	78	0.586 E-3
7	0.527 E-1	43	0.244 E-2	79	0.371 E-3
8	0.436 E-1	44	0.215 E-2	80	0.469 E-3
9	0.383 E-1	45	0.217 E-2	81	0.410 E-3
10	0.316 E-1	46	0.209 E-2	82	0.430 E-3
11	0.293 E-1	47	0.197 E-2	83	0.703 E-3
12	0.245 E-1	48	0.176 E-2	84	0.430 E-3
13	0.212 E-1	49	0.164 E-2	85	0.496 E-3
14	0.205 E-1	50	0.164 E-2	86	0.410 E-3
15	0.171 E-1	51	0.150 E-2	87	0.430 E-3
16	0.157 E-1	52	0.148 E-2	88	0.430 E-3
17	0.141 E-1	53	0.152 E-2	89	0.449 E-3
18	0.138 E-1	54	0.150 E-2	90	0.527 E-3
19	0.114 E-1	55	0.129 E-2	91	0.430 E-3
20	0.104 E-1	56	0.977 E-3	92	0.293 E-3
21	0.945 E-2	57	0.141 E-2	93	0.449 E-3
22	0.854 E-2	58	0.146 E-2	94	0.352 E-3
23	0.928 E-2	59	0.113 E-2	95	0.293 E-3
24	0.729 E-2	60	0.137 E-2	96	0.352 E-3
25	0.652 E-2	61	0.937 E-3	97	0.469 E-3
26	0.646 E-2	62	0.918 E-3	98	0.332 E-3
27	0.637 E-2	63	0.820 E-3	99	0.312 E-3
28	0.504 E-2	64	0.801 E-3	100	0.430 E-3
29	0.549 E-2	65	0.996 E-3	101	0.293 E-3
30	0.486 E-2	66	0.918 E-3	102	0.371 E-3
31	0.391 E-2	67	0.104 E-2	103	0.391 E-3
32	0.463 E-2	68	0.937 E-3	104	0.469 E-3
33	0.437 E-2	69	0.527 E-3	105	0.332 E-3
34	0.398 E-2	70	0.879 E-3	106	0.215 E-3
35	0.381 E-2	71	0.918 E-3	107	0.195 E-3

TABLE VIII-A, Continued

Count	Probability	Count	Probability	Count	Probability
108	0.273 E-3	122	0.234 E-3	136	0.273 E-3
109	0.273 E-3	123	0.137 E-3	137	0.293 E-3
110	0.391 E-3	124	0.156 E-3	138	0.195 E-3
111	0.215 E-3	125	0.332 E-3	139	0.234 E-3
112	0.352 E-3	126	0.137 E-3	140	0.254 E-3
113	0.273 E-3	127	0.234 E-3	141	0.176 E-3
114	0.312 E-3	128	0.273 E-3	142	0.312 E-3
115	0.273 E-3	129	0.215 E-3	143	0.273 E-3
116	0.391 E-3	130	0.254 E-3	144	0.723 E-2*
117	0.234 E-3	131	0.117 E-3	145	0.000 E 0
118	0.234 E-3	132	0.293 E-3	146	0.000 E 0
119	0.254 E-3	133	0.117 E-3	147	0.000 E 0
120	0.312 E-3	134	0.215 E-3	148	0.000 E 0
121	0.117 E-3	135	0.293 E-3	149	0.000 E 0

*See Appendix D.

TABLE VIII-B

EXPERIMENTALLY DETERMINED PROBABILITIES FOR PHOTON COUNTS

RUN 32

(N_S = 25.3, N_B = 1.9, σ_I^2 = 2.2, $(\sigma_I^2)_T$ = 7.6, $\langle v_\perp \rangle \simeq$ 7 mph.)

Count	Probability	Count	Probability	Count	Probability
0	0.113 E-1	36	0.596 E-2	72	0.195 E-2
1	0.299 E-1	37	0.561 E-2	73	0.170 E-2
2	0.460 E-1	38	0.582 E-2	74	0.143 E-2
3	0.569 E-1	39	0.455 E-2	75	0.166 E-2
4	0.581 E-1	40	0.510 E-2	76	0.164 E-2
5	0.545 E-1	41	0.473 E-2	77	0.148 E-2
6	0.490 E-1	42	0.512 E-2	78	0.154 E-2
7	0.431 E-1	43	0.410 E-2	79	0.162 E-2
8	0.377 E-1	44	0.389 E-2	80	0.141 E-2
9	0.363 E-1	45	0.424 E-2	81	0.143 E-2
10	0.316 E-1	46	0.428 E-2	82	0.129 E-2
11	0.287 E-1	47	0.373 E-2	83	0.162 E-2
12	0.260 E-1	48	0.322 E-2	84	0.107 E-2
13	0.221 E-1	49	0.348 E-2	85	0.113 E-2
14	0.214 E-1	50	0.332 E-2	86	0.801 E-3
15	0.204 E-1	51	0.314 E-2	87	0.137 E-2
16	0.190 E-1	52	0.289 E-2	88	0.133 E-2
17	0.173 E-1	53	0.299 E-2	89	0.133 E-2
18	0.153 E-1	54	0.295 E-2	90	0.109 E-2
19	0.148 E-1	55	0.299 E-2	91	0.115 E-2
20	0.139 E-1	56	0.283 E-2	92	0.105 E-2
21	0.131 E-1	57	0.289 E-2	93	0.129 E-2
22	0.128 E-1	58	0.262 E-2	94	0.918 E-3
23	0.111 E-1	59	0.209 E-2	95	0.104 E-2
24	0.961 E-2	60	0.189 E-2	96	0.113 E-2
25	0.108 E-1	61	0.244 E-2	97	0.625 E-3
26	0.947 E-2	62	0.238 E-2	98	0.957 E-3
27	0.957 E-2	63	0.273 E-2	99	0.977 E-3
28	0.885 E-2	64	0.187 E-2	100	0.820 E-3
29	0.824 E-2	65	0.229 E-2	101	0.918 E-3
30	0.852 E-2	66	0.193 E-2	102	0.840 E-3
31	0.684 E-2	67	0.209 E-2	103	0.996 E-3
32	0.709 E-2	68	0.184 E-2	104	0.879 E-3
33	0.645 E-2	69	0.189 E-2	105	0.820 E-3
34	0.707 E-2	70	0.164 E-2	106	0.664 E-3
35	0.617 E-2	71	0.189 E-2	107	0.625 E-3

TABLE VIII-B, Continued

Count	Probability	Count	Probability	Count	Probability
108	0.898 E-3	122	0.664 E-3	136	0.684 E-3
109	0.742 E-3	123	0.645 E-3	137	0.762 E-3
110	0.723 E-3	124	0.527 E-3	138	0.762 E-3
111	0.547 E-3	125	0.488 E-3	139	0.918 E-3
112	0.645 E-3	126	0.547 E-3	140	0.102 E-2
113	0.645 E-3	127	0.430 E-3	141	0.107 E-2
114	0.781 E-3	128	0.547 E-3	142	0.125 E-2
115	0.664 E-3	129	0.645 E-3	143	0.127 E-2
116	0.547 E-3	130	0.527 E-3	144	0.265 E-1*
117	0.508 E-3	131	0.781 E-3	145	0.000 E 0
118	0.547 E-3	132	0.430 E-3	146	0.000 E 0
119	0.605 E-3	133	0.449 E-3	147	0.000 E 0
120	0.566 E-3	134	0.723 E-3	148	0.000 E 0
121	0.488 E-3	135	0.547 E-3	149	0.000 E 0

*See Appendix D.

TABLE VIII-C

EXPERIMENTALLY DETERMINED PROBABILITIES FOR PHOTON COUNTS

RUN 33

(N_S = 31.0, N_B = 1.7, σ_I^2 = 2.3, $(\sigma_I^2)_T$ = 7.0, $\langle v_\perp \rangle \simeq 7$ mph.)

Count	Probability	Count	Probability	Count	Probability
0	0.119 E-1	36	0.652 E-2	72	0.201 E-2
1	0.306 E-1	37	0.582 E-2	73	0.170 E-2
2	0.440 E-1	38	0.613 E-2	74	0.213 E-2
3	0.507 E-1	39	0.512 E-2	75	0.211 E-2
4	0.466 E-1	40	0.535 E-2	76	0.221 E-2
5	0.466 E-1	41	0.535 E-2	77	0.189 E-2
6	0.417 E-1	42	0.521 E-2	78	0.158 E-2
7	0.380 E-1	43	0.520 E-2	79	0.211 E-2
8	0.328 E-1	44	0.508 E-2	80	0.217 E-2
9	0.308 E-1	45	0.482 E-2	81	0.131 E-2
10	0.306 E-1	46	0.400 E-2	82	0.168 E-2
11	0.258 E-1	47	0.385 E-2	83	0.191 E-2
12	0.233 E-1	48	0.402 E-2	84	0.154 E-2
13	0.209 E-1	49	0.408 E-2	85	0.215 E-2
14	0.198 E-1	50	0.400 E-2	86	0.170 E-2
15	0.172 E-1	51	0.377 E-2	87	0.162 E-2
16	0.187 E-1	52	0.367 E-2	88	0.162 E-2
17	0.149 E-1	53	0.357 E-2	89	0.156 E-2
18	0.153 E-1	54	0.311 E-2	90	0.160 E-2
19	0.143 E-1	55	0.299 E-2	91	0.143 E-2
20	0.151 E-1	56	0.324 E-2	92	0.164 E-2
21	0.137 E-1	57	0.307 E-2	93	0.146 E-2
22	0.121 E-1	58	0.285 E-2	94	0.150 E-2
23	0.115 E-1	59	0.301 E-2	95	0.117 E-2
24	0.104 E-1	60	0.316 E-2	96	0.146 E-2
25	0.111 E-1	61	0.295 E-2	97	0.139 E-2
26	0.842 E-2	62	0.289 E-2	98	0.127 E-2
27	0.943 E-2	63	0.266 E-2	99	0.996 E-3
28	0.932 E-2	64	0.256 E-2	100	0.137 E-2
29	0.832 E-2	65	0.309 E-2	101	0.125 E-2
30	0.828 E-2	66	0.234 E-2	102	0.127 E-2
31	0.721 E-2	67	0.242 E-2	103	0.137 E-2
32	0.805 E-2	68	0.223 E-2	104	0.117 E-2
33	0.707 E-2	69	0.209 E-2	105	0.111 E-2
34	0.660 E-2	70	0.234 E-2	106	0.111 E-2
35	0.664 E-2	71	0.221 E-2	107	0.164 E-2

TABLE VIII-C, Continued

Count	Probability	Count	Probability	Count	Probability
108	0.111 E-2	122	0.918 E-3	136	0.109 E-2
109	0.104 E-2	123	0.840 E-3	137	0.121 E-2
110	0.111 E-2	124	0.104 E-2	138	0.117 E-2
111	0.937 E-3	125	0.937 E-3	139	0.170 E-2
112	0.129 E-2	126	0.742 E-3	140	0.156 E-2
113	0.107 E-2	127	0.781 E-3	141	0.186 E-2
114	0.996 E-3	128	0.820 E-3	142	0.176 E-2
115	0.898 E-3	129	0.859 E-3	143	0.273 E-2
116	0.127 E-2	130	0.107 E-2	144	0.405 E-1*
117	0.859 E-3	131	0.898 E-3	145	0.000 E 0
118	0.109 E-2	132	0.820 E-3	146	0.000 E 0
119	0.801 E-3	133	0.996 E-3	147	0.000 E 0
120	0.957 E-3	134	0.801 E-3	148	0.000 E 0
121	0.840 E-3	135	0.109 E-2	149	0.000 E 0

*See Appendix D.

TABLE VIII-D

EXPERIMENTALLY DETERMINED PROBABILITIES FOR PHOTON COUNTS

RUN 34

(N_S = 41.0, N_B = 1.6, σ_I^2 = 2.1, $(\sigma_I^2)_T$ = 2.6, $\langle v_\perp \rangle \simeq$ 5 mph.)

Count	Probability	Count	Probability	Count	Probability
0	0.736 E-2	36	0.715 E-2	72	0.285 E-2
1	0.178 E-1	37	0.779 E-2	73	0.307 E-2
2	0.292 E-1	38	0.686 E-2	74	0.316 E-2
3	0.344 E-1	39	0.691 E-2	75	0.293 E-2
4	0.321 E-1	40	0.713 E-2	76	0.291 E-2
5	0.322 E-1	41	0.631 E-2	77	0.217 E-2
6	0.302 E-1	42	0.633 E-2	78	0.250 E-2
7	0.285 E-1	43	0.629 E-2	79	0.254 E-2
8	0.265 E-1	44	0.570 E-2	80	0.271 E-2
9	0.262 E-1	45	0.572 E-2	81	0.229 E-2
10	0.236 E-1	46	0.541 E-2	82	0.293 E-2
11	0.238 E-1	47	0.586 E-2	83	0.246 E-2
12	0.225 E-1	48	0.520 E-2	84	0.205 E-2
13	0.196 E-1	49	0.520 E-2	85	0.201 E-2
14	0.192 E-1	50	0.473 E-2	86	0.205 E-2
15	0.182 E-1	51	0.516 E-2	87	0.248 E-2
16	0.176 E-1	52	0.455 E-2	88	0.213 E-2
17	0.174 E-1	53	0.484 E-2	89	0.201 E-2
18	0.157 E-1	54	0.441 E-2	90	0.232 E-2
19	0.158 E-1	55	0.432 E-2	91	0.205 E-2
20	0.143 E-1	56	0.437 E-2	92	0.189 E-2
21	0.137 E-1	57	0.424 E-2	93	0.232 E-2
22	0.138 E-1	58	0.369 E-2	94	0.230 E-2
23	0.136 E-1	59	0.453 E-2	95	0.221 E-2
24	0.119 E-1	60	0.393 E-2	96	0.195 E-2
25	0.118 E-1	61	0.389 E-2	97	0.135 E-2
26	0.109 E-1	62	0.432 E-2	98	0.162 E-2
27	0.112 E-1	63	0.404 E-2	99	0.150 E-2
28	0.101 E-1	64	0.277 E-2	100	0.193 E-2
29	0.967 E-2	65	0.355 E-2	101	0.195 E-2
30	0.988 E-2	66	0.361 E-2	102	0.111 E-2
31	0.896 E-2	67	0.334 E-2	103	0.160 E-2
32	0.961 E-2	68	0.277 E-2	104	0.172 E-2
33	0.850 E-2	69	0.281 E-2	105	0.203 E-2
34	0.836 E-2	70	0.322 E-2	106	0.123 E-2
35	0.824 E-2	71	0.295 E-2	107	0.127 E-2

TABLE VIII-D, Continued

Count	Probability	Count	Probability	Count	Probability
108	0.168 E-2	122	0.131 E-2	136	0.121 E-2
109	0.121 E-2	123	0.158 E-2	137	0.174 E-2
110	0.123 E-2	124	0.937 E-3	138	0.145 E-2
111	0.117 E-2	125	0.111 E-2	139	0.162 E-2
112	0.152 E-2	126	0.107 E-2	140	0.195 E-2
113	0.137 E-2	127	0.123 E-2	141	0.187 E-2
114	0.127 E-2	128	0.117 E-2	142	0.184 E-2
115	0.123 E-2	129	0.121 E-2	143	0.283 E-2
116	0.119 E-2	130	0.840 E-3	144	0.668 E-1*
117	0.104 E-2	131	0.164 E-2	145	0.000 E 0
118	0.937 E-3	132	0.137 E-2	146	0.000 E 0
119	0.957 E-3	133	0.123 E-2	147	0.000 E 0
120	0.152 E-2	134	0.115 E-2	148	0.000 E 0
121	0.119 E-2	135	0.127 E-2	149	0.000 E 0

*See Appendix D.

TABLE VIII-E

EXPERIMENTALLY DETERMINED PROBABILITIES FOR PHOTON COUNTS

RUN 35

(N_S = 44.2, N_B = 0.29, σ_I^2 = 2.2, $(\sigma_I^2)_T$ = 5.2, $\langle v_\perp \rangle \simeq$ 8 mph.)

Count	Probability	Count	Probability	Count	Probability
0	0.270 E-1	36	0.693 E-2	72	0.276 E-2
1	0.370 E-1	37	0.710 E-2	73	0.267 E-2
2	0.352 E-1	38	0.684 E-2	74	0.320 E-2
3	0.349 E-1	39	0.620 E-2	75	0.270 E-2
4	0.319 E-1	40	0.628 E-2	76	0.276 E-2
5	0.303 E-1	41	0.592 E-2	77	0.249 E-2
6	0.279 E-1	42	0.626 E-2	78	0.241 E-2
7	0.249 E-1	43	0.616 E-2	79	0.214 E-2
8	0.242 E-1	44	0.539 E-2	80	0.243 E-2
9	0.219 E-1	45	0.566 E-2	81	0.259 E-2
10	0.221 E-1	46	0.513 E-2	82	0.221 E-2
11	0.209 E-1	47	0.573 E-2	83	0.242 E-2
12	0.201 E-1	48	0.490 E-2	84	0.219 E-2
13	0.170 E-1	49	0.478 E-2	85	0.221 E-2
14	0.167 E-1	50	0.513 E-2	86	0.190 E-2
15	0.160 E-1	51	0.427 E-2	87	0.211 E-2
16	0.163 E-1	52	0.474 E-2	88	0.171 E-2
17	0.145 E-1	53	0.427 E-2	89	0.178 E-2
18	0.143 E-1	54	0.473 E-2	90	0.190 E-2
19	0.138 E-1	55	0.434 E-2	91	0.194 E-2
20	0.131 E-1	56	0.379 E-2	92	0.210 E-2
21	0.126 E-1	57	0.368 E-2	93	0.173 E-2
22	0.118 E-1	58	0.342 E-2	94	0.194 E-2
23	0.119 E-1	59	0.374 E-2	95	0.210 E-2
24	0.104 E-1	60	0.357 E-2	96	0.180 E-2
25	0.115 E-1	61	0.349 E-2	97	0.165 E-2
26	0.978 E-2	62	0.344 E-2	98	0.171 E-2
27	0.107 E-1	63	0.345 E-2	99	0.191 E-2
28	0.909 E-2	64	0.316 E-2	100	0.178 E-2
29	0.897 E-2	65	0.329 E-2	101	0.204 E-2
30	0.895 E-2	66	0.335 E-2	102	0.145 E-2
31	0.842 E-2	67	0.310 E-2	103	0.177 E-2
32	0.807 E-2	68	0.277 E-2	104	0.148 E-2
33	0.828 E-2	69	0.305 E-2	105	0.135 E-2
34	0.727 E-2	70	0.280 E-2	106	0.161 E-2
35	0.758 E-2	71	0.301 E-2	107	0.163 E-2

TABLE VIII-E, Continued

Count	Probability	Count	Probability	Count	Probability
108	0.163 E-2	122	0.132 E-2	136	0.159 E-2
109	0.138 E-2	123	0.138 E-2	137	0.173 E-2
110	0.137 E-2	124	0.121 E-2	138	0.177 E-2
111	0.141 E-2	125	0.134 E-2	139	0.214 E-2
112	0.138 E-2	126	0.125 E-2	140	0.223 E-2
113	0.145 E-2	127	0.159 E-2	141	0.251 E-2
114	0.115 E-2	128	0.104 E-2	142	0.286 E-2
115	0.143 E-2	129	0.142 E-2	143	0.306 E-2
116	0.154 E-2	130	0.133 E-2	144	0.308 E-1*
117	0.135 E-2	131	0.137 E-2	145	0.000 E 0
118	0.112 E-2	132	0.139 E-2	146	0.000 E 0
119	0.138 E-2	133	0.152 E-2	147	0.000 E 0
120	0.133 E-2	134	0.116 E-2	148	0.000 E 0
121	0.124 E-2	135	0.133 E-2	149	0.000 E 0

*See Appendix D.

TABLE IX-A

EXPERIMENTALLY DETERMINED ERROR RATES

(Data Set I, November 10, 1978, Tape PCR 1)

Run	No. of Detectors	EER	AOR	SOR I	SOR II	ATR	Parameters
1	1	3.6 E-1	3.6 E-1	3.6 E-1	3.6 E-1	3.6 E-1	N_S = 1.9
	2	3.9 E-1	2.9 E-1	3.3 E-1	3.3 E-1	2.8 E-1	N_B = 1.0
	3	2.4 E-1	2.4 E-1	3.2 E-1	3.5 E-1	2.3 E-1	σ_I^2 = 2.7
	4	2.0 E-1	2.0 E-1	2.8 E-1	3.8 E-1	1.9 E-1	v = 0
	5	1.7 E-1	1.7 E-1	2.9 E-1	4.0 E-1		
	6	1.5 E-1	1.5 E-1	3.1 E-1	4.3 E-1		
	7	1.3 E-1	1.3 E-1	3.2 E-1	4.5 E-1		
	8	1.1 E-1	1.1 E-1	3.0 E-1	4.6 E-1		
	9	9.7 E-2	9.7 E-2	3.1 E-1	4.7 E-1		
	10	8.4 E-2	8.4 E-2	3.2 E-1	4.8 E-1		
2	1	3.5 E-1	3.5 E-1	3.5 E-1	3.5 E-1	3.5 E-1	N_S = 2.5
	2	2.3 E-1	2.3 E-1	3.3 E-1	3.3 E-1	2.6 E-1	N_B = 1.0
	3	2.2 E-1	2.2 E-1	2.8 E-1	3.5 E-1	2.0 E-1	σ_I^2 = 2.8
	4	1.7 E-1	1.7 E-1	2.8 E-1	3.8 E-1	1.6 E-1	v = 0
3	1	2.9 E-1	2.9 E-1	3.0 E-1	3.0 E-1	2.9 E-1	N_S = 4.5
	2	2.0 E-1	2.0 E-1	2.5 E-1	2.9 E-1	1.8 E-1	N_B = 1.0
	3	1.4 E-1	1.4 E-1	2.4 E-1	3.3 E-1	1.2 E-1	σ_I^2 = 2.8
	4	9.9 E-2	9.9 E-2	2.3 E-1	3.7 E-1	8.4 E-2	v = 0
4	1	2.7 E-1	2.7 E-1	2.7 E-1	3.5 E-1	2.5 E-1	N_S = 5.1
	2	1.6 E-1	1.6 E-1	2.4 E-1	4.2 E-1	1.4 E-1	N_B = 0.85
	3	1.0 E-1	1.0 E-1	2.3 E-1	4.6 E-1	8.4 E-2	σ_I^2 = 2.7
	4	7.4 E-2	7.4 E-2	1.8 E-1	4.8 E-1	5.6 E-2	v = 0
5	1	2.2 E-1	2.2 E-1	2.3 E-1	3.3 E-1	2.1 E-1	N_S = 6.9
	2	1.2 E-1	1.2 E-1	2.1 E-1	4.1 E-1	1.0 E-1	N_B = 0.82
	3	7.0 E-2	7.0 E-2	1.5 E-1	4.6 E-1	5.2 E-2	σ_I^2 = 2.5
	4	3.8 E-2	3.9 E-2	1.7 E-1	4.8 E-1	2.5 E-2	v = 0

TABLE IX-B

EXPERIMENTALLY DETERMINED ERROR RATES

(Data Set II, March 1, 1979, Tape PCR 2, 1st Half)

Run	No. of Detectors	EER	AOR	SOR I	SOR II	ATR	Parameters
6	1	3.6 E-1	3.6 E-1	3.6 E-1	4.0 E-1	3.7 E-1	N_S = 1.6
	2	2.9 E-1	2.9 E-1	3.2 E-1	4.4 E-1	2.9 E-1	N_B = 0.94
	3	2.4 E-1	2.4 E-1	3.0 E-1	4.7 E-1	2.4 E-1	σ_I^2 = 2.3
	4	2.0 E-1	2.0 E-1	3.0 E-1	4.5 E-1	1.9 E-1	$(\sigma_I^2)_T$ = 2.5
							$\langle v_\perp \rangle$ ≈ 2.5 mph
7	1	3.1 E-1	3.1 E-1	3.1 E-1	3.8 E-1	3.1 E-1	N_S = 2.9
	2	2.2 E-1	2.2 E-1	2.8 E-1	4.3 E-1	2.1 E-1	N_B = 0.94
	3	1.6 E-1	1.6 E-1	2.7 E-1	4.7 E-1	1.5 E-1	σ_I^2 = 2.7
	4	1.2 E-1	1.2 E-1	2.2 E-1	4.4 E-1	1.1 E-1	$(\sigma_I^2)_T$ = 2.5
							$\langle v_\perp \rangle$ ≈ 2.5 mph
8	1	2.7 E-1	2.7 E-1	2.7 E-1	3.6 E-1	2.6 E-1	N_S = 4.9
	2	1.7 E-1	1.7 E-1	2.1 E-1	4.3 E-1	1.7 E-1	N_B = 0.95
	3	1.1 E-1	1.1 E-1	2.0 E-1	3.9 E-1	1.1 E-1	σ_I^2 = 2.2
	4	7.7 E-2	7.8 E-2	1.8 E-1	4.4 E-1	7.4 E-2	$(\sigma_I^2)_T$ = 3.5
							$\langle v_\perp \rangle$ ≈ 2.5 mph
9	1	2.4 E-1	2.4 E-1	2.5 E-1	3.5 E-1	2.4 E-1	N_S = 5.8
	2	1.4 E-1	1.4 E-1	2.0 E-1	4.3 E-1	1.5 E-1	N_B = 0.95
	3	9.0 E-2	9.0 E-2	1.7 E-1	3.9 E-1	9.5 E-2	σ_I^2 = 2.1
	4	5.9 E-2	5.9 E-2	1.8 E-1	4.4 E-1	6.6 E-2	$(\sigma_I)_T^2$ = 3.7
							$\langle v_\perp \rangle$ ≈ 2.5 mph

TABLE IX-B, Continued

Run	No. of Detectors	EER	AOR	SOR I	SOR II	ATR	Parameters
10	1	2.3 E-1	2.3 E-1	2.6 E-1	2.6 E-1	2.2 E-1	N_S = 7.1
	2	1.3 E-1	1.3 E-1	1.7 E-1	2.8 E-1	1.1 E-1	N_B = 1.1
	3	7.7 E-2	7.7 E-2	1.5 E-1	3.3 E-1	6.0 E-2	σ_I^2 = 1.7
	4	4.5 E-2	4.6 E-2	1.3 E-1	3.8 E-1	3.3 E-2	$(\sigma_I^2)_T$ = 2.8
							$\langle v_\perp \rangle$ ≈ 2 mph

TABLE IX-C

EXPERIMENTALLY DETERMINED ERROR RATES

(Data Set III, March 1, 1979, Tape PCR 2, 2nd Half)

Run	No. of Detectors	EER	AOR	SOR I	SOR II	ATR	Parameters
11	1	3.4 E-1	3.4 E-1	3.6 E-1	3.6 E-1	3.4 E-1	N_S = 2.8
	2	2.7 E-1	2.7 E-1	3.0 E-1	3.7 E-1	2.6 E-1	N_B = 2.3
	3	2.1 E-1	2.1 E-1	2.7 E-1	4.1 E-1	2.0 E-1	σ_I^2 = 2.0
	4	1.8 E-1	1.8 E-1	2.7 E-1	4.4 E-1	1.6 E-1	$(\sigma_I^2)_T$ = 2.8
							$\langle v_\perp \rangle \approx$ 1.5 mph
12	1	2.9 E-1	2.9 E-1	3.0 E-1	3.4 E-1	2.9 E-1	N_S = 4.7
	2	2.0 E-1	2.0 E-1	2.5 E-1	3.8 E-1	1.9 E-1	N_B = 2.5
	3	1.5 E-1	1.5 E-1	2.4 E-1	4.3 E-1	1.3 E-1	σ_I^2 = 2.3
	4	1.0 E-1	1.0 E-1	2.4 E-1	4.6 E-1	8.8 E-2	$(\sigma_I^2)_T$ = 3.5
							$\langle v_\perp \rangle \approx$ 2.5 mph
13	1	2.6 E-1	2.6 E-1	2.7 E-1	3.2 E-1	2.5 E-1	N_S = 6.9
	2	1.6 E-1	1.6 E-1	2.4 E-1	3.8 E-1	1.5 E-1	N_B = 2.6
	3	1.1 E-1	1.1 E-1	2.1 E-1	4.3 E-1	9.0 E-2	σ_I^2 = 2.3
	4	6.9 E-2	7.0 E-2	2.1 E-1	4.6 E-1	5.6 E-2	$(\sigma_I^2)_T$ = 4.2
							$\langle v_\perp \rangle \approx$ 0 mph
14	1	2.0 E-1	2.0 E-1	2.5 E-1	3.2 E-1	2.1 E-1	N_S = 13.2
	2	9.8 E-2	9.8 E-2	1.8 E-1	3.2 E-1	1.2 E-1	N_B = 3.0
	3	5.2 E-2	5.2 E-2	1.7 E-1	3.7 E-1	7.9 E-2	σ_I^2 = 2.3
	4	2.8 E-2	2.8 E-2	1.6 E-1	4.2 E-1	5.5 E-2	$(\sigma_I^2)_T$ = 5.5
							$\langle v_\perp \rangle \approx$ 2.5 mph

TABLE IX-C, Continued

Run	No. of Detectors	EER	AOR	SOR I	SOR II	ATR	Parameters
15	1	1.7 E-1	1.7 E-1	2.0 E-1	2.8 E-1	1.9 E-1	N_S = 17.5
	2	7.6 E-2	7.5 E-2	1.6 E-1	3.6 E-1	9.3 E-2	N_B = 2.5
	3	3.6 E-2	3.6 E-2	1.4 E-1	4.2 E-1	5.4 E-2	σ_I^2 = 2.2
	4	1.8 E-2	1.8 E-2	1.3 E-1	4.6 E-1	3.4 E-2	$(\sigma_I^2)_T$ = 3.5
							$\langle v_I \rangle \approx$ 2.5 mph

TABLE IX-D

EXPERIMENTALLY DETERMINED ERROR RATES

(Data Set IV, March 1, 1979, Tape PCR 3, 1st Half)

Run	No. of Detectors	EER	AOR	SOR I	SOR II	ATR	Parameters
16	1	3.6 E-1	3.6 E-1	3.7 E-1	3.9 E-1	3.8 E-1	N_S = 3.6
	2	2.9 E-1	2.9 E-1	3.3 E-1	4.1 E-1	3.1 E-1	N_B = 4.6
	3	2.4 E-1	2.4 E-1	3.2 E-1	4.5 E-1	2.6 E-1	σ_I^2 = 2.6
	4	2.0 E-1	2.1 E-1	3.2 E-1	4.7 E-1	2.2 E-1	$(\sigma_I^2)_T$ = 5.6
							$\langle v_\perp \rangle \approx$ 3.5 mph
17	1	2.6 E-1	2.7 E-1	2.9 E-1	3.4 E-1	2.7 E-1	N_S = 9.5
	2	1.6 E-1	1.6 E-1	2.5 E-1	3.9 E-1	1.8 E-1	N_B = 4.7
	3	1.0 E-1	1.0 E-1	2.3 E-1	4.4 E-1	1.2 E-1	σ_I^2 = 2.5
	4	6.7 E-2	6.7 E-2	2.3 E-1	4.7 E-1	8.6 E-2	$(\sigma_I^2)_T$ = 4.3
							$(v_\perp)_T \approx$ 3.5 mph
18	1	2.3 E-1	2.3 E-1	2.7 E-1	3.2 E-1	2.4 E-1	N_S = 12.6
	2	1.3 E-1	1.3 E-1	2.1 E-1	3.9 E-1	1.5 E-1	N_B = 4.7
	3	7.7 E-2	7.6 E-2	2.1 E-1	4.4 E-1	9.8 E-2	σ_I^2 = 2.5
	4	4.9 E-2	4.9 E-2	2.1 E-1	4.7 E-1	7.0 E-2	$(\sigma_I^2)_T$ = 5.6
							$\langle v_\perp \rangle \approx$ 1 mph
19	1	1.8 E-1	1.8 E-1	2.3 E-1	2.8 E-1	1.9 E-1	N_S = 19.7
	2	8.2 E-2	8.3 E-2	1.9 E-1	3.7 E-1	1.0 E-1	N_B = 4.5
	3	3.9 E-2	4.0 E-2	1.8 E-1	4.3 E-1	6.1 E-2	σ_I^2 = 2.7
	4	1.9 E-2	2.0 E-2	1.8 E-1	4.6 E-1	4.0 E-2	$(\sigma_I^2)_T$ = 4.9
							$\langle v_\perp \rangle \approx$ 2 mph
	1	P_T = 2.0 E-1					

TABLE IX-D, Continued

Run	No. of Detectors	EER	AOR	SOR I	SOR II	ATR	Parameters
20	1	1.7 E-1	1.7 E-1	2.0 E-1	2.6 E-1	1.8 E-1	N_S = 19.8
	2	7.3 E-2	7.5 E-2	1.7 E-1	3.4 E-1	9.8 E-2	N_B = 4.3
	3	3.4 E-2	3.5 E-2	1.7 E-1	4.0 E-1	5.9 E-2	σ_I^2 = 2.5
	4	1.6 E-2	1.7 E-2	1.6 E-1	4.4 E-1	3.9 E-2	$(\sigma_I^2)_T$ = 4.9

TABLE IX-E

EXPERIMENTALLY DETERMINED ERROR RATES

(Data Set V, March 1, 1979, Tape PCR 3, 2nd Half)

Run	No. of Detectors	EER	AOR	SOR I	SOR II	ATR	Parameters
21	1	2.9 E-1	2.9 E-1	3.3 E-1	3.3 E-1	3.1 E-1	N_S = 8.5
	2	2.0 E-1	2.0 E-1	2.7 E-1	3.6 E-1	2.2 E-1	N_B = 7.2
	3	1.4 E-1	1.4 E-1	2.5 E-1	4.1 E-1	1.6 E-1	σ_I^2 = 2.4
	4	9.9 E-2	9.9 E-2	2.5 E-1	4.5 E-1	1.3 E-1	$(\sigma_I^2)_T$ = 2.8
							$\langle v_\perp \rangle \approx$ 0.5 mph
22	1	2.4 E-1	2.4 E-1	2.7 E-1	3.0 E-1	2.5 E-1	N_S = 15.0
	2	1.4 E-1	1.4 E-1	2.2 E-1	3.5 E-1	1.6 E-1	N_B = 7.2
	3	8.7 E-2	8.7 E-2	2.1 E-1	4.1 E-1	1.1 E-1	σ_I^2 = 2.6
	4	5.5 E-2	5.5 E-2	2.1 E-1	4.5 E-1	8.1 E-2	$\langle v_\perp \rangle$ = 3.5 mph
23	1	2.0 E-1	2.0 E-1	2.3 E-1	2.7 E-1	2.1 E-1	N_S = 20.5
	2	9.6 E-2	9.6 E-2	1.9 E-1	3.3 E-1	1.2 E-1	N_B = 7.0
	3	5.0 E-2	5.0 E-2	1.8 E-1	3.9 E-1	7.9 E-2	σ_I^2 = 2.5
	4	2.7 E-2	2.8 E-2	1.8 E-1	4.4 E-1	5.5 E-2	$(\sigma_I^2)_T$ = 2.8
							$\langle v_\perp \rangle$ = 5 mph
24	1	1.3 E-1	1.3 E-1	2.2 E-1	2.7 E-1	1.4 E-1	N_S = 31.4
	2	4.7 E-2	4.8 E-2	1.5 E-1	3.7 E-1	6.3 E-2	N_B = 6.6
	3	1.7 E-2	1.9 E-2	1.4 E-1	4.3 E-1	3.3 E-2	σ_I^2 = 2.4
	4	6.4 E-3	7.3 E-3	1.4 E-1	4.6 E-1	1.8 E-2	$\langle v_\perp \rangle$ = 2.5 mph
25	1	1.3 E-1	1.3 E-1	1.8 E-1	2.8 E-1	1.3 E-1	N_S = 36.0
	2	4.5 E-2	4.8 E-2	1.4 E-1	3.8 E-1	5.0 E-2	N_B = 6.7
	3	1.6 E-2	1.8 E-2	1.4 E-1	4.4 E-1	2.3 E-2	σ_I^2 = 2.4
	4	6.5 E-3	7.2 E-3	1.3 E-1	4.7 E-1	1.1 E-2	$(\sigma_I^2)_T$ = 3.5
							$\langle v_\perp \rangle$ = 0.5 mph

TABLE IX-F

EXPERIMENTALLY DETERMINED ERROR RATES

(Data Set VI, March 29, 1979, Tape PCR 4, 2nd Half)

Run	No. of Detectors	EER	AOR	SOR I	SOR II	ATR	Parameters
26	1	2.9 E-1	2.9 E-1	3.1 E-1	3.1 E-1	3.1 E-1	N_S = 4.1
	2	2.0 E-1	2.0 E-1	2.3 E-1	3.2 E-1	2.3 E-1	N_B = 1.2
	3	1.4 E-1	1.4 E-1	2.3 E-1	3.7 E-1	1.7 E-1	σ_I^2 = 2.4
	4	1.0 E-1	1.0 E-1	2.2 E-1	4.1 E-1	1.3 E-1	$(\sigma_I^2)_T$ = 9.6
27	1	2.4 E-1	2.4 E-1	2.8 E-1	2.8 E-1	2.6 E-1	N_S = 7.0
	2	1.5 E-1	1.5 E-1	2.0 E-1	3.2 E-1	1.6 E-1	N_B = 1.3
	3	9.1 E-2	9.1 E-2	2.0 E-1	3.7 E-1	1.1 E-1	σ_I^2 = 2.4
	4	6.0 E-2	6.0 E-2	1.8 E-1	4.2 E-1	7.5 E-2	$(\sigma_I^2)_T$ = 10.0
							$\langle v_\perp \rangle \approx$ 7 mph
28	1	1.7 E-1	1.7 E-1	2.4 E-1	2.4 E-1	1.8 E-1	N_S = 13.8
	2	7.5 E-2	7.4 E-2	1.7 E-1	3.0 E-1	9.2 E-2	N_B = 1.2
	3	3.5 E-2	3.4 E-2	1.3 E-1	3.7 E-1	5.3 E-2	σ_I^2 = 2.3
	4	1.7 E-2	1.6 E-2	1.3 E-1	4.1 E-1	3.3 E-2	$(\sigma_I^2)_T$ = 14.7
							$\langle v_\perp \rangle \approx$ 4 mph
29	1	1.7 E-1	1.7 E-1	2.4 E-1	2.4 E-1	1.8 E-1	N_S = 15.5
	2	7.5 E-2	7.5 E-2	1.7 E-1	3.0 E-1	9.2 E-2	N_B = 1.3
	3	3.4 E-2	3.4 E-2	1.3 E-1	3.7 E-1	5.3 E-2	σ_I^2 = 2.3
	4	1.6 E-2	1.6 E-2	1.1 E-1	4.2 E-1	3.4 E-2	$(\sigma_I^2)_T$ = 8.4
							$\langle v_\perp \rangle \approx$ 6 mph

TABLE IX-F, Continued

Run	No. of Detectors	EER	AOR	SOR I	SOR II	ATR	Parameters
30	1	1.0 E-1	1.0 E-1	1.2 E-1	2.1 E-1	1.1 E-1	N_S = 30
	2	3.1 E-2	3.2 E-2	1.1 E-1	3.0 E-1	4.4 E-2	N_B = 1.3
	3	1.1 E-2	1.1 E-2	1.0 E-1	3.7 E-1	2.1 E-2	σ_I^2 = 2.5
	4	3.7 E-3	4.0 E-3	9.5 E-2	4.2 E-1	1.1 E-2	$(\sigma_I^2)_T$ = 10.0

TABLE IX-G

EXPERIMENTALLY DETERMINED ERROR RATES

(Data Set VII, March 29, 1979, Tape PCR 5)

Run	No. of Detectors	EER	AOR	SOR I	SOR II	ATR	Parameters
31	1	2.0 E-1	2.0 E-1	2.6 E-1	2.6 E-1	2.3 E-1	N_S = 12.4
	2	1.0 E-1	1.0 E-1	1.8 E-1	3.2 E-1	1.3 E-1	N_B = 2.2
	3	5.5 E-1	5.5 E-1	1.6 E-1	3.8 E-1	8.4 E-2	σ_I^2 = 2.3
	4	3.0 E-2	3.1 E-2	1.5 E-1	4.2 E-1	5.1 E-2	$(\sigma_I^2)_T$ = 10.5
							$\langle v_\perp \rangle \approx$ 5 mph
32	1	1.3 E-1	1.3 E-1	1.9 E-1	3.0 E-1	1.5 E-1	N_S = 25.3
	2	4.3 E-2	4.4 E-2	1.3 E-1	4.1 E-1	7.2 E-2	N_B = 1.9
	3	1.4 E-2	1.5 E-2	1.2 E-1	4.6 E-1	4.1 E-2	σ_I^2 = 2.2
	4	5.2 E-3	5.6 E-3	1.1 E-1	4.7 E-1	2.5 E-2	$(\sigma_I^2)_T$ = 7.6
							$\langle v_\perp \rangle \approx$ 7 mph
33	1	1.1 E-1	1.1 E-1	1.6 E-1	2.7 E-1	1.2 E-1	N_S = 31.0
	2	3.3 E-2	3.3 E-2	1.1 E-1	3.7 E-1	5.0 E-2	N_B = 1.7
	3	1.1 E-2	1.1 E-2	1.1 E-1	4.4 E-1	2.4 E-2	σ_I^2 = 2.3
	4	3.7 E-3	4.0 E-3	9.6 E-2	4.7 E-1	1.4 E-2	$(\sigma_I^2)_T$ = 7.0
							$\langle v_\perp \rangle \approx$ 7 mph
34	1	7.4 E-2	7.4 E-2	1.4 E-1	2.5 E-1	9.5 E-2	N_S = 41.0
	2	1.7 E-2	1.7 E-2	8.1 E-2	3.6 E-1	3.9 E-2	N_B = 1.6
	3	3.8 E-3	4.2 E-3	7.2 E-2	4.3 E-1	1.9 E-2	σ_I^2 = 2.1
	4	7.4 E-4	9.4 E-4	6.5 E-2	4.6 E-1	9.5 E-3	$(\sigma_I^2)_T$ = 2.6
							$\langle v_\perp \rangle \approx$ 5 mph

TABLE IX-G, Continued

Run	No. of Detectors	EER	AOR	SOR I	SOR II	ATR	Parameters
35	1	5.4 E-2	5.5 E-2	1.3 E-1	1.3 E-1	6.6 E-2	N_S = 44.2
	2	8.6 E-3	9.4 E-3	6.4 E-2	2.0 E-1	2.1 E-2	N_B = 0.29
	3	1.3 E-3	3.9 E-3	3.8 E-2	2.7 E-1	9.7 E-3	σ_I^2 = 2.2
	4	2.7 E-4	4.1 E-4	3.1 E-2	3.2 E-1	6.5 E-3	$(\sigma_I^2)_T$ = 5.2
							$\langle v_\perp \rangle \approx$ 8 mph

TABLE X

THEORETICALLY CALCULATED VS. EXPERIMENTALLY MEASURED ERROR RATES FOR AOR (SINGLE DETECTOR ARRAY)

Run	Probability of Error		Run	Probability of Error	
	Experiment	Theory		Experiment	Theory
1	3.6 E-1	3.8 E-1	19	1.8 E-1	2.1 E-1
2	3.5 E-1	3.6 E-1	20	1.7 E-1	2.0 E-1
3	2.9 E-1	3.0 E-1	21	2.9 E-1	3.1 E-1
4	2.7 E-1	2.8 E-1	22	2.4 E-1	2.5 E-1
5	2.2 E-1	2.4 E-1	23	2.0 E-1	2.2 E-1
6	3.6 E-1	3.7 E-1	24	1.3 E-1	1.7 E-1
7	3.1 E-1	3.4 E-1	25	1.3 E-1	1.6 E-1
8	2.7 E-1	2.7 E-1	26	2.9 E-1	3.0 E-1
9	2.4 E-1	2.5 E-1	27	2.4 E-1	2.5 E-1
10	2.3 E-1	2.0 E-1	28	1.7 E-1	1.8 E-1
11	3.4 E-1	3.5 E-1	29	1.7 E-1	1.7 E-1
12	2.9 E-1	3.2 E-1	30	1.0 E-1	1.2 E-1
13	2.6 E-1	2.8 E-1	31	2.0 E-1	2.1 E-1
14	2.0 E-1	2.1 E-1	32	1.3 E-1	1.3 E-1
15	1.7 E-1	1.8 E-1	33	1.1 E-1	1.2 E-1
16	3.6 E-1	3.8 E-1	34	7.4 E-2	8.4 E-2
17	2.7 E-1	2.8 E-1	35	5.5 E-2	5.4 E-2
18	2.3 E-1	2.5 E-1			

TABLE XI

THEORETICALLY CALCULATED VS. EXPERIMENTALLY MEASURED

ERROR RATES FOR AOR (TWO DETECTOR ARRAY)

Run	Probability of Error		Run	Probability of Error	
	Experiment	Theory		Experiment	Theory
1	2.9 E-1	3.1 E-1	19	8.3 E-2	1.1 E-1
2	2.3 E-1	2.8 E-1	20	7.5 E-2	9.7 E-2
3	2.0 E-1	2.1 E-1	21	2.0 E-1	2.1 E-1
4	1.6 E-1	1.8 E-1	22	1.4 E-1	1.5 E-1
5	1.2 E-1	1.4 E-1	23	9.6 E-2	1.1 E-1
6	2.9 E-1	3.2 E-1	24	4.8 E-2	7.1 E-2
7	2.2 E-1	2.5 E-1	25	4.8 E-2	6.2 E-2
8	1.7 E-1	1.7 E-1	26	2.0 E-1	2.1 E-1
9	1.4 E-1	1.4 E-1	27	1.5 E-1	1.5 E-1
10	1.3 E-1	1.1 E-1	28	7.4 E-2	8.0 E-2
11	2.7 E-1	2.7 E-1	29	7.5 E-2	7.3 E-2
12	2.0 E-1	2.3 E-1	30	3.2 E-2	4.1 E-2
13	1.6 E-1	1.8 E-1	31	1.0 E-1	1.1 E-1
14	9.8 E-2	1.1 E-1	32	4.4 E-2	4.6 E-2
15	7.5 E-2	8.0 E-2	33	3.3 E-2	3.9 E-2
16	2.9 E-1	3.2 E-1	34	1.7 E-2	2.0 E-2
17	1.6 E-1	1.8 E-1	35	9.4 E-3	8.9 E-3
18	1.3 E-1	1.5 E-1			

TABLE XII

THEORETICALLY CALCULATED VS. EXPERIMENTALLY MEASURED ERROR RATES FOR AOR (FOUR DETECTOR ARRAY)

Run	Probability of error	
	Experiment	Theory
16	2.1 E-1	2.3 E-1
17	6.7 E-2	8.3 E-2
18	4.9 E-2	5.8 E-2
19	2.0 E-2	3.3 E-2
20	1.7 E-2	2.7 E-2
26	1.0 E-1	1.1 E-2
27	6.0 E-2	6.1 E-2
28	1.6 E-2	1.9 E-2
29	1.6 E-2	1.6 E-2
30	4.0 E-3	5.3 E-3
31	3.1 E-2	5.5 E-2
32	5.6 E-3	6.8 E-3
33	4.0 E-3	4.9 E-3
34	9.4 E-4	1.5 E-3
35	4.1 E-4	3.2 E-4

APPENDIX D

APPENDIX D

I. Circuit Description

The integrating circuits following the discriminator (for the photon detector) and the irradiance detector can be understood in terms of the five elemental circuits in Figure 69.

(a) is a pulse integrator. A negative pulse at the emitter terminal of the transistor causes a current pulse at the collector, which charges up the capacitor and increases the voltage across it by a small step. To the extent that the collector current is independent of the collector voltage the magnitude of the step will be of constant height. In the actual circuit the collector current can be considered to be independent if the collector voltage is in the range of 2-5 volts. The height of the step can be changed by changing either R_1 or C_1. S_1 is an electronic switch. S_1 is closed at the end of the bit interval to dump the charges across the capacitor. S_1 is opened at the beginning of the next interval to start the pulse integration once again. In the actual circuit, S_1 is made of four CD4016 switches in parallel. The closed circuit impedance is then about 70 ohms and the open impedance is several giga ohms. The switch is closed by applying +12 volts and opened by applying 0 volt. The capacitor C_1 must be of very high quality with no internal leakage. Also the immediate vicinity of C_1 in the circuit board must be clean to prevent any leakage.

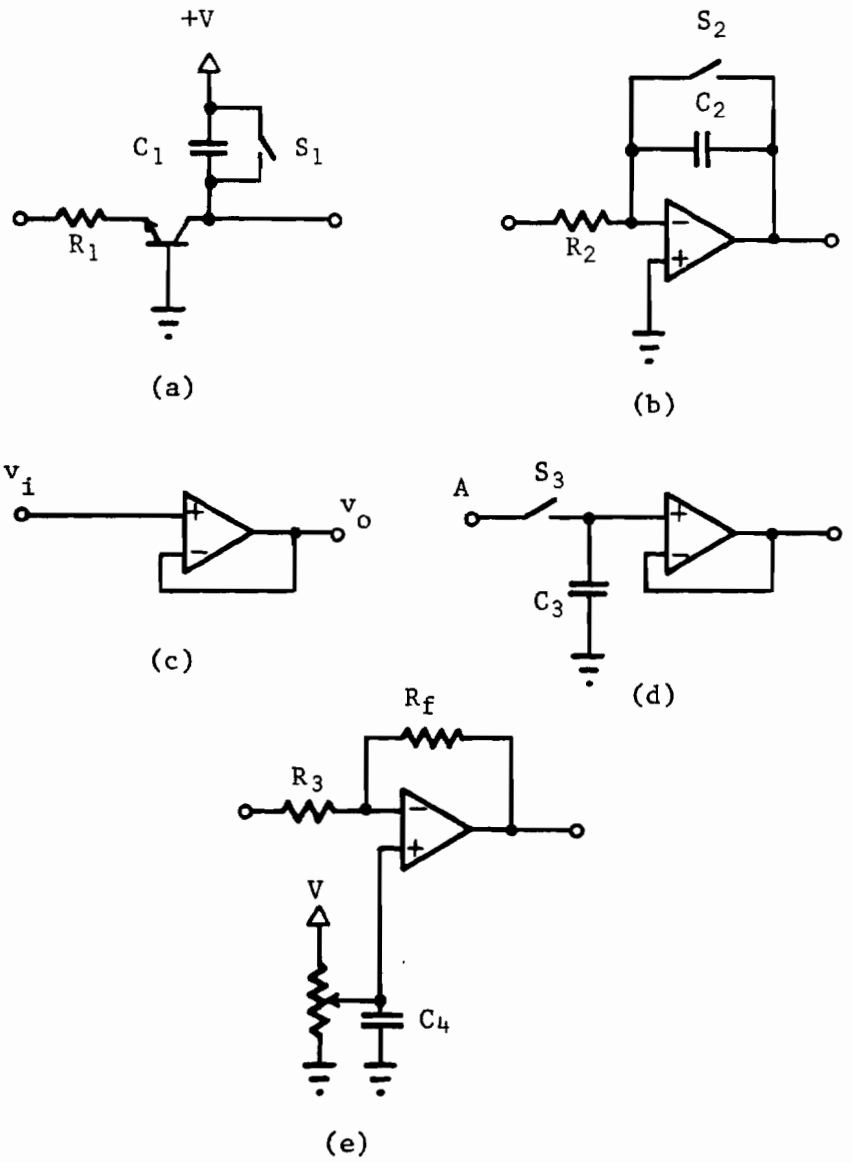

Figure 69. Circuits used in voltage integrations of Figures 70A-72B.

(a) pulse integrator
(b) continuous voltage integration
(c) voltage follower
(d) voltage hold circuit
(e) amplifier with d.c. adjustment

(b) is a conventional integrator using an operational amplifier. The functions and features relating to R_2, C_2 and S_2 are very much the same as in case (a). The switch S_2 has two CD4016 switches in parallel.

(c) is a voltage follower. Because of the 100% feedback this circuit provides an extremely high input impedance (several giga ohms) and a very low output impedance (a few ohms). Such circuits are used in impedance matching between a high impedance output and a low impedance input.

(d) is a voltage hold circuit. When the switch S_3 is closed, the voltage at point A is quickly transferred to the capacitor. When S_3 is open, the capacitor maintains the voltage to the extent that there is very little leakage. This means that C_3 must be of very high quality as were C_1 and C_2. The voltage follower is used to obtain a low impedance.

(e) is a traditional, inverting, feedback amplifier with provisions for adjusting the d.c. level of the output.

Figures 70A and 70B give the overall pulse integrator circuit. Figure 71 gives the various wave forms and control pulses involved in the pulse integration.

(a) is the clock pulse generated from the reference signal and given as input to the pulse generator (see Figures 19 and 76). This pulse generator outputs the pulses d, f and h (Figure 71).

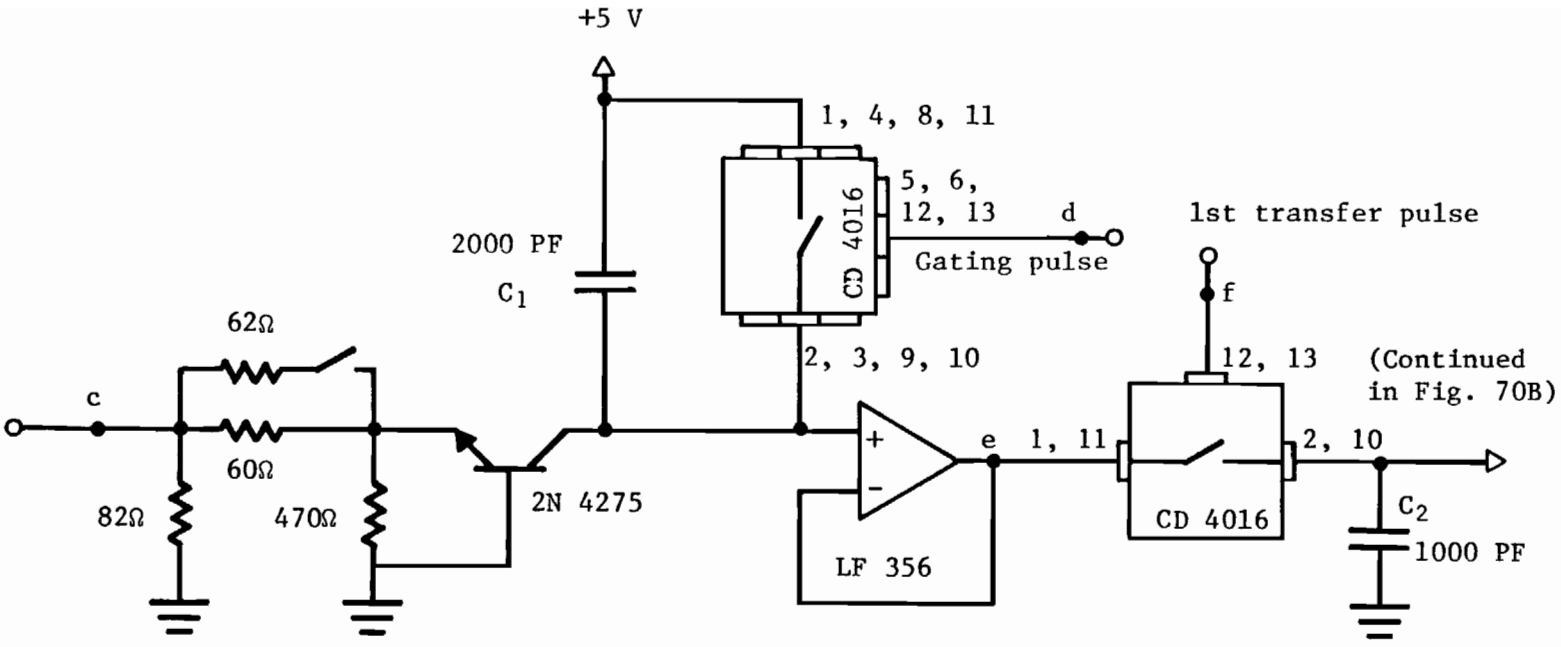

Fig. 70A. Pulse integrator for photon counting. (Wave forms at points marked with lower case alphabets are shown in Fig. 71.) C_1, C_2 are low leakage capacitors.

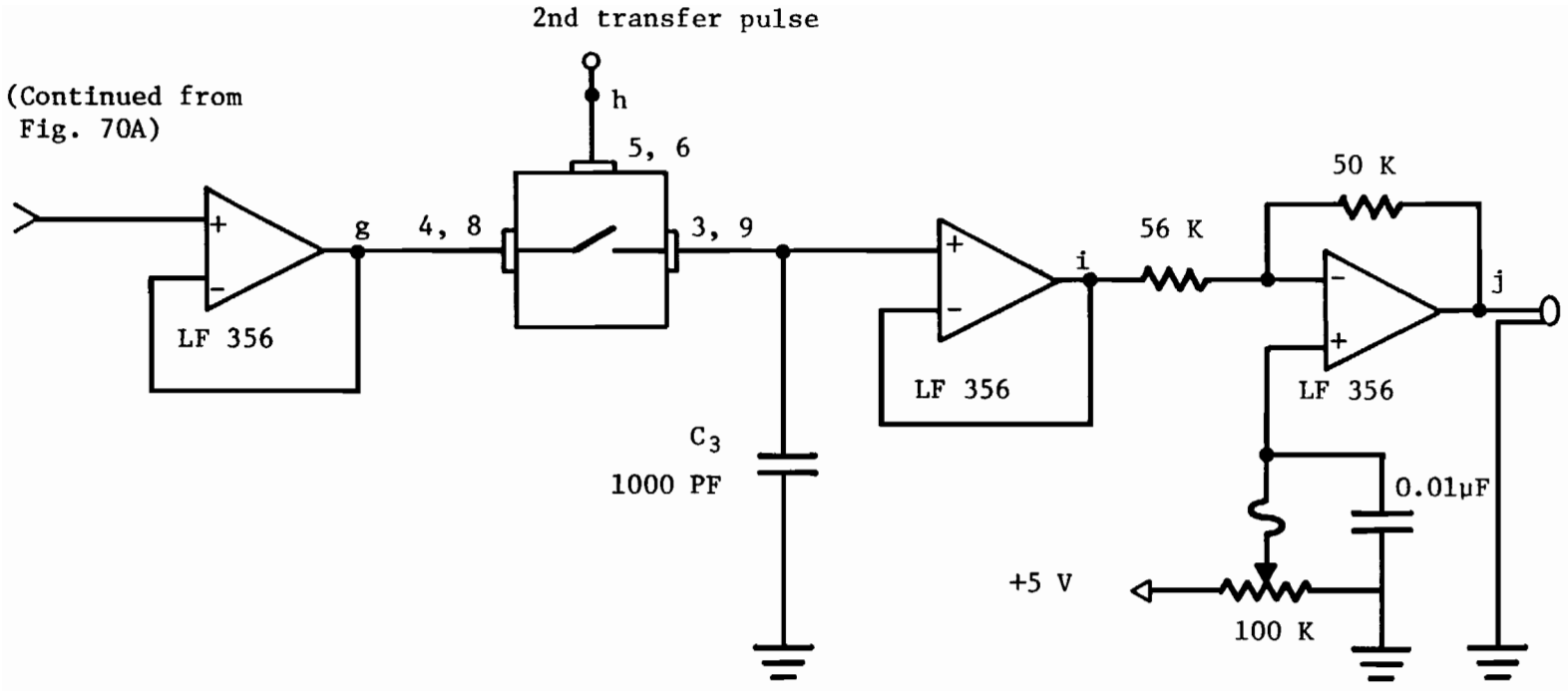

Fig. 70B. Pulse integrator for photon counting. (Wave forms at points marked with lower case alphabets are shown in Fig. 71.) C_3 is a low leakage capacitor.

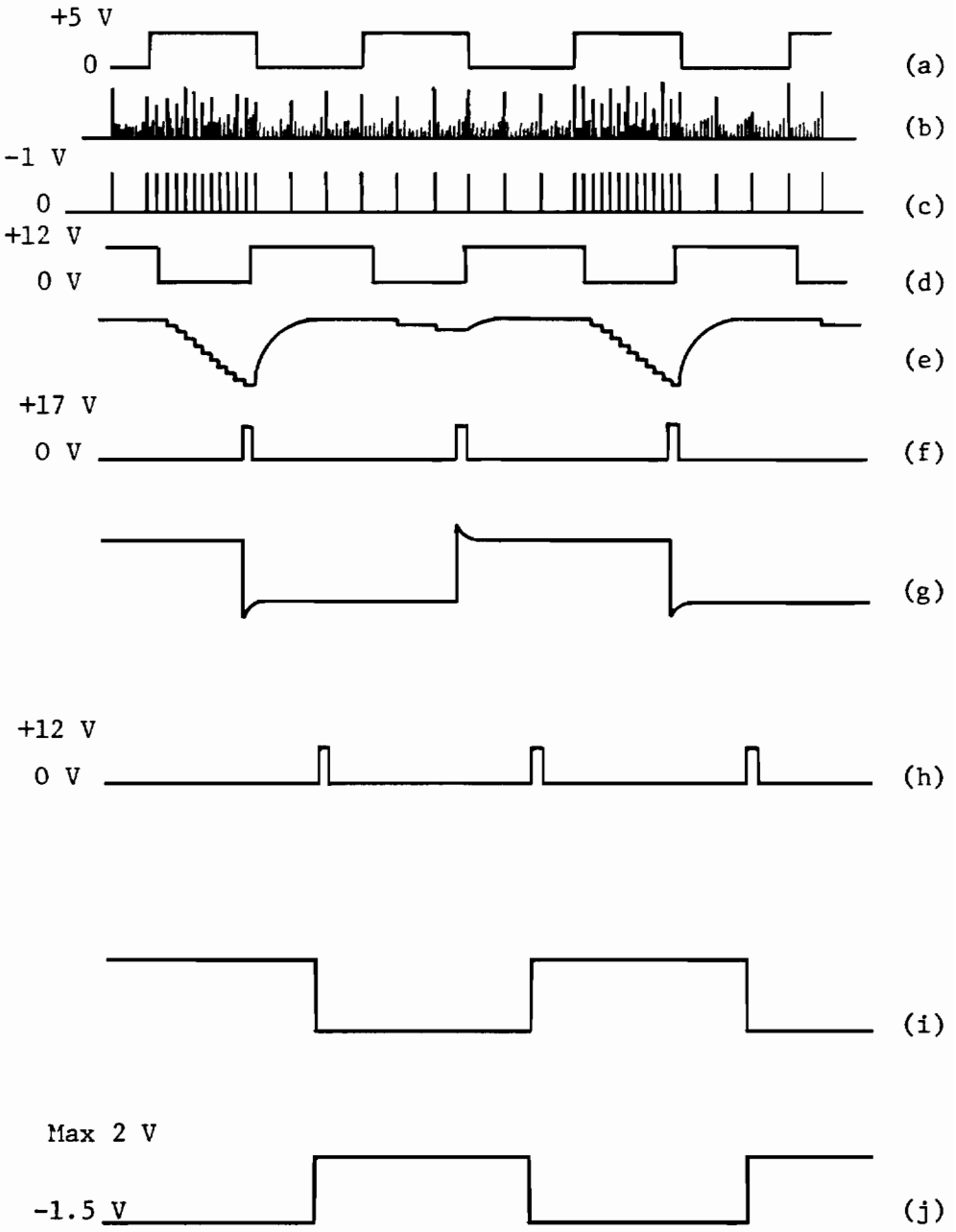

Fig. 71. Wave forms at various stages of pulse integration.

(b) is the output of the photon counting PMT and the input for the discriminator. It contains both the noise as well as photo-electron pulses.

(c) is the output of the discriminator. The noise pulses are suppressed and the output pulses are of constant height ($\sim$ -1V) and width ($\sim$ 15 nsec).

(d) is the gating pulse. When this voltage is low the integration starts, and when it is high, the integration stops. By using a delay circuit, the gating pulse was made to coincide with the bit interval timings.

(e) is the integrating voltage. It decreases by a step for each pulse integrated.

(f) is the first transfer pulse which turns on the switch, and transfers the integrating voltage to the first hold circuit at the end of the integration for the bit interval.

(g) is the output of the first hold circuit. As can be seen, it contains slight spikes. These spikes posed a very difficult filtering problem and the subsequent stage is intended for eliminating these spikes.

(h) is the second transfer pulse. This pulse is used to transfer the integrated voltage to the next hold circuit at a time when the spikes of the previous wave form have died out.

(i) is the resulting wave form of the previous operation.

(j) is the final output after an inversion and d.c. adjustment. At this stage the voltage wave form is recorded on the instrument tape recorder.

Figures 72A and 72B give the overall circuit diagram for the integration of the irradiance signal. Except for the obvious differences at the input and an additional inverting amplification, the general features and functions of the circuit are the same as for the previous circuit.

Figures 73-75 describe the reproduction of the data. The functions are explained in Chapter 4.

Figure 76 shows a typical case of the number of occurrences of the values of the reproduced voltage vs. the voltage. This is a set of approximate delta functions. The area under each delta function corresponds to the number of instances that a certain number of photoelectrons were counted during the bit intervals. The first one on the left should correspond to a zero count, the second to a count of one, the third to a count of two, and so on.

Figure 77 shows the schematics for the pulse generator for generating the gating and switching pulses for the integrators shown in Figures 70A, 70B, 72A and 72B.

Figure 78 shows the circuit for detecting the irradiance of the received signal using the PMT (RCA 931A).

Figure 79 shows the schematics for obtaining voltages +12, -12 and +5 from TM50 (Tektronix) power supplies.

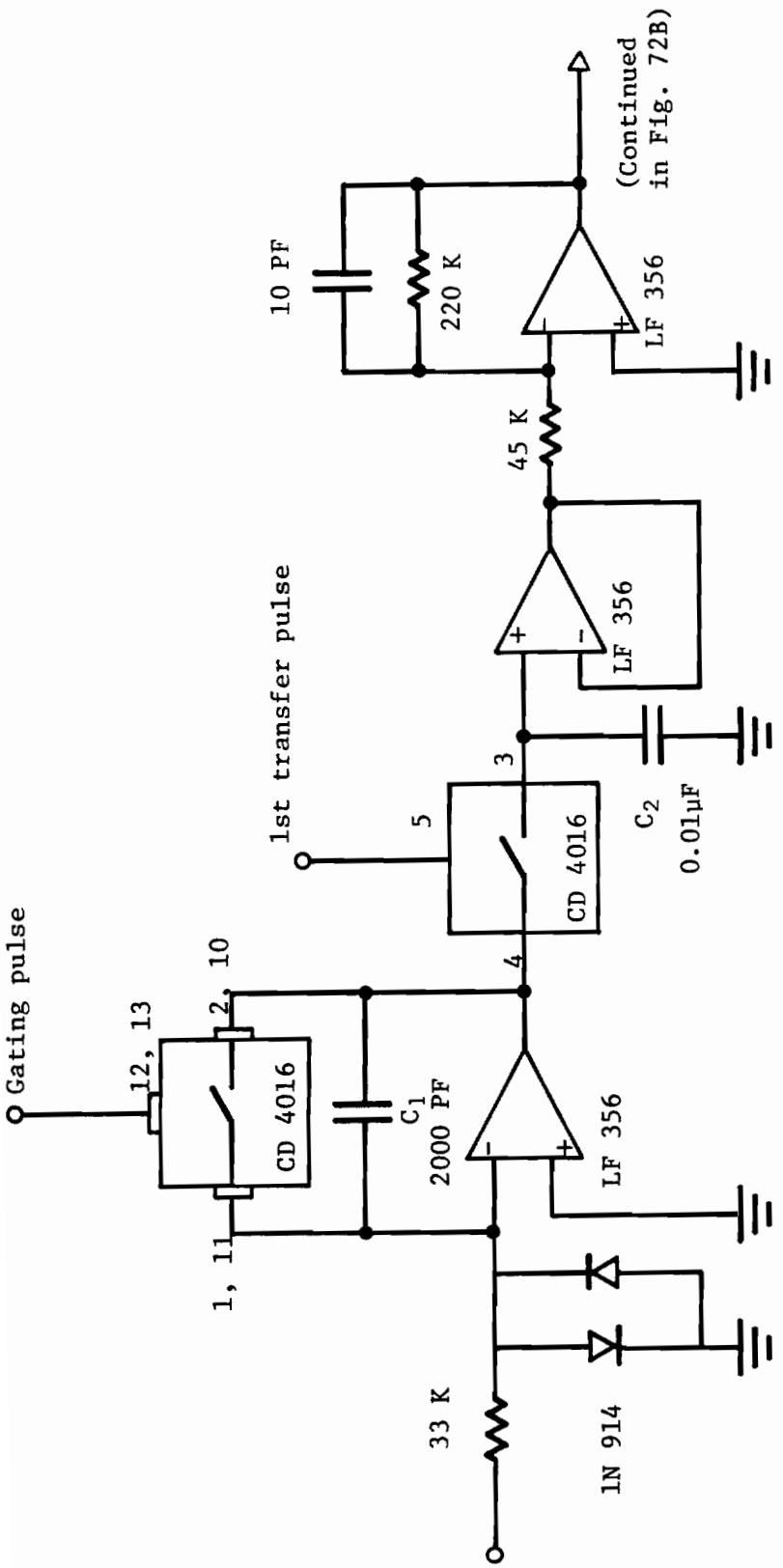

Fig. 72A. Integrator for irradiance signal. C_1 and C_2 are low leakage capacitors.

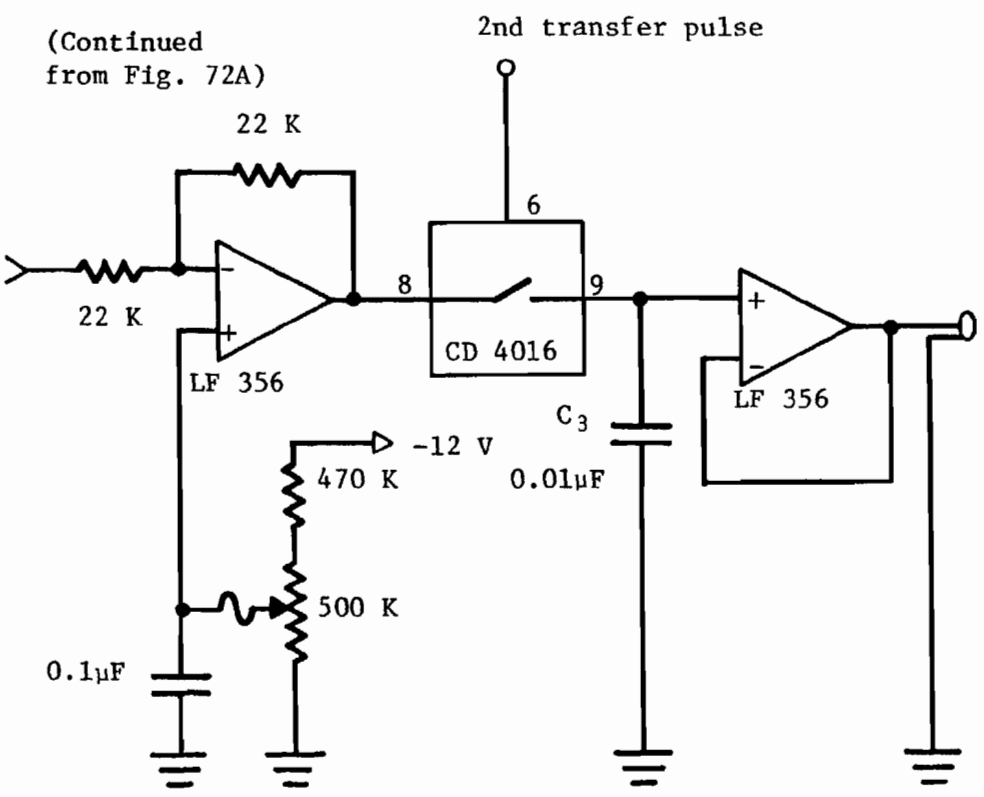

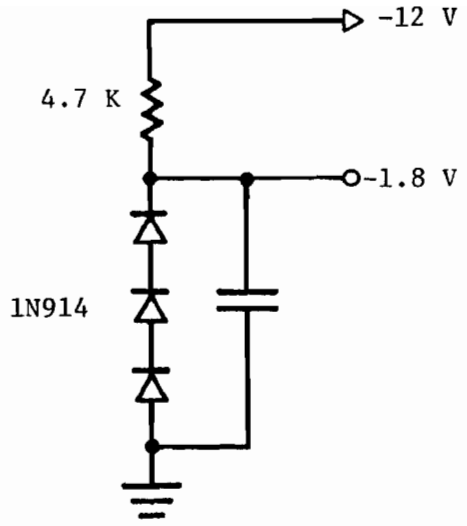

Pin 7 of CD 4016 is connected to -1.8 V (instead of ground) through the above circuit.

Fig. 72B. Integrator for irradiance signal. C_3 is a low leakage capacitor.

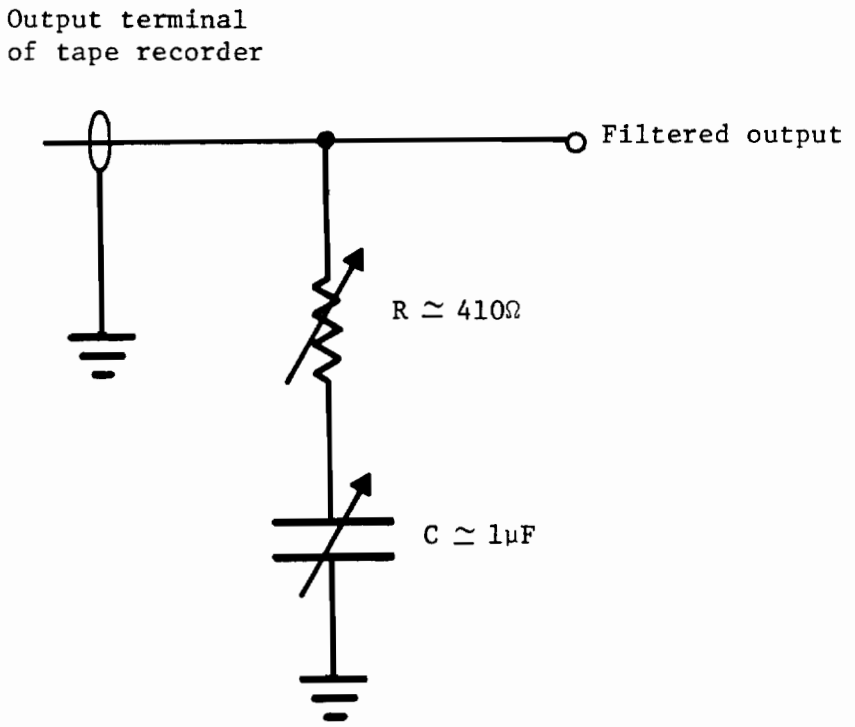

Fig. 73. Output filter shown in Fig. 74.

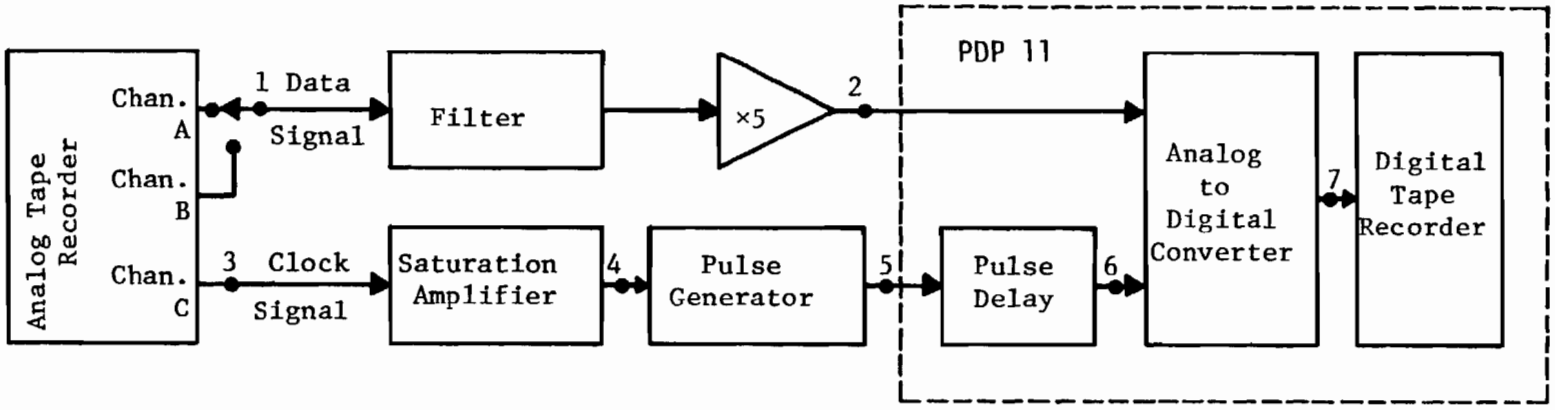

Fig. 74. Block diagram of playback and data retrieval. (Wave forms at points marked with numerals are shown in Fig. 75.)

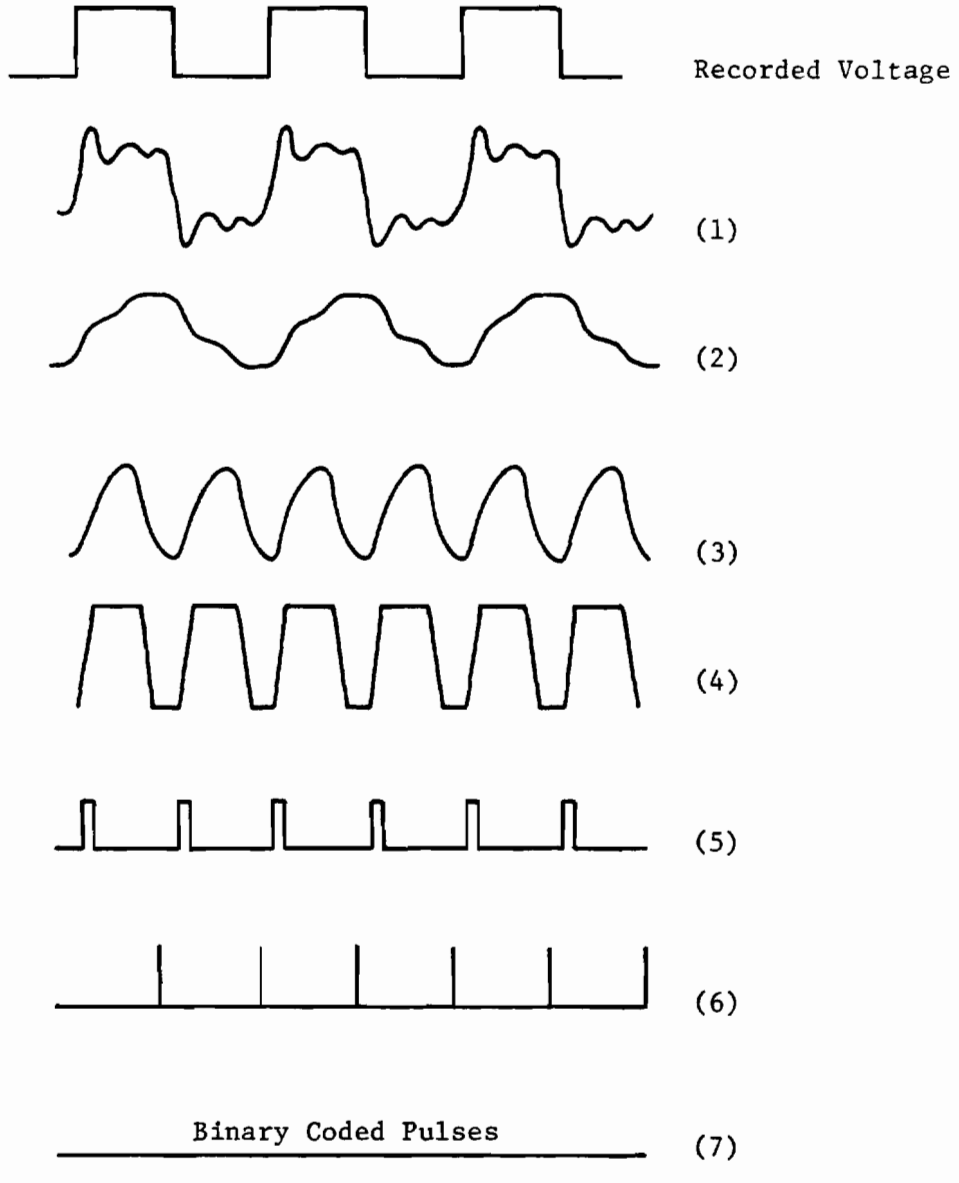

Fig. 75. Wave forms at various stages of data reproduction.

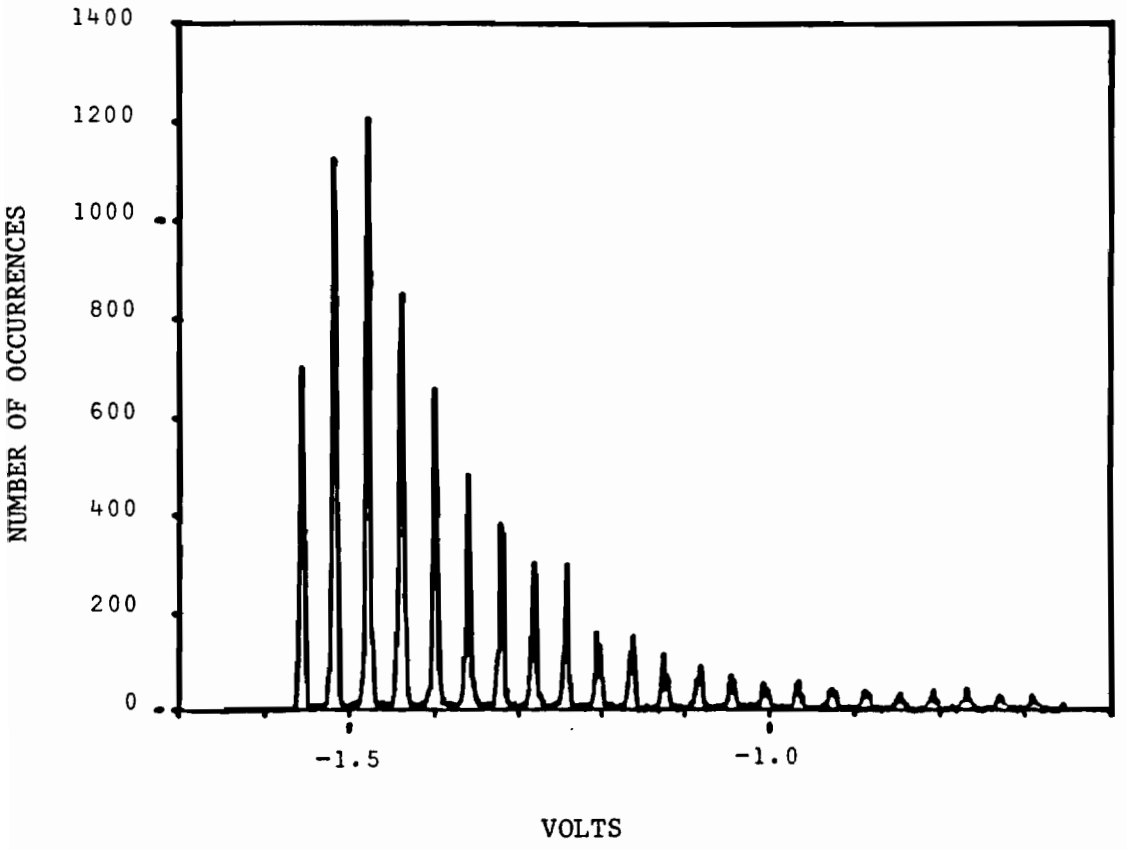

Figure 76. A typical probability density curve for reproduced voltage.

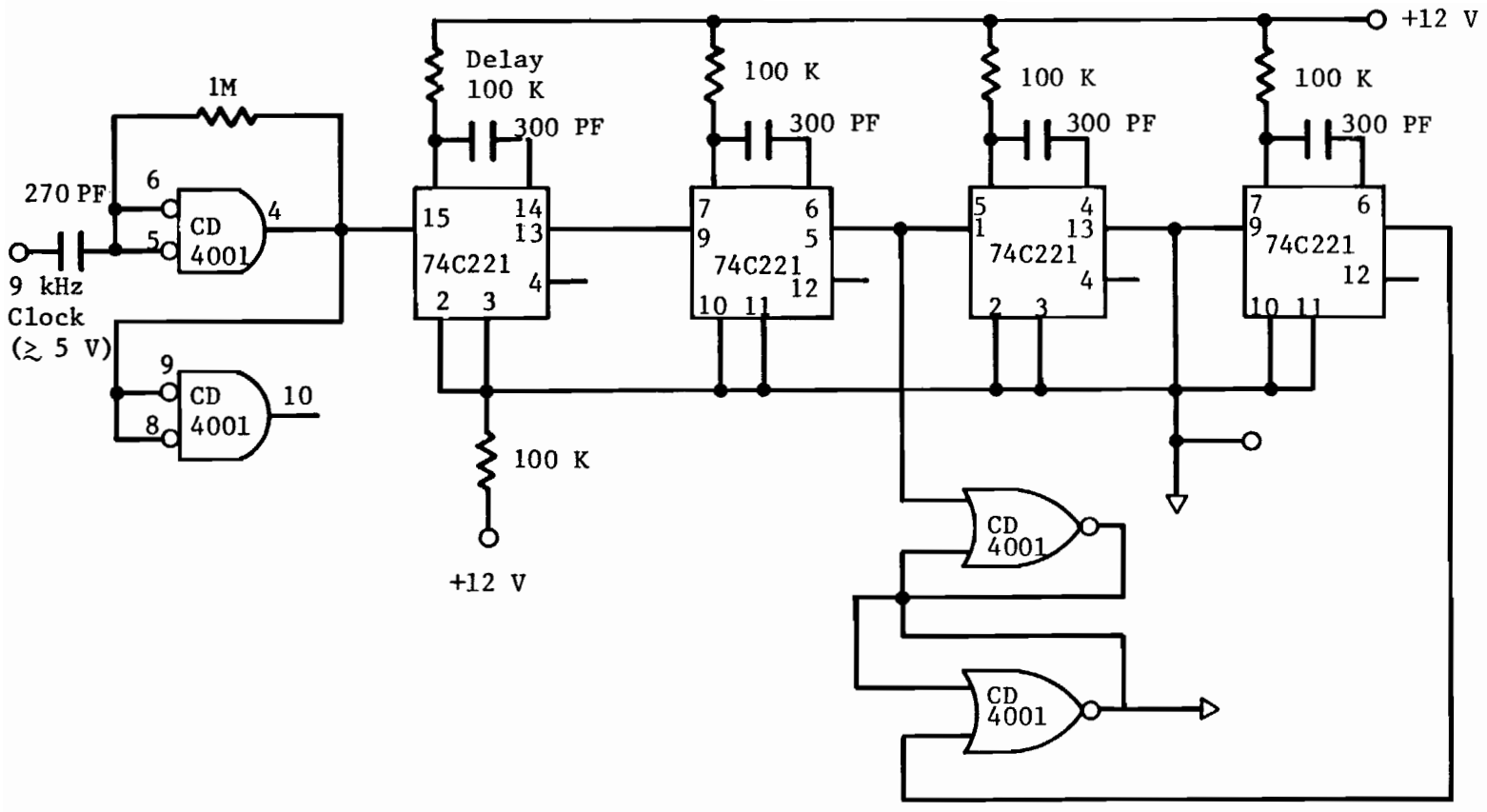

Fig. 77. Gating and switching pulse generator.

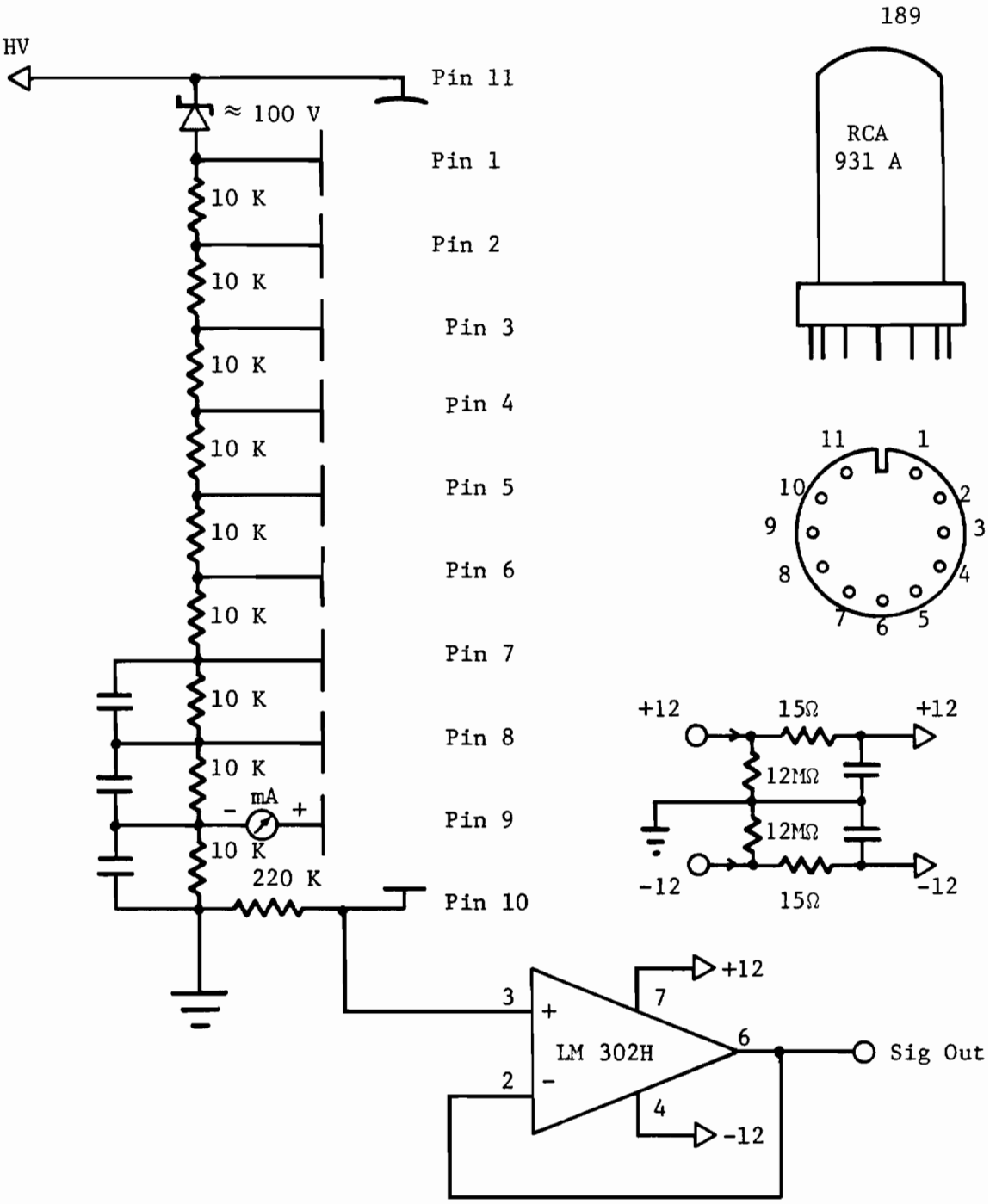

Fig. 78. Schematics for PMT, measuring irradiance.

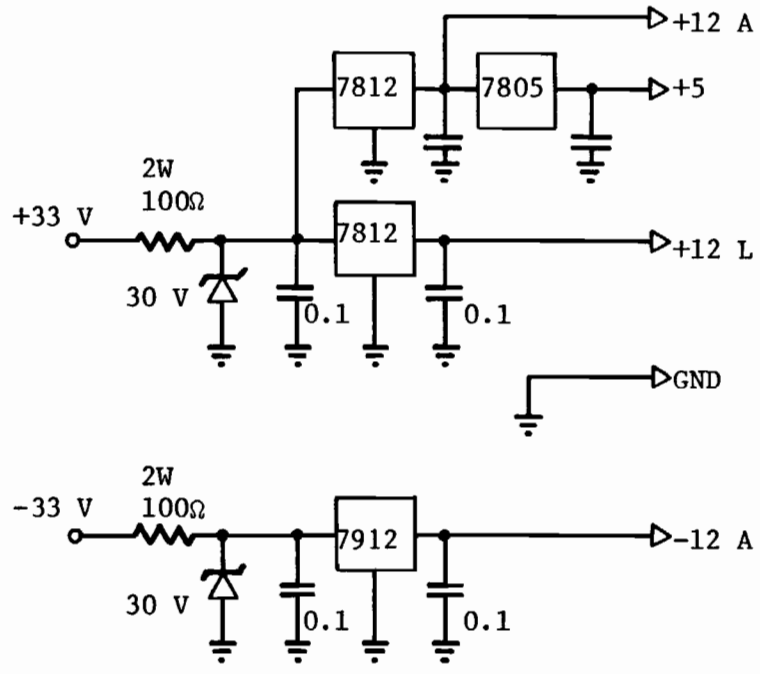

POWER DISTRIBUTION				
CHIP	+12A	+12L	-12A	GND
LF 356	7		4	
CD 4001		14		7
CD 4016		14		7
74 C 221		16		8

Fig. 79. Low voltage power supply for circuits in Figs. 70, 72, 77, 78.

II. Correction for N_S Calculated from the Data

After the data were read from the analog tape and written on the digital tape, the data were used to determine the exact values of N_B and N_S. For this, all the odd-numbered data were collected and the probability distribution for the photon counts and the mean photon counts per bit were determined. The same was done for the even-numbered data. The smaller of the two means gives N_B. The value of N_S was determined from equation (38).

However, a little correction may sometimes be necessary. This is because the receiver system we used here can count up to a maximum of only 143 per bit interval. If during any bit time the count exceeds 143, the same will be counted as 143. When high values of N_S are used or when the turbulence is very high the counts in a bit may exceed 143 in many cases, but all of them will be counted as 143. The value of N_S calculated from such data would be smaller than the actual value.

Figure 80 shows the probability distribution for photoelectron counts for the case of run 35. The peaking at 143 is due to the fact that all counts above 143 were counted as 143, thereby causing an abnormally high probability at 143. The error in the estimation of N_S as calculated from the above case was estimated and proper correction applied before the value of N_S was used elsewhere in calculation. This estimation was done by assuming that in case there had been no peaking at N, the distribution would taper off uniformly up to $N + N'$ as shown by the dashed line in Figure 81.

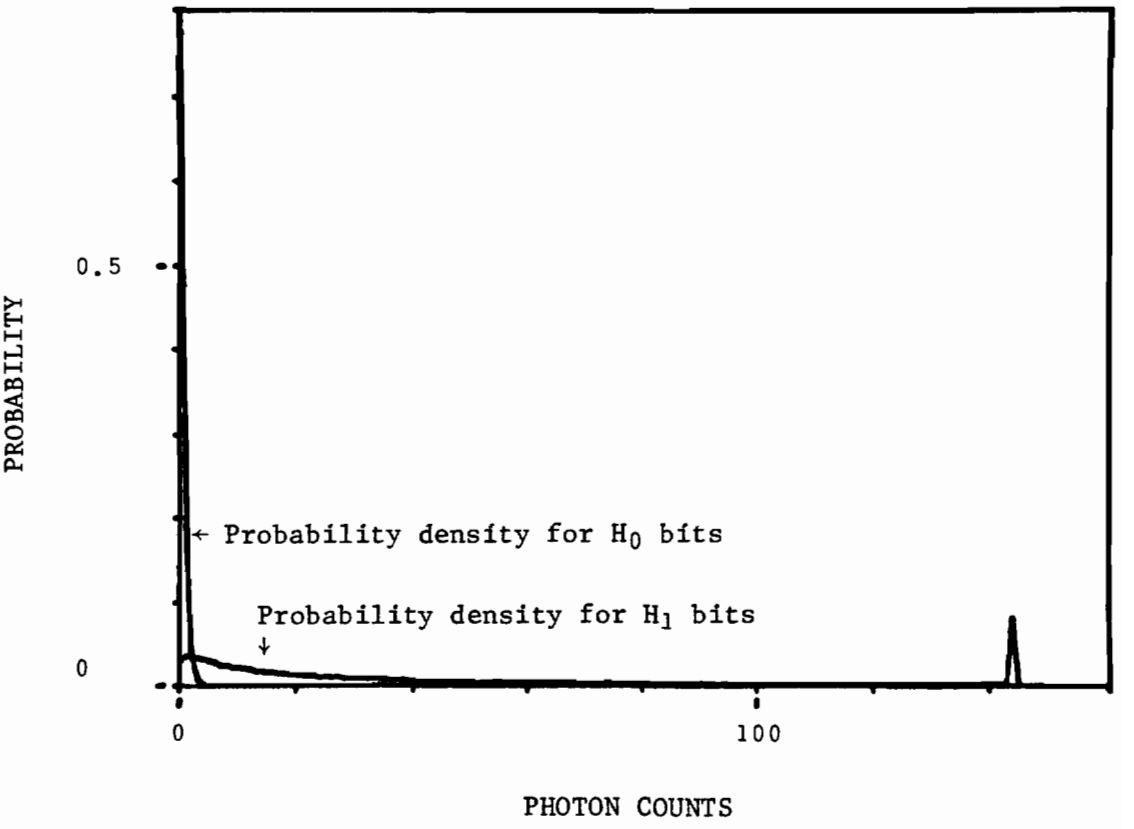

Figure 80. Probability density of photon counts for H_1 bits showing abnormally high values at n = 143.

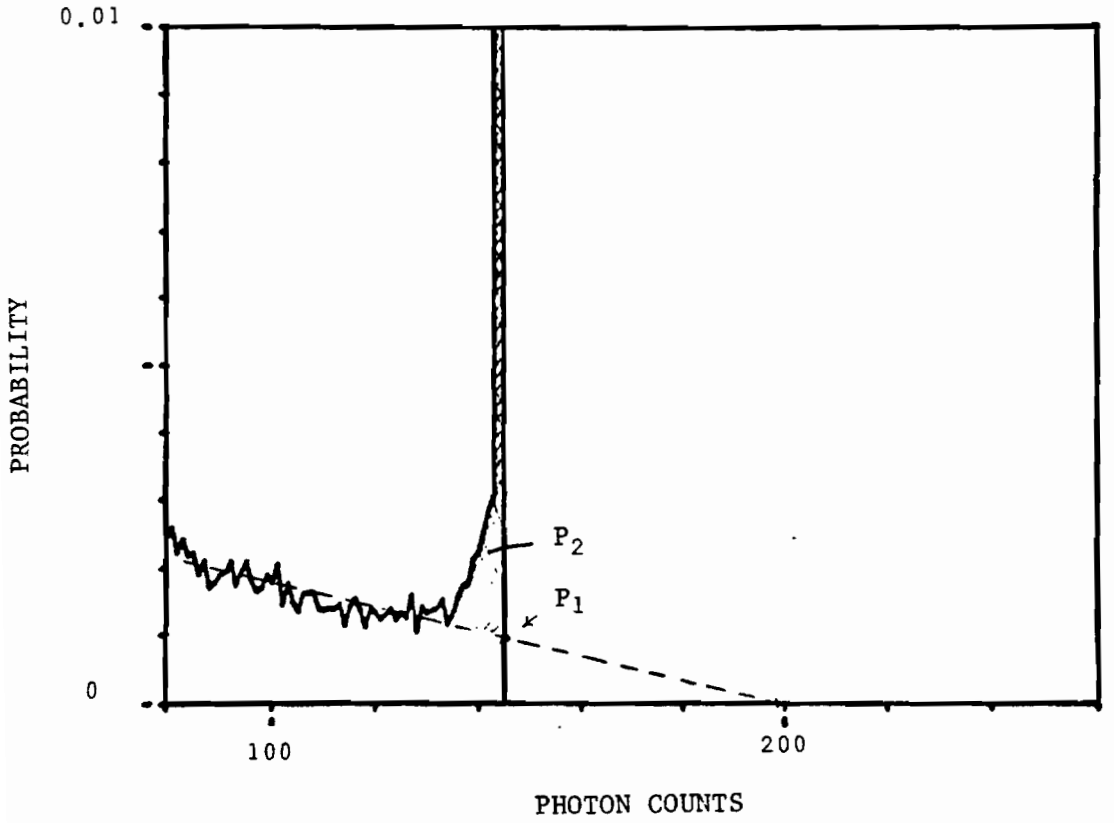

Figure 81. Same as Figure 80 but magnified at the peak at n = 143.

Let the probability of having a count n be P(n).

Let the probability represented by the hatched area be P_2.

Let the probability of the count N be P_1 as determined from Fig. 81 under the assumption of uniform tapering of probability.

$$\therefore \sum_{n=N+1}^{N+N'} P(n) = P_2$$

$$P(n) = P_1 - \frac{(n - N)P_1}{N'} , \quad n > N$$

$$\therefore \sum_{n=N+1}^{N+N'} \left\{ P_1 - (n - N) \frac{P_1}{N'} \right\} = P_2 , \quad n > N$$

$$\text{or} \quad N'P_1 - \frac{(N' + 1)N'}{2} \frac{P_1}{N'} = P_2$$

$$\text{Solving for } N', \quad N' = \frac{2P_2 + P_1}{P_1}$$

$$\simeq \frac{2P_2}{P_1} \quad \text{if } N' >> 1$$

$$\therefore P(n) = P_1 - (n - N) P_1 \frac{P_1}{2P_2} , \quad n > N$$

$$= P_1 - \frac{(n - N)P_1^2}{2P_2}$$

Let M by the total number of bits used in evaluating the mean value of counts for H_1 bits.

$\therefore$ Total number of photons counted = $M \cdot (N'_S + N_B) + C$

where N'_S is the uncorrected value of N_S and C is a correction term.

$$\text{Now,} \quad C = \left[\sum_{n=N+1}^{N+N'} P(n)Mn \right] - P_2MN, \quad n > N$$

$$= \sum_{n=N+1}^{N+N'} \left\{ P_1 - \frac{(n - N)}{2P_2} P_1^2 \right\} Mn - P\,MN$$

$$= M \left[\sum_{n=N+1}^{N+N'} \left\{ P_1 - \frac{(n - N)}{2P_2} P_1^2 \right\} n - P_2N \right]$$

$$\text{Now,} \quad (N_S + N_B) = (N'_S + N_B) + C_1$$

where C_1 is the correction to be applied.

From the above,

$$C_1 = \frac{C}{M}$$

$$= \sum_{n=N+1}^{N+N'} P_1 n \left\{ 1 - \frac{P_1}{2P_2} (n - N) \right\} - P_2N$$

$$\text{with} \quad N' = \frac{2P_2}{P_1}$$

The value of C_1 was calculated and applied to $(N_S' + N_B)$ from which the correct value of N_S was calculated using equation (38).

III. Some Miscellaneous Details of the Experiment

1) The recording of the data was done at a tape speed of 60 inches per second, which is the maximum speed available. This was done to avail of the maximum band width for recording. The FM mode was used since d.c. levels were important. The reproduction speed had to match the tape drive speed for PDP 11. The speed used in this case was 60/32 inches per second, though 60/16 inches speed could have been used.

2) While handling the tape in Ampex 1300, any change of operation (from fast forward to drive, etc.) must always be done after stopping the tape and giving sufficient time so that the tape might come to a complete stop. Any impatience to observe this will result in tape squeezing or, worse still, the tape may snap.

3) Cleaning and demagnetizing the head every time before recording and reproduction is necessary.

4) The difference in the temperature between the two micro thermal probes was recorded in channel 4 of the tape, though these readings were not used in the calculation so far. But the same could be reproduced from tapes PCR 1-4 if necessary.

5) To prevent the transmission of the vibrations from the sync motor to the optical components is important in view of the large distance involved. The best method to do this was found to be mounting the motor on a 4 or more inch thick foam.

REFERENCES

1. E. V. Hoversten and R. S. Kennedy, "Efficient optical communication with the earth's atmosphere," AGARD conference proceedings on Opto-Electronics Signal Processing Techniques 50, 5-1 (1970).
2. E. V. Hoversten, R. O. Harger and S. J. Halme, "Communication theory for the turbulent atmosphere," Proc. IEEE 58, 1626-50 (1970).
3. M. C. Teich and S. Rosenberg, "Photocounting array receivers for optical communication through the lognormal atmospheric channel 1: Optimum and suboptimum receiver structures," Appl. Opt. 12, 2616-24 (1973).
4. J. Dunphy and J. R. Kerr, "Scintillation measurements for large integrated path turbulence," J. Opt. Soc. Am. 63, 981-86 (1973).
5. T. Kobayashi, K. Kohiyama and K. Nishino, "Atmospheric optical communication system," IEEE Trans. Com. Com-25, 1508-11 (1977).
6. T. P. Symera, P. A. Uusmaa, Kh. V. Khinrikus, Yu. E. Mal'sub, "Probability of error in an atmospheric laser communication line," Soviet J. Quant. Elec. 6, 759-6 (1976).
7. M. Ross, P. Freedman, J. Abernathy, G. Matassov, J. Wolf and J. D. Barry, "Space optical communications with Nd:Yag laser," Proc. IEEE 66, 319-44 (1978).
8. S. Chandrasekar, Radiative Transfer (Dover Pub. 1970).
9. R. R. Meier, J. S. Lee and D. E. Anderson, "Atmospheric scattering of middle UV radiation from an internal source," Appl. Opt. 17, 3216-25 (1978).

10. G. W. Kattawar and G. N. Plass, "Asymptotic radiance and polarization in optically thick media: Ocean and clouds," Appl. Opt. 15, 3166-78 (1976).

11. B. W. Fowler and C. C. Sung, "Radiative transfer in two dimensions through fog," Appl. Opt. 17, 1797-805 (1978).

12. G. W. Sutton, "Hole boring with pulsed high energy lasers: An exact solution including scattering and absorption," Appl. Opt. 17, 3424-30 (1978).

13. R. C. Harney, "Hole boring in clouds by high intensity lasers: Theory," Appl. Opt. 16, 2974-78 (1977).

14. Akira Ishimaru, "Theory and application of wave propagation and scattering in random media," Proc. IEEE 65, 1030-61 (1977).

15. E. A. Bucher and R. M. Lerner, "Experiments on light pulse communication and propagation through atmospheric clouds," Appl. Opt. 12, 2401-14 (1973).

16. W. H. Paik, M. Tebyani, D. J. Epstein, R. S. Kennedy and J. H. Shapiro, "Propagation experiments in low visibility atmosphere, Appl. Opt. 17, 899-905 (1978).

17. J. R. Clark and J. R. Baird, "Low visibility communications," Appl. Opt. 15, 314-16 (1976).

18. R. L. Fante, "Electromagnetic beam propagation in turbulent media," Proc. IEEE 63, 1669-91 (1975).

19. R. S. Lawrence and J. W. Strohbehn, "A survey of clear air propagation effects relevant to optical communications," Proc. IEEE 58, 1523-45 (1970).

20. Eli Brookner, "Atmospheric propagation and communication channel model for laser wave lengths," IEEE Trans. Com. Tech. Com-18, 396-416 (1970).

21. R. A. Elliott, J. R. Dunphy and J. R. Kerr, "Statistical tests of distributional hypothesis applied to irradiance fluctuations," OSA Topical mtg. on Optical Propagation Through Turbulence, Rain and Fog at Boulder, Colorado (Aug. 1977).

22. G. R. Ochs and R. S. Lawrence, "Saturation of laser scintillation under conditions of strong atmospheric turbulence," J. Opt. Soc. Am. 59, 226-27 (1969).

23. P. H. Deitz and N. J. Wright, "Saturation of scintillation magnitude in near earth optical propagation," J. Opt. Soc. Am. 59, 527-35 (1969).

24. M. H. Lee, R. A. Elliott, J. F. Holmes, and J. R. Kerr, "Variance of irradiance for saturated scintillations," J. Opt. Soc. Am. 66, 1389-92 (1976).

25. R. L. Fante, "Irradiance scintillations: Comparison of theory with experiment," J. Opt. Soc. Am. 65, 548-50 (1975).

26. L. R. Bissonnette and P. L. Wizinowich, "Probability distribution of turbulent irradiance in a saturation regime," Appl. Opt. 18, 1590-99 (1979).

27. D. L. Fried, G. E. Mevers and M. P. Keister Jr., "Measurements of laser beam scintillations in the atmosphere," J. Opt. Soc. Am. 57, 787-97 (1967).

28. H. L. Van Trees, Detection, Estimation and Modulation Theory: Part 1 (John Wiley 1968), p. 26.

29. J. H. Churnside and C. M. McIntyre, "Averaged threshold receiver for direct detection of optical communication through the log normal atmospheric channel," Appl. Opt. 16, 2669-76 (1977).

30. H. Z. Cummins and E. R. Pike, Photon Correlation and Light Beating Spectroscopy (Plenun 1974), p. 45.

31. M. C. Teich and S. Rosenberg, "Photocounting array receivers for optical communication through the log normal atmospheric channel 2: Optimum and suboptimum receiver performance for binary signaling," Appl. Opt. 12, 2625-35 (1973).

32. P. Diament and M. C. Teich, "Photo detection of low level radiation through the turbulent atmosphere," J. Opt. Soc. Am. 60, 1489-94 (1970).

33. Hans Eklund, "Signal distribution due to beam pointing error in a chopper modulated laser system," Appl. Opt. 17, 289-95 (1978).

34. V. I. Stuk, R. D. Mukhamed'yarov, V. N. Zhukov and O. Yu. Blinov, "Radiation modulator with synchronous motor," Soviet J. Tech. (USA) 44, 154-55 (1977).

35. S. F. Clifford, G. R. Ochs and R. S. Lawrence, "Saturation of optical scintillation by strong turbulence," J. Opt. Soc. Am. 64, 148-53 (1974).

36. R. W. Boyd, "Wave length dependence on seeing," J. Opt. Soc. Am. 68, 877-83 (1978).

37. J. Borgnino and F. Martin, "Correlation between angle of arrival fluctuations on the entrance pupil of a solar telescope," J. Opt. Soc. Am. 67, 1065-72 (1977).

38. A. R. Lewis and V. H. Rumsey, "Angular spectrum measurements of atmospheric turbulence," J. Opt. Soc. Am. 67, 178-81 (1977).

39. B. I. Cantor and M. C. Teich, "Dead time correlated photo counting distributions for laser radiation," J. Opt. Soc. Am. 65, 786-91 (1975).

40. L. Stephens and F. Davidson, "Photo electron counter dead time effects on direct detection optical communication systems," IEEE Trans. Com. Com-25, 615-21 (1977).

41. R. B. Fluchel, D. F. Fogle, and G. M. Lee, "Nonideal photoelectron counting," IEEE Trans. Com. Com-22, 1836-41 (1974).

42. R. M. Gagliardi and S. Karp, Optical Communications (John Wiley 1976), Ch. 9 & 10.

43. R. M. Gagliardi, "Effects of timing errors in optical digital systems," IEEE Trans. Com. Com-20, 87-93 (1972).

44. P. J. Titterton, "Effects of system inaccuracies on the probability of bit error for pulsed communication systems," Appl. Opt. 13, 1034-40 (1974).

BIOGRAPHICAL NOTE

Kaliappan Shanmuganathan was born July 6, 1946 in Bodinayakanur, Tamil Nadu, India. He graduated from high school in 1962 in that city. He received his B.Sc. degree in Physics in 1966 from Madras University and his M.Sc. degree in 1968 from Madurai University, both in India. After receiving his M.Sc. degree he worked as a lecturer in Physics for six years. During 1971-72 he attended the Indian Institute of Science at Bangolav and the Indian Institute of Technology in Kanpur to study advanced experimental techniques in Physics. In 1975 he left his job as a lecturer to pursue further studies in Physics at the Oregon Graduate Center, Beaverton, Oregon, where he completed the requirements for his Ph.D. in Applied Physics and Electronic Science in June, 1980. He was employed as a post-doctoral research fellow at the Oregon Graduate Center for six months. He will be returning to The American College, Madurai, India, as an assistant professor of Physics in July, 1980.